General Disclaimer

One or more of the Following Statements may affect this Document

- This document has been reproduced from the best copy furnished by the organizational source. It is being released in the interest of making available as much information as possible.

- This document may contain data, which exceeds the sheet parameters. It was furnished in this condition by the organizational source and is the best copy available.

- This document may contain tone-on-tone or color graphs, charts and/or pictures, which have been reproduced in black and white.

- This document is paginated as submitted by the original source.

- Portions of this document are not fully legible due to the historical nature of some of the material. However, it is the best reproduction available from the original submission.

A MODEL OF THE 0.4-GHz SCATTEROMETER

Job Order 73-215

Prepared By

Lockheed Electronics Company, Inc.
Systems and Services Division
Houston, Texas
Contract NAS 9-15200

For

EARTH OBSERVATIONS DIVISION
SPACE AND LIFE SCIENCES DIRECTORATE

National Aeronautics and Space Administration
LYNDON B. JOHNSON SPACE CENTER
Houston, Texas
January 1978

LEC-11087

1. Report No.	2. Government Accession No.	3. Recipient's Catalog No.

4. Title and Subtitle	5. Report Date
A MODEL OF THE 0.4-GHz SCATTEROMETER	January 1978
	6. Performing Organization Code
7. Author(s)	8. Performing Organization Report No.
S. T. Wu	LEC-11087
	10. Work Unit No.
9. Performing Organization Name and Address Lockheed Electronics Company, Inc. Systems and Services Division 1830 Nasa Road I Houston, Texas 77058	11. Contract or Grant No. NAS 9-15200
	13. Type of Report and Period Covered Technical Report
12. Sponsoring Agency Name and Address National Aeronautics and Space Administration Lyndon B. Johnson Space Center Houston, Texas 77058	14. Sponsoring Agency Code

15. Supplementary Notes

16. Abstract

The 0.4 GHz aircraft scatterometer system used for the Agricultural Soil Moisture Estimation Program is analyzed for the antenna pattern, the signal flow in the receiver data channels, and the errors in the signal outputs. The operational principal, system sensitivity, data handling, and resolution cell length requirement are also described. The backscattering characteristics of the agriculture scenes is contained in the form of the functional dependence of the backscattering coefficient on the incidence angle.

The substantial gains of the cross-polarization term of the horizontal and vertical antennas have profound effects on the cross-polarized backscattered signals. If these signals are not corrected properly, large errors could result in the estimate of the cross-polarized backscattering coefficient. It is also necessary to correct the variations of the aircraft parameters during data processing to minimize the error in the σ° estimation.

Recommendations are made to improve the overall performance of the scatterometer system.

17. Key Words (Suggested by Author(s))	18. Distribution Statement
airborne equipment/remote sensors/ scatterometers/soil moisture/back-scattering/microwave scattering/ signal analysis/antenna patterns	

19. Security Classif. (of this report)	20. Security Classif. (of this page)	21. No. of Pages	22. Price*
Unclassified	Unclassified		

*For sale by the National Technical Information Service, Springfield, Virginia 22161

A MODEL OF THE 0.4-GHz SCATTEROMETER

Job Order 73-215

PREPARED BY

S. T. Wu
Principal Engineer

APPROVED BY

P. J. Walsh, Supervisor
Exploratory Investigations Section

J. E. Davis, Manager
Earth Observations Exploratory
Studies Department

PREPARED BY

Lockheed Electronics Company, Inc.

For

Earth Observations Division
NATIONAL AERONAUTICS AND SPACE ADMINISTRATION
LYNDON B. JOHNSON SPACE CENTER
HOUSTON, TEXAS

January 1978

CONTENTS

TABLES

FIGURES

ACRONYMS AND ABBREVIATIONS

ac	alternating current
ADAS	Aircraft Data Acquisitions System
AGC	automatic gain control
ASME	Agricultural Soil Moisture Estimation
C	centigrade
CAD	Computation and Analysis Division
cm	centimeter
CW	continuous wave
dB	decibel
dBm	decibels referred to 1 milliwatt in 600 ohms
dc	direct current
DDC	Data Distribution Center
EOD	Earth Observations Division
ESD	Engineering Systems Division
FM	frequency modulation
g	gram
GDSD	Ground Data System Division
GHz	gigahertz
GSFC	Goddard Space Flight Center
HH	horizontal-horizontal
HV	horizontal-vertical
Hz	hertz
ICW	interrupted continuous wave
IF	intermediate frequency

IRIG	Inter-Range Instrumentation Group
JSC	Lyndon B. Johnson Space Center
K	kelvin
KHz	kilohertz
LO	local oscillator
m	meter
MHz	megahertz
NASA	National Aeronautics and Space Administration
PCM	pulse code modulation
PRF	pulse repetition frequency
PW	pulse width
REC	record
RF	radio frequency
rms	root-mean-square
UK	University of Kansas
VH	vertical-horizontal
VSWR	voltage standing wave ratio
VV	vertical-vertical

ACKNOWLEDGMENT

It is a pleasure to acknowledge A. E. Dillinger for her effort in putting the 0.4-GHz scatterometer antenna pattern data into a magnetic tape in a form suitable for numerical computation of antenna coupling effects. Particular thanks are due to S. C. Reid, who provided the laboratory calibrations data.

1. INTRODUCTION

Three scatterometer systems at frequencies of 0.4, 1.6, and 13.3 GHz have been installed on a National Aeronautics and Space Administration (NASA) aircraft as additional microwave sensors for the Joint Soil Moisture Experiment (ref. 1), which is now the Agricultural Soil Moisture Estimation Program (ASME). These scatterometers transmit radio frequency (RF) waves downward and measure the power of the waves backscattered from an agricultural scene. The final results of the operation are expressed in terms of the backscattering coefficient σ° as a function of the incident angle θ of the RF waves. Because $\sigma^\circ(\theta)$ at a given frequency, depends only on the scene parameters such as soil moisture content, surface roughness, vegetative cover, and soil type, these scene parameters can be estimated (remotely sensed) by studying the magnitude and variations of σ° with θ.

The 13.3-GHz scatterometer system has been studied rather extensively in the past (refs. 2, 3, 4). The results of recent study, which was based on the new laboratory measurements of the system parameters, was reported by Rosenkranz (ref. 5). Using the same approach, an up-to-date analysis of the 1.6-GHz scatterometer system was reported by Wang (ref. 6). Reports on the 0.4-GHz system are limited to a general system description by Reid (ref. 7) and by the vendors (refs. 8, 9). Therefore, because of component replacement and antenna redesign a current analysis on

the 0.4-GHz system is required in order to assess the performances and limitations of the system. It is the objective of this report to provide an up-to-date analysis of the 0.4-GHz scatterometer system, based on the most recent measurements of the system parameters.

The specification, configuration, and functional description of the system are discussed in section 2. This section also includes the signal frequency spectrum, data processing procedures, and the expected receiver signal level at aircraft altitudes. The scatterometer system analysis is given in section 3. In this section, the backscattering coefficient algorithms used to calculate σ° are presented. A return signal power, which uses a continuous system calibration approach is traced through the receiver channels. Resolution cell length requirements are also discussed in section 3. Section 4 includes the antenna patterns data, which are studied for the configuration of main lobe, the effects of side lobe, and the cross-polarization levels. Section 5 gives the numerical results, including the estimates of σ° and the effect of cross-polarization levels. Section 6 presents the major conclusions of this study and several suggestions on future endeavors for studying the 0.4-GHz scatterometer.

2. SYSTEM DESCRIPTION

2.1 SYSTEM SPECIFICATION

The 0.4-GHz scatterometer, which is flown on a Lyndon B. Johnson Space Center (JSC) aircraft, is an interrupted continuous-wave (ICW) Doppler radar system (refs. 7, 8, 9), designed to measure the backscattering coefficient σ° as a function of the angle of incidence θ for various types of terrain. The scatterometer transmits an ICW of 400.85 MHz radio frequency (RF) waves alternately from the horizontal and vertical antennas. The backscattered signals are received by both antennas and processed by individual receivers for each transmitted polarization. As a result of the forward motion of the aircraft, different Doppler frequency shifts are introduced in the return signals from different angles of incidence. The power of the return signal from a ground-resolution cell which is associated with a given incidence angle is finally retrieved by bandpass filtering at the corresponding Doppler frequency during data processing.

The system specifications and capabilities are given in table 2-1. There are three manual models of operation depending on the altitude of the aircraft. There is also an automode operation in which the pulse width (PW) and pulse repetition frequency (PRF) are automatically controlled by an altimeter. For ASME application, only manual mode 1-5 is used. The 1-5 indicates aircraft altitudes from 1000 to 5000 feet (304.8 to 1524 meters).

TABLE 2-1. — THE 0.4-GHz SCATTEROMETER SYSTEM CHARACTERISTICS

Terms	
Transmit frequency	400.85 ± 1 MHz
Transmitter power output	40.8 dBm (peak); 25.4 dBm (average)
Modulation	Interrupted continuous wave (ICW)
Pulse width (PW)	Manual 1-5, 1.35 ± 0.1 μs Manual 4-20, 6.9 ± 0.2 μs Manual 16-40, 29.5 ± 0.74 μs
Pulse repetition frequency (PRF)	Manual 1-5, 42 ± 0.8 KHz Manual 4-20, 10.5 ± 0.25 KHz Manual 16-40, 4.9 ± 0.125 KHz
Transmitter/receiver (T/R) isolation	120 dB during transmit
Number of antennas	Two, horizontal and vertical
Isolation between antennas	25 dB minimum
Antenna gain (two-way)	~ 25 dB
Antenna beam width (two-way)	~ 18°
Antenna alongtrack coverage	0 to 60° cosecant squared beam
Position of peak antenna gain	44° (angle of incidence) horizontal antenna 68° (angle of incidence) vertical antenna
Maximum skew angle	0.25°
Polarization	HH, HV, VH, VV
Dynamic range	120 dB
Receiver sensitivity	- 148 dBm (6 Hz bandwidth)
Receiver noise figure	~ 20 dB

TABLE 2-1. — Concluded.

Terms	
Signal-to-noise ratio (1500 ft. altitude)	> 10 dB
Calibration	Simultaneous with data processing
Receiver output	Four fixed-receiver gate channels; one calibration channel; signal level - 0 to 5 volts

The scatterometer is a multiple data channel system. Multiple receivers and switches automatically separate the backscattered signal into the following data channels.

a. Horizontally polarized return when transmitting a horizontally polarized wave using a fixed-receiver gate (HHFG)
b. Vertically polarized return when transmitting a vertically polarized wave using a fixed-receiver gate (VVFG)
c. Vertically polarized return when transmitting a horizontally polarized wave using a fixed-receiver gate (HVFG)
d. Horizontally polarized return when transmitting a vertically polarized wave using a fixed-receiver gate (VHFG)

The scatterometer continuously calibrates the backscattered signal by injecting a calibrate signal into each channel and monitoring the transmitter power using a calibrate channel. The ratio of power return to power transmitted is obtained by measuring the ratio of power return to calibrate signal in the channel of interest and by measuring the ratio of transmitted power to calibrate power in the calibrate channel. The ratio of a calibrate signal in the data channel to calibrate signal in the calibrate channel is a predetermined system constant. This calibration method eliminates uncertainties which, otherwise, would be introduced because of transmitter output and receiver gain variation.

2.2 SYSTEM CONFIGURATIONS

The 0.4-GHz scatterometer was installed in the NASA C-130 aircraft. The horizontal and vertical antennas were mounted near the aircraft tail such that the plane of the antennas made a 22° angle with the horizontal plane. Figures 2-1 and 2-2 show the side and back views of the antennas, respectively. Each antenna consists of 24 dipoles. Every crosstrack array contains eight equally spaced dipoles; there are three crosstrack arrays equally spaced in the alongtrack plane to form the complete antenna system. The dipole orientation of the horizontal and vertical antenna arrays are orthogonal to each other so that either the vertically or the horizontally polarized, cosecant-squared beam can be generated. The antenna pattern was shaped to cover an illumination area bounded by a crosstrack angular extent of approximately 18° and an alongtrack angular extent ranging from nadir to approximately 60° in the aft direction.

The transmitter/receiver (T/R) unit and the tape recorder were placed in a rack inside the aircraft. Coaxial cables were used to connect the T/R unit input and output to the respective antenna port.

2.3 PRINCIPLE OF OPERATION

The operational principle of the 0.4-GHz scatterometer has been described in several reports (refs. 7, 8, 9). A brief description is presented here to facilitate understanding the signal analysis, which is discussed in section 3.2.

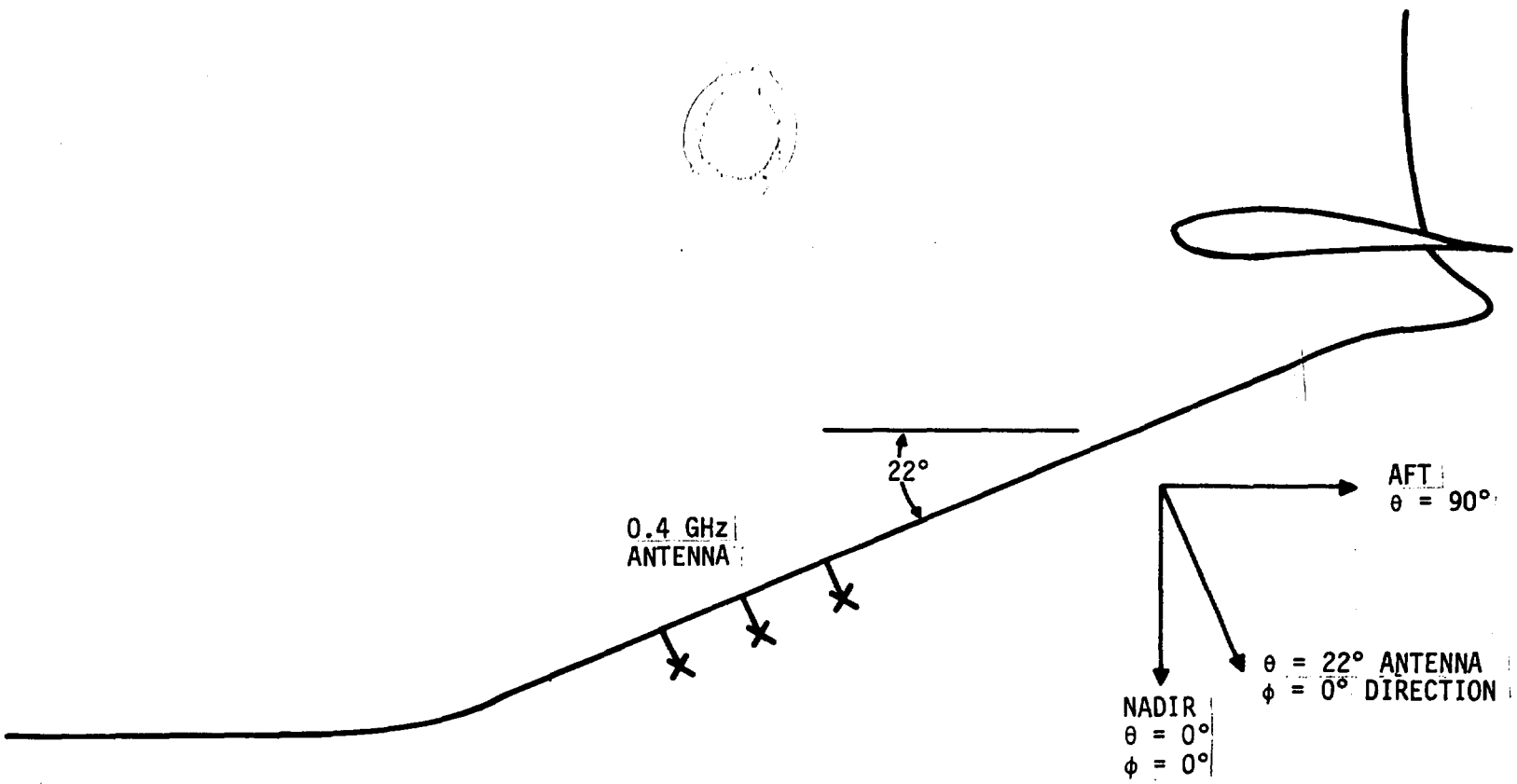

Figure 2-1.— Side view of C-130 showing coordinates for the 0.4 GHz scatterometer.

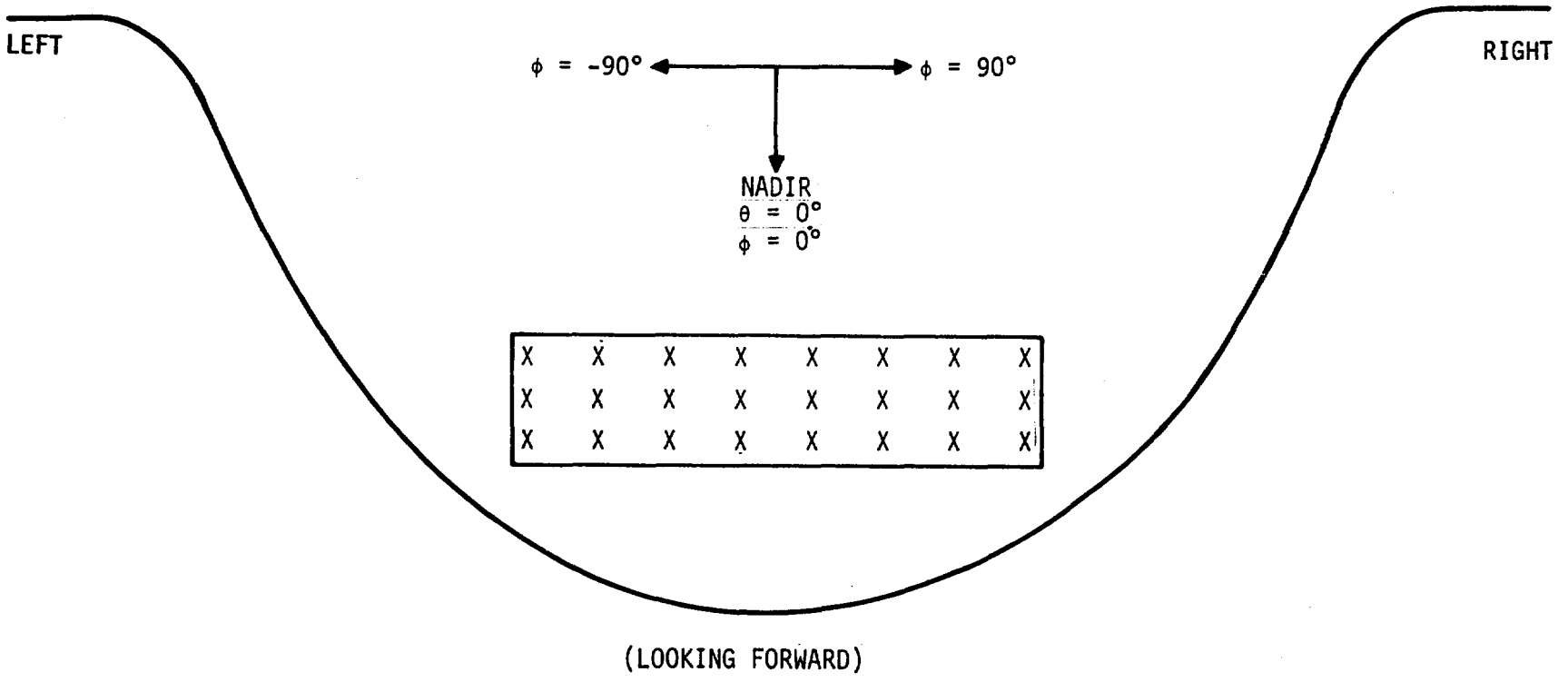

Figure 2-2.— Back view of C-130 showing coordinates for the 0.4 GHz scatterometer.

Figure 2-3 shows the block diagram of the scatterometer system. (It is a slight modification of figure 2-1 in reference 7.) The functions of major components of the system are described in the following paragraphs.

The transmitted signal is an interrupted continuous-wave (ICW) whose width and duty cycle are controlled by the synchronizer. The frequency of the transmitted signal is determined by a crystal controlled oscillator in the transmitter/modulator. In addition to providing the 20-watt peak 400.85 MHz ICW output signal, the transmitter/modulator provides a 400.85 MHz signal to the first local oscillator (LO) source and a transmitter sample signal (approximately 50 dB down) to the calibrate receiver. The timing signal is generated by the synchronizer. These include the modulator trigger supplied to the transmitter/modulator and the switching signals to the RF and intermediate frequency (IF) switches. The pulse width (PW) and the pulse repetition frequency (PRF) are determined by the mode selected by the operator. In the manual mode, the PW and PRF are fixed by the selected altitude range (table 2-1).

The scatterometer timing waveforms are shown in figure 2-4. The transmitter/modulator is turned on by the modulator trigger pulse and has a fixed 0.2μsec delay. The RF energy from the transmitter/modulator is alternately switched between the horizontally polarized antenna and the vertically polarized antenna by the antenna switch

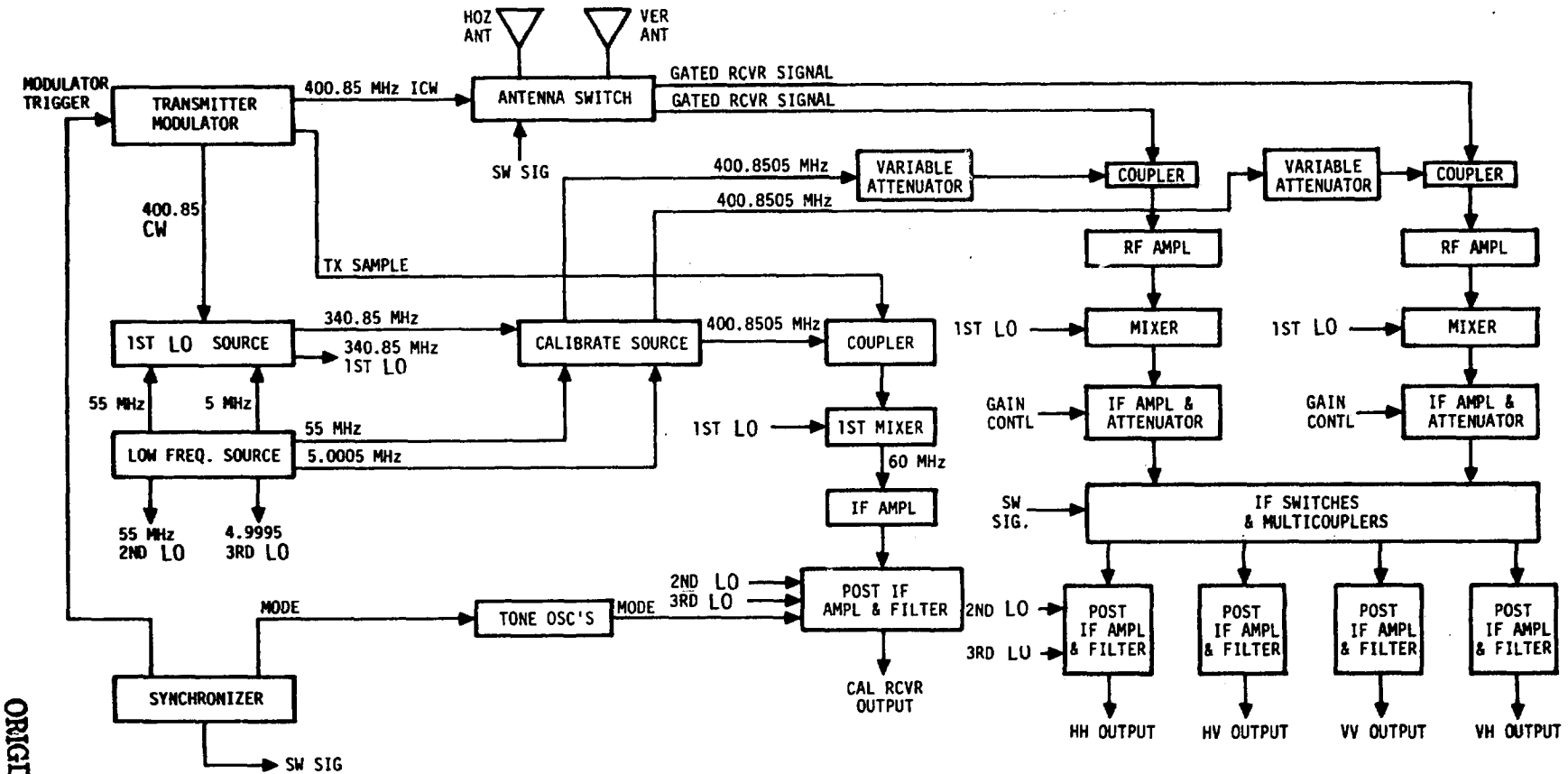

Figure 2-3.— The 0.4-GHz scatterometer block diagram.

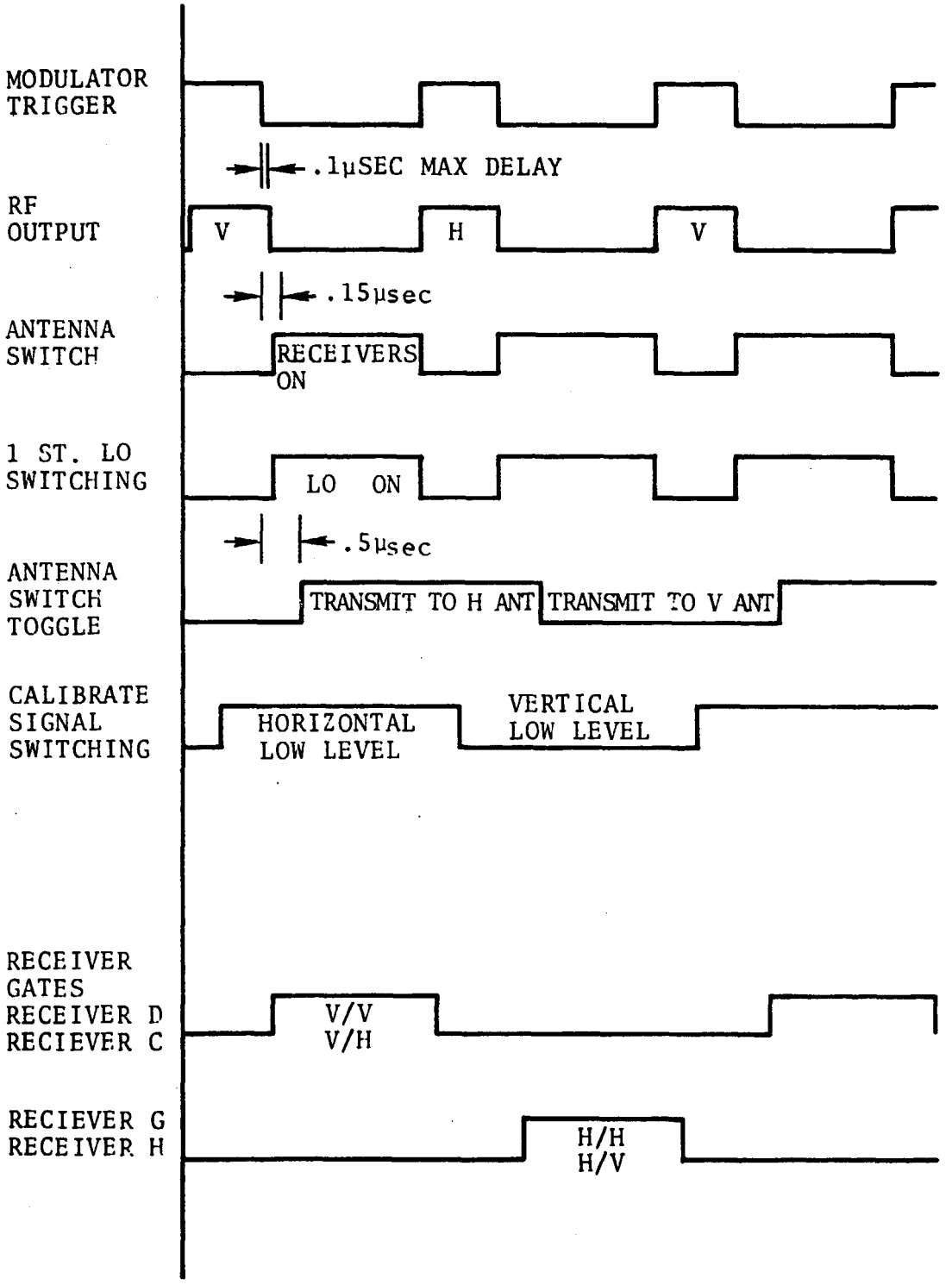

Figure 2-4.– Scatterometer timing waveforms.

toggle waveform. Both receiving channels are coupled to their respective antenna by the antenna switch waveform. An inherent delay is built into this waveform to ensure that the transmitter is turned off before the antennas are switched to their receivers. The first LO switching waveform controls the LO input to the first receiver mixers. The first LO excitation is removed during transmission to provide additional transmitter/receiver isolation. Further isolation is accomplished in the IF switches, where receiver gating is done. The signals received from the antennas are gated by the antenna switch and applied to a directional coupler which provides a means of injecting the calibrate signal. The gated signal is attenuated very little by the coupler (i.e., introduced by the insertion loss of the coupler) and the calibrate signal is attenuated by 20 dB (i.e., the coupling value).

There are three amplification stages in the receiver units; namely, the RF amplification, IF amplification, and the post IF amplification. The combined backscattered and calibrate signal from the directional coupler are first amplified by a 27-dB gain RF amplifier which has a noise figure of less than 4 dB. The amplified signals are then fed to a mixer and down converted to the 60 MHz IF amplification stage. The input signal to the IF amplifier are subjected to an adjustable gain control in 10 dB steps over a 50-dB range. The output signals from the 60-MHz IF amplifier is fed to the IF switch and multicoupler assembly, where they are gated and distributed to the proper post-IF amplifier. The

post-IF amplifier provides both manual and automatic gain control, each having a range of 40 dB. The 60-MHz signals are first converted down to 5 MHz using the 55-MHz second LO and then converted down again to 500 Hz using the 4.995-MHz third LO. The 500-Hz signals are fed to a low-frequency amplifier where a direct current (dc) offset is added to form an output compatible for tape recording.

There are four data channels, one calibrate channel, and three telemetry signals in the scatterometer system output. Each of the four data channels occupies a bandwidth of 1 kHz and is maintained at a nominal level of 0.9 V root mean square by an automatic gain control (AGC) circuit. In addition, the alternating current (ac) output signal is superimposed on a dc offset voltage of 2.5 Vdc. The calibrate receiver channel also contains IF and post-IF amplifiers, and the output consists of two discrete data signals and three discrete signals for telemetry of control positions. The data signals are located at 500 Hz and 1 kHz for the transmitter sample and the calibrate signal, respectively. The telemetry signals are obtained from three voltage-controlled subcarrier oscillators designed for operation on bands 1, 2, and 3 of the Inter-Range Instrumentation Group (IRIG) standard. The mode selector switch is assigned to band 1; the horizontal gain control, band 2; and the vertical gain control, band 3.

2.4 SIGNAL FREQUENCY SPECTRUM

To investigate the waveform of transmitted signal and its power spectrums distribution, a signal frequency spectrum is discussed in this subsection. In figure 2-4, the RF output of 400.85 MHz CW can be represented by $A \cos 2\pi f_o \tau$ [fig. 2-5(a)]. The modulator trigger provides a unit pulse train, $\sum_{n=-\infty}^{\infty} S(t-nT)$, with period T and pulse width τ as shown in figure 2-5(b). The transmitter output is a combination of the two sources [fig. 2-5(c)]. This signal output from the transmitter can be expressed by

$$f(t) = A \cos 2\pi f_o t \sum_{N=-\infty}^{\infty} S(t-nT) \qquad (2\text{-}1)$$

where

$S(t-nT) = 1$ for $nT - \frac{\tau}{2} \leq t \leq nT + \frac{\tau}{2}$

$= 0$ elsewhere $\quad n = 0, \pm 1, \pm 2, \ldots$

A = amplitude of the ICW at the transmitter output, and

f_o = frequency transmitted = 400.85 MHz

The frequency spectrum is obtained by applying Fourier transform on f(t). It is shown in reference 10 that if $f(t) = f_1(t)\, f_2(t)$, then $F[f(t)] = F[f_1(t)] \otimes F[f_2(t)]$, where $F[\ ]$ denotes the Fourier transform of the function in the bracket and $\otimes$ denotes the convolution integral of the two functions in the expression. Now let

$$f_1(t) = A \cos 2\pi f_o t \qquad (2\text{-}2)$$

and

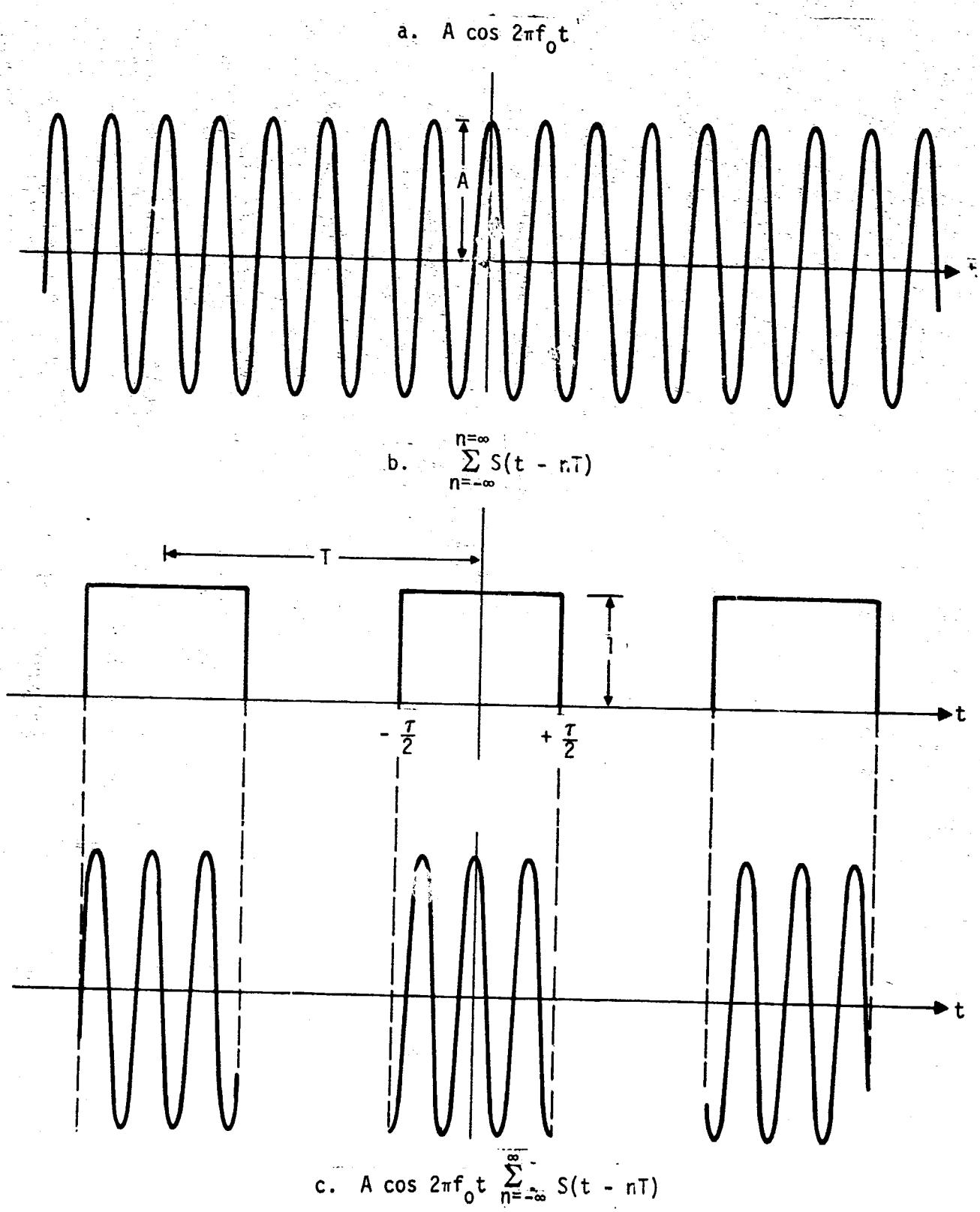

Figure 2-5.– Transmitted signal waveforms.

$$f_2(t) = \sum_{n=-\infty}^{\infty} S(t-nT) \tag{2-2}$$

Then, the transform of $f_1(t)$ is

$$F[f_1(t)] = A \int_{-\infty}^{\infty} \cos 2\pi f_o t e^{-j2\pi ft}\, dt$$

$$= \frac{A}{2} \int_{-\infty}^{\infty} e^{-j2\pi(f - f_o)t} + e^{-j2\pi(f + f_o)t}\, dt$$

$$= \frac{A}{2} \delta(f - f_o) + \delta(f + f_o) \tag{2-3}$$

where $\delta(f - f_o)$ and $\delta(f + f_o)$ are the delta functions which represent unit impulse at $f = f_o$ and $f = -f_o$, respectively.

The transform of $f_2(t)$ is

$$F[f_2(t)] = \int_{-\infty}^{\infty} \sum_{n=\infty}^{\infty} S(t - nT) e^{-j2\pi ft}\, dt \tag{2-4}$$

Observe that for $n = 0$

$$\int_{-\infty}^{\infty} S(t) e^{-j2\pi ft}\, dt = \int_{-\tau/2}^{\tau/2} e^{-j2\pi ft}\, dt = \frac{\sin \pi f\tau}{\pi f} \tag{2-5}$$

and for $n = K$

$$\int_{-\infty}^{\infty} S(t - KT) e^{-j2\pi ft}\, dt = \int_{-\infty}^{\infty} S(t') e^{-j2\pi f(t' + KT)}\, dt'$$

$$= e^{-j2\pi fKT} \int_{-\tau/2}^{\tau/2} e^{-j2\pi ft'}\, dt'$$

$$= \frac{\sin \pi f\tau}{\pi f} e^{-j2\pi fKT} \tag{2-6}$$

Thus

$$F[f_2(t)] = \frac{\sin \pi f\tau}{\pi f} \sum_{n=-\infty}^{\infty} e^{-j2\pi nfT} \qquad (2\text{-}7)$$

Therefore, the Fourier transform of f(t) is

$$F[f(t)] = \frac{A}{2} \int_{-\infty}^{\infty} [\delta(f - f_o - \nu) + \delta(f + f_o - \nu) \frac{\sin \pi\nu\tau}{\pi\tau} \sum_{n=-\infty}^{\infty} e^{-j2\pi n\nu T} \, d\nu$$

$$= \frac{A}{2} \frac{\sin \pi(f - f_o)\tau}{\pi(f - f_o)} \sum_{n=-\infty}^{\infty} e^{-j2\pi n(f - f_o)T}$$

$$+ \frac{A}{2} \frac{\sin \pi(f + f_o)\tau}{\pi(f + f_o)} \sum_{n=-\infty}^{\infty} e^{-j2\pi n(f + f_o)T} \qquad (2\text{-}8)$$

The frequency spectra, as derived in equations (2-1) through (2-8), are shown sequentially in figure 2-6. The summation, $\sum_{n=-\infty}^{\infty} e^{-j2\pi nfT}$, gives unit impulse train spacing at PRF, $f_r = \frac{1}{T}$ [fig. 2-6(a)]. The shape of the function $\frac{\sin \pi f\tau}{\pi f}$ is given in figure 2-6(b). The spectrum of $F[f_2(t)]$, [fig. 2-6(c)], results from the multiplication of figures 2-6(a) and 2-6(b). Finally, the convolution operation of $F[f_2(t)]$ with respect to $F[f_1(t)]$ transfers the total spectrum to the center positions at $f = f_o$ and at $f = -f_o$. Figure 2-6(d) shows the spectrum of $F[f(t)]$. Only the spectrum positioned at $f = f_o$ will be of interest in the present discussion.

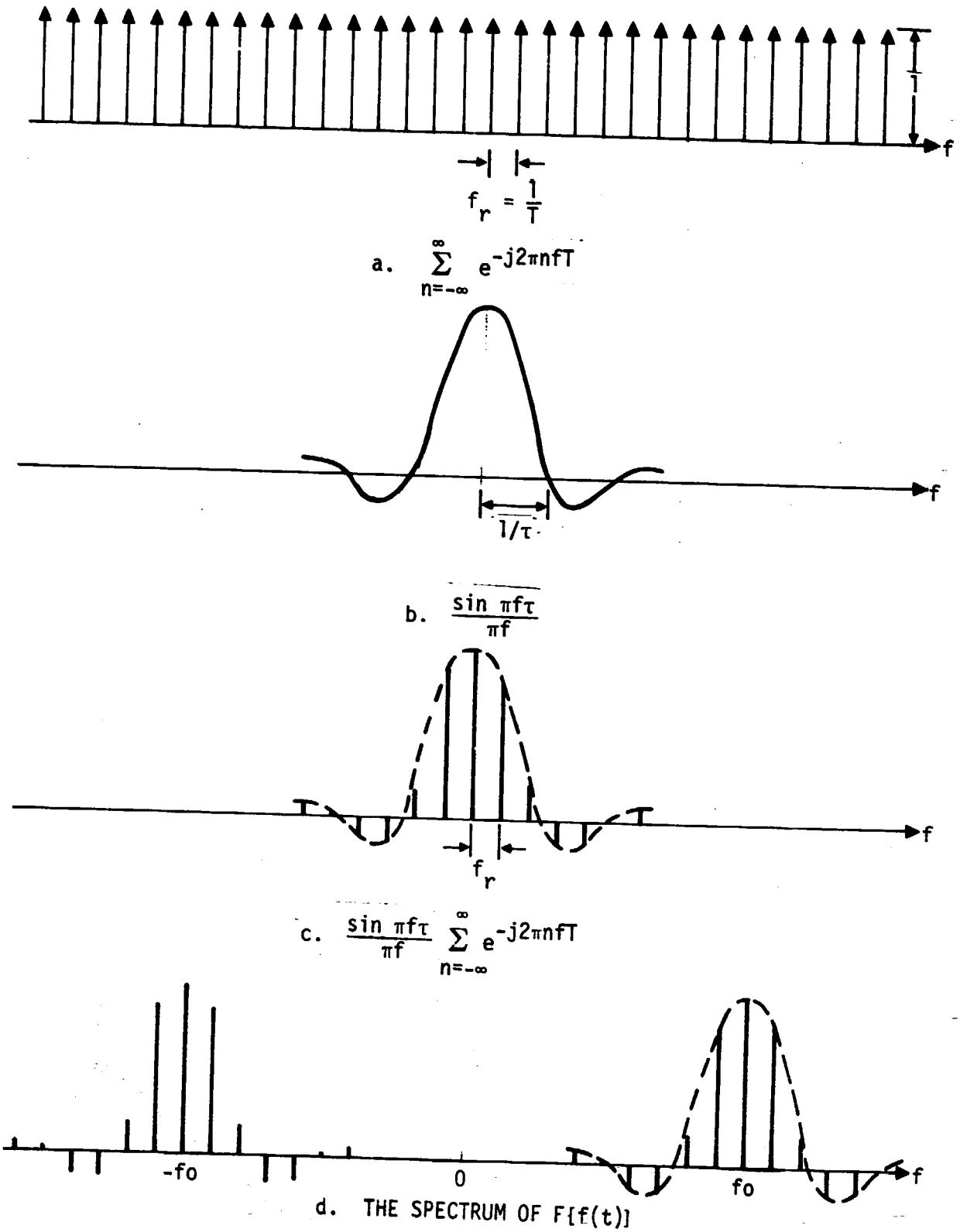

Figure 2-6.– Frequency spectra of transmitted waveforms.

The spectrum of a transmitted signal with a 42-KHz PRF, a 1.35-μsec PW, and positioned at the 400-MHz carrier frequency is shown in figure 2-7. The spectrum of the received signal after a third-down conversion is also shown.

2.5 RECEIVER SENSITIVITY

One way to estimate the sensitivity of the scatterometer system is by examining the signal-to-noise ratio at the receiver output. The power P_r reflected from a target and collected by a receiving antenna can be expressed in terms of the radar equation (ref. 11) as

$$P_r = \frac{P_t G_t G_r \sigma \lambda^2}{(4\pi)^3 R^4} \qquad (2\text{-}9)$$

where

P_t = power transmitted by the radar in watts

G_t = gain of the transmitting antenna in watts

G_r = gain of the receiving antenna in the direction of the target

σ = radar cross section of the target

λ = radar wavelength

R = distance between the radar and the target

To compute the signal-to-noise ratio at the receiver output, the radar equation needs to include the effects of duty cycle and several loss factors; it is derived as follows. The antenna pattern factor can be expressed by:

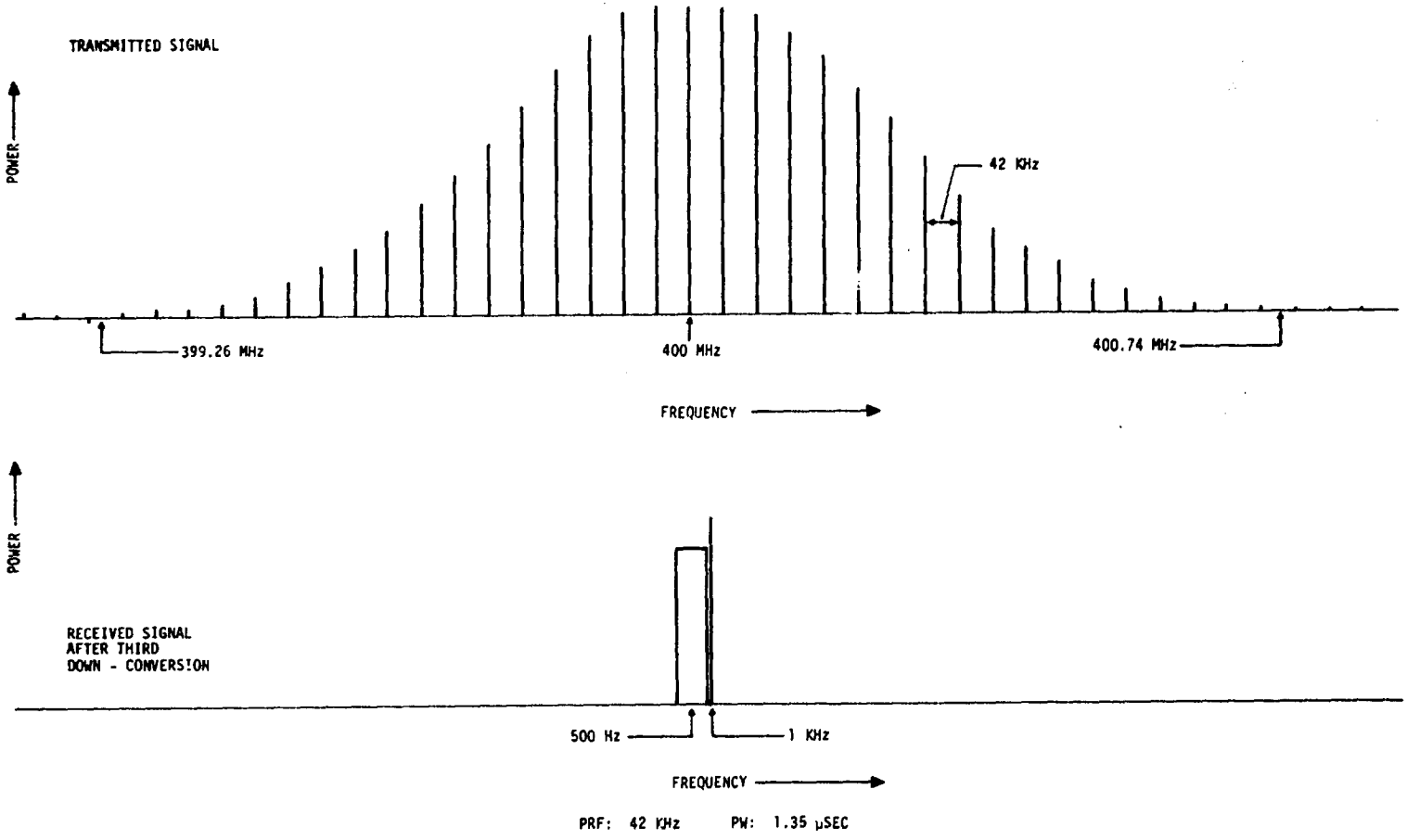

Figure 2-7.— A signal frequency spectrum of the 0.4-GHz scatterometer.

$$G_t G_r = G_0^2 f_1(\theta,\phi) \tag{2-10}$$

where $f_1(\theta,\phi)$ is the two-way antenna pattern factor.

The radar cross section of the target can be expressed by:

$$\sigma = \int \sigma^\circ(\theta)\, dA \tag{2-11}$$

where $\sigma^\circ(\theta)$ is the backscattering coefficient per unit area; the integration is taken over the illuminated region.

The differential area dA is

$$dA = R^2 d\theta d\phi \tag{2-12}$$

Substituting equations (2-10) through (2-12) into equation (2-9) yield

$$P_r(\theta_o) = \frac{P_t G_0^2 \lambda^2}{(4\pi)^3} \int_{\theta_o - \frac{\Delta\theta}{2}}^{\theta_o + \frac{\Delta\theta}{2}} \frac{\sigma^o(\theta)}{R^2} \left[\int_{-\pi/2}^{\pi/2} f_1(\theta,\phi) d\phi \right] d\theta \tag{2-13}$$

The Doppler frequency at the angle of incidence (θ_o) and the aircraft ground velocity (V) is expressed as:

$$f_D = \frac{2V}{\lambda} \sin \theta_o \tag{2-14}$$

and

$$\Delta f_D = \frac{2V}{\lambda} \cos \theta \, \Delta\theta \tag{2-15}$$

Since a wide aft beam antenna is being considered, $f_1(\theta,\phi)$ is a slowly varying function of θ and may be written as

$$\int_{-\pi/2}^{\pi/2} f_1(\theta,\phi)d\phi = B_\phi F\ (\theta) \qquad (2\text{-}16)$$

where B_ϕ is the two-way crosstrack effective antenna beam width.

The power density in watts per hertz $W_r(\theta_o)$, received at the receiving antenna, is obtained by substituting equation (2-16) and the relation $h = R \cos \theta$ for equation (2-13) and by dividing by Δf_D.

$$W_r(\theta_o) = \frac{P_r(\theta_o)}{\Delta f_D} = \frac{P_t G_o^2 F\ (\theta_o)\lambda^3 \sigma^o(\theta_o) B_\phi \cos \theta_o}{2(4\pi)^3 Vh^2} \qquad (2\text{-}17)$$

where h is the aircraft altitudes.

Figures 2-8 and 2-9 show the resolution cell as defined by the Doppler frequency bandwidth and antenna beam width and the geometry of a scatterometer ground-resolution cell, respectively.

The average power transmitted is $P_{avg} = D_T P_t$, where D_T is the duty cycle of the transmitter. The duty cycle D_T is expressed by:

$$D_T = \tau \cdot f_r \qquad (2\text{-}18)$$

where τ and f_r are PW and PRF, respectively. Of this transmitted

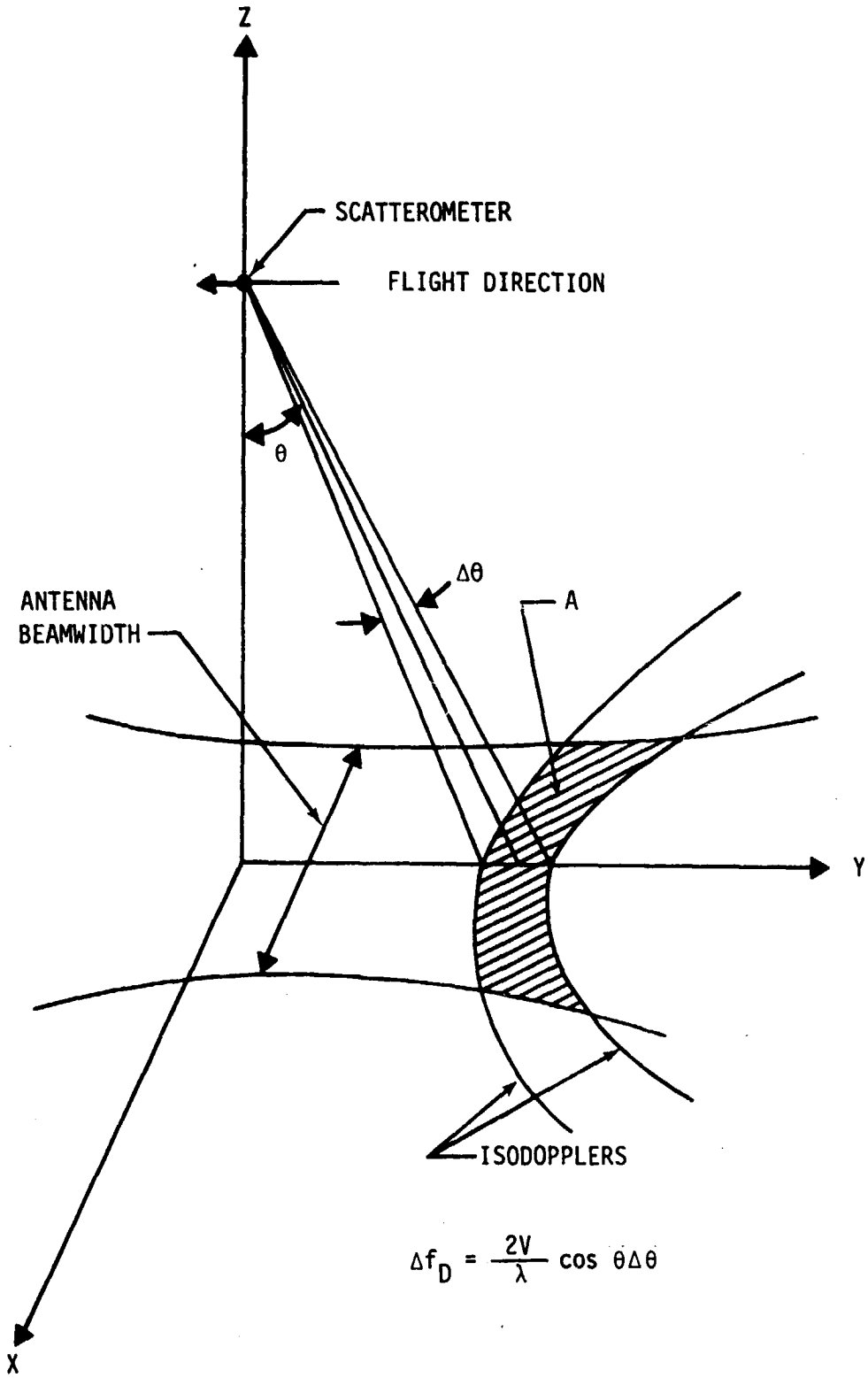

Figure 2-8.– The resolution cell as defined by Doppler frequency bandwidth and antenna beam width.

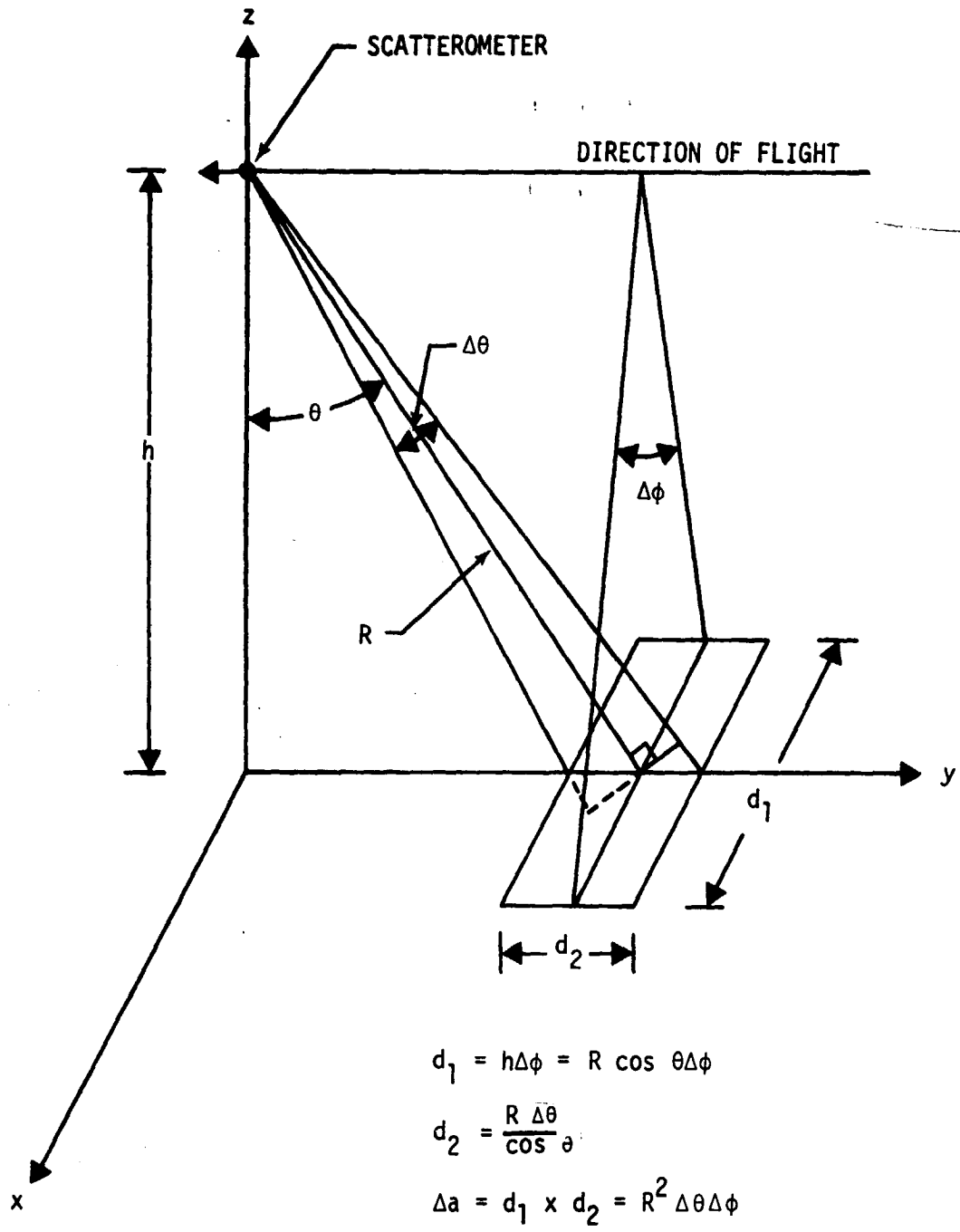

$$d_1 = h\Delta\phi = R \cos\theta\Delta\phi$$

$$d_2 = \frac{R\,\Delta\theta}{\cos\theta}$$

$$\Delta a = d_1 \times d_2 = R^2\,\Delta\theta\Delta\phi$$

Figure 2-9.-- Geometry of a scatterometer ground resolution cell.

power, only D_T amount is usable; the remainder is redistributed as harmonics of the PRF. Therefore, the relative power contained in the fundamental waveform (fig. 2-7) is $D_T^2 P_t$.

The received signal power density becomes

$$W_{rs}(\theta) = \frac{P_t G^2(\theta) \lambda^2 \sigma^o(\theta) B_\phi \cos \theta \, D_T^2}{2(4\pi)^3 V h^2 L_m} \tag{2-19}$$

where L_m is the miscellaneous loss, including the two-way antenna coaxial cable loss and switching loss; $G^2(\theta) = G_o^2 F(\theta)$ and θ_o have been generalized to θ.

The noise power per hertz is expressed by:

$$W_n = KTF \, D_R \tag{2-20}$$

where F is the receiver noise figure, and D_R is the receiver gated on duty cycle.

The signal-to-noise power density ratio is

$$\frac{W_{rs}}{W_n} = \frac{P_t G^2(\theta) \lambda^3 \sigma^o(\theta) B_\phi \cos \theta \, D_T^2}{2(4\pi)^3 V h^2 L_m KTF D_R} \tag{2-21}$$

The numerical values of the system parameters in equation (2-21) were evaluated using the measured data and were included in table

2-2 for the estimate of the signal-to-noise ratio. The aircraft altitudes and the speed were assumed to be approximately 457 m (1500 feet) and 77 m/sec (253 ft/sec), respectively. The incidence angle was taken to be 60°, where low signal return was expected. The $\sigma°$ value at a 60°-incidence angle was taken from figure 3-3; the calm sea value was used for low signal return. A duty cycle of 0.0567 for manual mode 1-5 was computed from equation (2-18). All of the remaining parameters appeared in equation (2-20) are self-explanatory. The gain of the receiver amplifier was not entered in the computation because it applied equally to signal and noise and was eliminated when the signal-to-noise ratio was taken. In calculating the receiver noise level, the ambient temperature (T) was assumed to be approximately 290 K. The Boltzmann constant (K) is 1.38×10^{-23} J/K. The 5.4-dB noise was obtained from the report by the Emerson Electric Company (ref. 9). The signal power density received is the sum (in dB) of all items given in equation (2-19) and is -131.9 dBm/Hz. The receiver noise power density is -173.1 dBm/Hz, which results in a signal-to-noise ratio of approximately 41 dB. However, the signal-to-noise ratio of the tape recorder system as reported in reference 6 is approximately 40 dB, which represents the best value attainable with the 0.4-GHz scatterometer and data recording system.

TABLE 2-2. – THE 0.4-GHz SCATTEROMETER SIGNAL-TO-NOISE RATIO

Parameters	Power Level
Transmitter output power P_t	40.8 dBm
$G^2(\theta)$ (VV gain at θ = 60°)	19.3 dB
B_ϕ (at θ = 60°, VV beam width is 23.3°)	-3.9 dB
λ^3 (wavelength - 0.75 m)	-3.7 dB
$\sigma^\circ(\theta)$ (θ = 60°)	-40.0 dB
cos θ (θ = 60°)	-3.0 dB
$1/[2(4\pi)^3]$	-36.0 dB
1/V (aircraft velocity - 77 m/sec)	-18.9 dB
$1/h^2$ (aircraft altitudes - 457 m)	-53.2 dB
$1/L_m$ (coaxial cable loss)	-8.4 dB
D_T^2 (duty cycle - 0.0567)	-24.9 dB
Received signal power density	-131.9 dBm/Hz
KT	-174 dBm/Hz
Receiver noise figure (F)	5.4 dB
Receiver gated on duty cycle (D_R)	-4.5 dB
Receiver noise power density	-173.1 dBm/Hz
Signal-to-noise ratio	41.2 dB

2.6 DATA PROCESSING

The output of the scatterometer is recorded by a Mincom Series 110 Recorder/Reproducer System, Wideband Group I.[1] The specifications of the recorder for the three scatterometers can be found in reference 6. The channel number assignments for various data output of the scatterometers are shown in figure 2-10. The 0.4-GHz scatterometer outputs are recorded on five adjacent data channels (4, 6, 10, 12, and 14) of the same tape.

The data-taking time is recorded through the IRIG Standard Time Code and the Aircraft Data Acquisitions System (ADAS) in channels 9 and 2, respectively. In addition to the time information, ADAS acquires the aircraft parameters such as altitude, speed, roll, pitch, and drift angles.

The time and aircraft parameters provided by ADAS are recorded sequentially in pulse code modulation (PCM) format and frequency modulated at 225 KHz. All of this information is derived during data reduction and is used in data processing for the derivation of σ° as shown in figure 2-11.

Figure 2-11 is a brief data processing block diagram of the Texas A&M University software processor which processes the three scatterometer analog data tapes. In addition to the recorded

---

[1] This model is used for identification purposes only and does not constitute a recommendation.

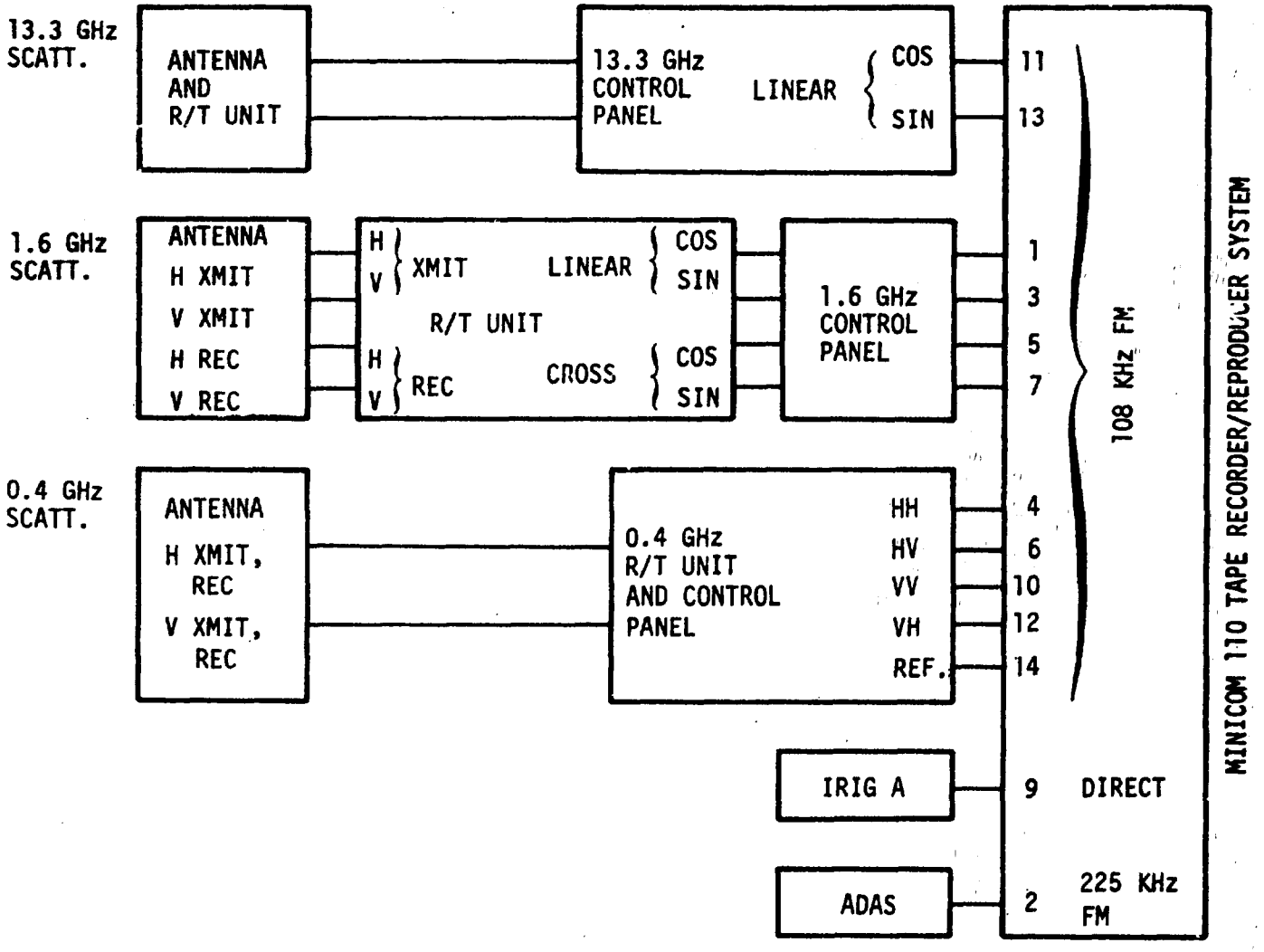

Figure 2-10.— Channel assignment of signal outputs for three scatterometers.

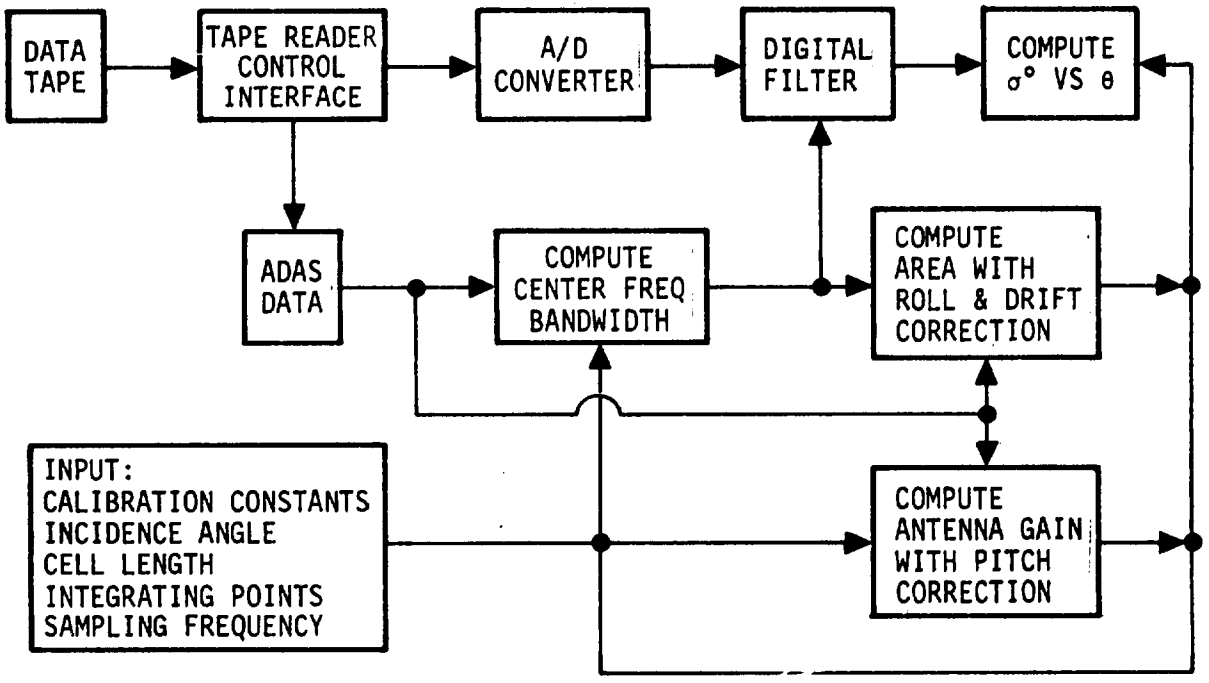

Figure 2-11.– Data processing block diagram.

signals and ADAS data in the tape, the system calibration constants, the resolution cell length, and the angle of incidence are required as inputs. Digital filtering is employed in the processor to obtain the signal spectrum at the required center frequency and bandwidth which corresponds to the specific incidence angle and area, respectively. At the same time, the computations of antenna gain and area, with pitch, roll and drift corrections, result in the computation of σ° versus θ_o. The output of σ° is tabulated with respect to incidence angle and flight time.

3. SYSTEM ANALYSIS

3.1 BACKSCATTERING COEFFICIENT ALGORITHMS

The power density $W_r(\theta)$ at the receiving antenna is given in equation (2-17). Expressed in terms of $\sigma^\circ(\theta)$, equation (2-17) becomes

$$\sigma^\circ(\theta) = \frac{2(4\pi)^3 Vh^2 W_r(\theta)}{\lambda^3 \cos\theta\, G^2(\theta) B_\phi P_t} \tag{3-1}$$

Since $W_r(\theta) = P_r(\theta)/\Delta f_D$, equation (3-1) can also be written as:

$$\sigma^\circ(\theta) = \frac{2(4\pi)^3 Vh^2 P_r(\theta)}{\lambda^3 \cos\theta\, G^2(\theta) B_\phi\, \Delta f_D P_t} \tag{3-2}$$

where Δf_D is related to the ground cell length $\Delta\rho_f$ in the following form (ref. 11).

$$\Delta f_D = \frac{2V \cos^3\theta}{\lambda h} \Delta\rho_f \tag{3-3}$$

Equation (3-2) is the simple, direct, and most used approach of determining σ° as a function of incidence angle, θ. As derived in the previous section, it associates a ground resolution cell, $A(\theta)$, with a single average value of $\sigma^\circ(\theta)$ (fig. 2-8) and then expresses $\sigma^\circ(\theta)$ in terms of all measurable parameters.

The σ° derived from this approach contains two sources of error, both resulting from the approximation of a rectangular area (fig. 2-9) for an actual Doppler cell defined by two iso-dopplers (fig. 2-8). The first source of error comes from the assignment of a single value of σ° for a given rectangular ground cell. Actually, σ° is observed to vary with incidence angle θ, and the contribution to the observed signal return within a given bandwidth, Δf_D, is the sum of the backscattered signals from all the small area elements with different θ_i's in the Doppler cell. The second source of error is the results of crudeness of the area approximation itself. Both of the error sources depend on the scatterometer antenna beam width. For the 0.4-GHz scatterometer, the antenna beam width, B_ϕ, varies from approximately 14° to 25° over the range of θ, from 0° to 60° (fig. 4-5). In this case, it is desirable to explore the amount of error introduced in the σ° derivation by using equation (3-2).

For deriving received power, P_r, without error-introduced approximation, refer to the radar equation

$$P_r = \frac{P_t G_t G_r \sigma \lambda^2}{(4\pi)^3 R^4} \qquad (3\text{-}4)$$

The radar cross section of the target σ is the integration of backscattering coefficient σ° through the differential area

element, dA, and is expressed as:

$$d\sigma = \sigma^{\circ} dA \tag{3-5}$$

In terms of equation (3-5), the radar equation becomes

$$P_r = \int_A \frac{P_t G_t G_r \sigma^{\circ} \lambda^2}{(4\pi)^3 R^4} dA \tag{3-6}$$

The power, $P_r(\Theta)$, observed at a given central Doppler frequency, $f_D(\Theta)$, and within a bandwidth, $\Delta f_D(\Theta)$, is uniquely related to a ground cell, A, as shown in figure 2-8. The integration in equation (3-6) is computed by numerical summation because only a discrete value of measured antenna gain pattern is available and the ground cell, A, is further divided into N elements. Equation (3-6) is then expressed as:

$$P_r(\theta) = \frac{P_t \lambda^2}{(4\pi)^3} \sum_{i=1}^{N} \frac{G_t(\theta_i) G_l(\theta_i) \sigma^{o}(\theta_i)}{R^4(\theta_i)} \Delta A_i \tag{3-7}$$

The power density, $W_r(\Theta)$, is simply

$$W_r(\theta) = \frac{P_r(\theta)}{\Delta f_D(\theta)} = \frac{P_t \lambda^2}{\Delta f_D(\theta)(4\pi)^3} \sum_{i=1}^{N} \frac{G_t(\theta_i) G_r(\theta_i) \sigma^{o}(\theta_i)}{R^4(\theta_i)} \Delta A_i \tag{3-8}$$

Examining equations (3-7) and (3-8), it is obvious that no explicit expression for $\sigma^\circ(\theta)$ is available for the exact derivation which makes equation (3-7) or (3-8) very difficult to use for data reduction purposes. But it can be used for comparison to evaluate the error induced in equations (3-1) or (3-2) when large antenna beam width and Doppler bandwidth are used.

To derive the backscattering coefficient, σ°, as a function of incidence angle, θ, from equation (3-8) requires an iteration process. First, a functional dependence of σ° on θ has to be assumed. Then the power density, $W_r(\theta)$, of the backscattered signal is calculated from equation (3-8) for a series of θ and $\Delta\theta$. The calculated $W_r(\theta)$ is compared with the power spectrum which is derived from the observations. If the computed and observed power spectra do not match well over the incidence angles of interest, another form of $\sigma^\circ(\theta)$ is assumed and the procedure is repeated. The final functional dependence of σ° on θ is attained when the best match between the computed and the observed power spectra is obtained.

Equations (3-1), (3-2), (3-7), and (3-8) apply to each of the four polarization combinations as described in section 2. Thus, P_r, P_t, G_r, and G_t can be in either the horizontal or the vertical polarization state. Depending on the polarization state of P_r (or G_r) and P_t (or G_t), four different backscattering coefficients can be derived from the operation of the scatterometer;

namely, σ°_{HH}, σ°_{VV}, σ°_{VH}, and σ°_{HV}. (The subscripts indicate the polarization state of P_r, P_t, G_r, G_t, and σ°, which are not explicitly written in the expression above.) The power received, P_r, is the power of the backscattered signal at the receiving antenna output port. As the signal passes through the receiver data channels, it experiences losses as well as gains because of the presence of many subsystems. These factors will have to be considered in order to correctly interpret the observed data.

Both approaches for the determination of σ° versus θ relationship [namely, the σ° values from equations (3-2) and (3-7)] are attempted in section 5, where the numerical calculation is performed. A comparison is made on the results from both approaches.

The backscattered signal in the receiver data channel and its continuous calibration technique is analyzed further, and the backscattering coefficient, σ°, is discussed in the following sections. The antenna gain pattern, side lobe level, and cross coupling effects are discussed in detail in section 4.

3.2 RECEIVER SIGNAL ANALYSIS – CALIBRATION CONSTANTS APPROACH

The desired data in equations (3-2) and (3-7) are the relationship between P_t and P_r. If this relationship is established at a common point in the system, then combined with antenna pattern, aircraft velocity, and aircraft altitude data, it is possible to obtain the desired backscattering coefficient. The antenna

gain data must be referenced to the common point selected in the system. In the 0.4-GHz scatterometer system, calibrate signals are generated, which serve as a reference in the receiver channel. These calibrate signals provide information in the recorded data which can be used to eliminate uncertainties which would otherwise be introduced because of transmitter output and receiver gain variations.

The various signals in the 0.4-GHz scatterometer system are indicated in figures 3-1 and 3-2. Figure 3-1 shows the relationship between the received signals and the calibration signals. As indicated, the desired relationship is the ratio of P_r to P_t. Referring to figure 3-2, the transmitted power, P_{TH} (at the horizontal antenna port), is equal to the peak transmitter power P_o less the attenuation through the antenna switch and the RF filter.

$$P_{TH} = K_{TH1}K_{TH2}P_o \tag{3-10}$$

A sample of the transmitted power $K_{T1}P_o$ is fed to the calibrate receiver through a directional coupler. The coupling is designated as K_{T2}. Thus, the transmitted power sample in the calibrate receiver has a value of $K_{T1}K_{T2}P_o$. The calibrate signal which is supplied to the calibrate receiver is designated C_c; the value at the front end of the calibrate receiver is $K_{cc}C_c$, where K_{cc} is the constant introduced by the insertion loss of the directional coupler.

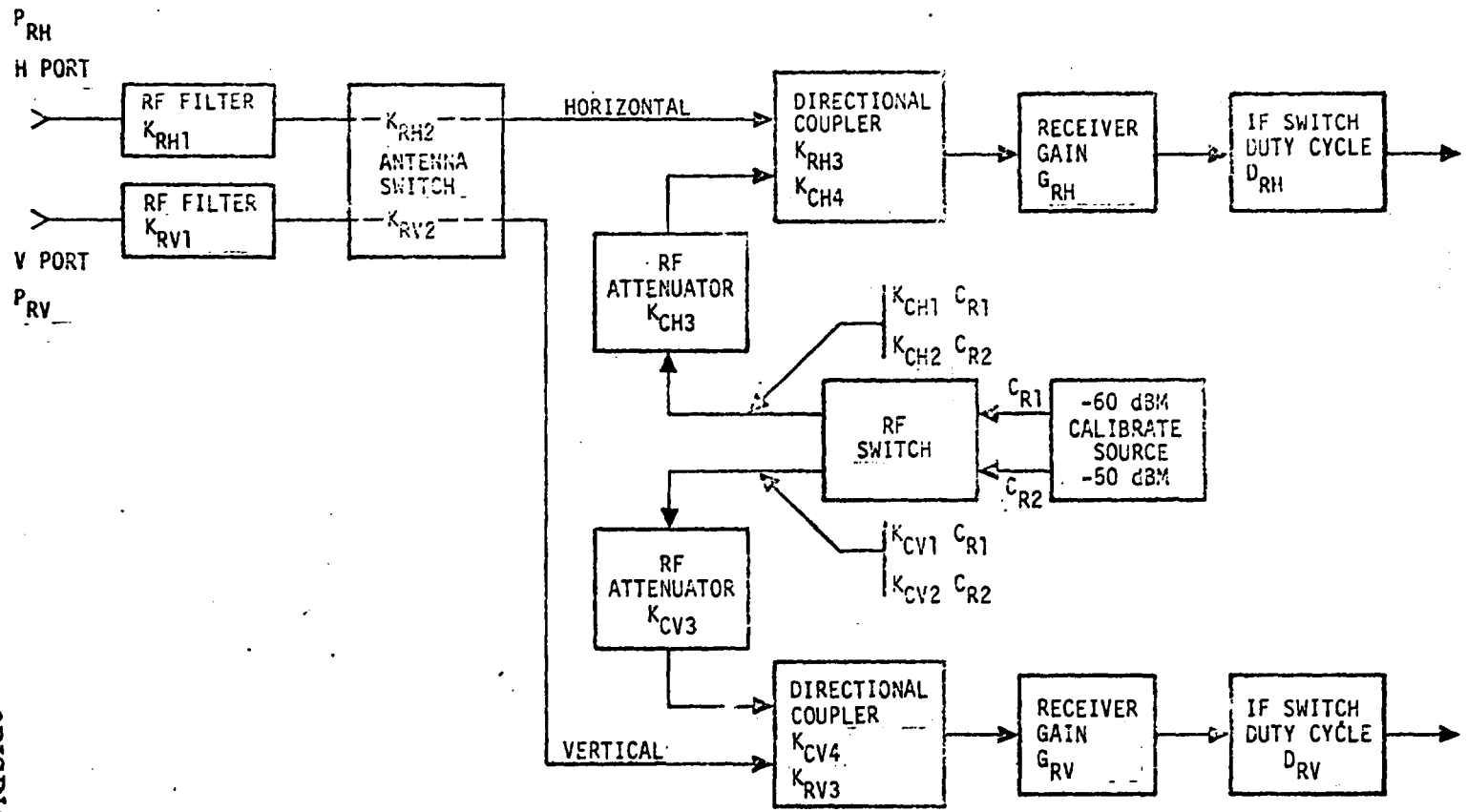

Figure 3-1.— Received signal calibration.

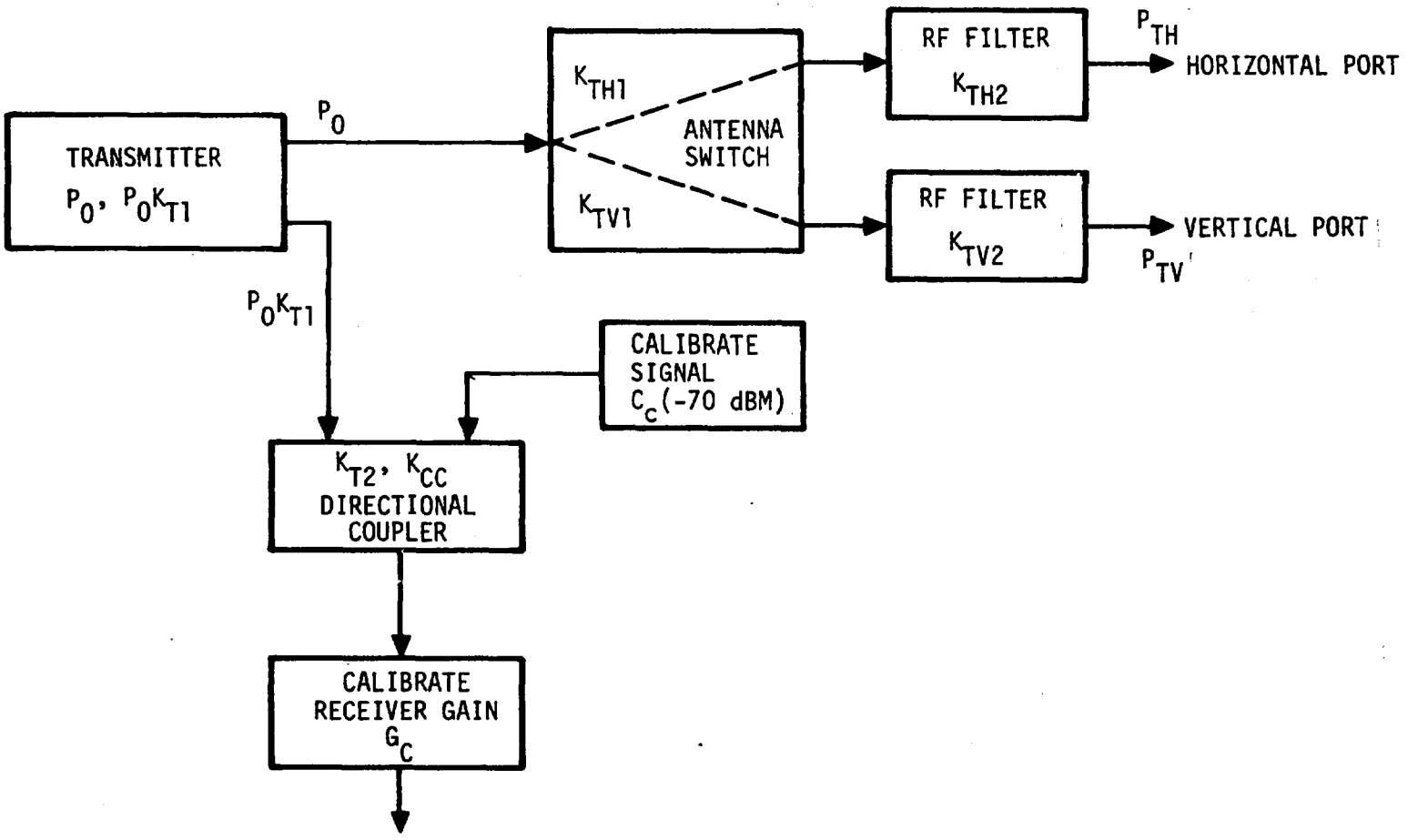

Figure 3-2.— Transmitted signal calibration.

The receivers used in the 0.4-GHz scatterometer pass only the central spectral line. Thus, the transmitter sample signal from the calibrate receiver is modified by the square of the transmitter duty cycle.

$$\text{Transmitter sample} = G_c K_{T2} K_{T1} D_T^2 P_o \qquad (3\text{-}10)$$

where G_c is the gain of the calibrate receiver, and D_t is the transmitter duty cycle. The calibrate signal from the calibrate receiver is equal to $G_c K_{cc} C_c$.

The received signal is processed in four separate receivers. Figure 3-1 shows the relationships between the received signals and the calibration signals in the receiver channels. The relationship of the horizontal receiver will be discussed here. Similar relationships are valid for all of the fixed-gate receivers.

The received signal, P_{RH}, is attenuated by the RF filter, the antenna switch, and the directional coupler. The received signal in the horizontal receiver is given by $K_{RH1} K_{RH2} K_{RH3} P_{RH}$. The calibrate and received signals from the horizontal receiver are:

$$\text{Calibrate signal} = G_{RH} K_{CH1} K_{CH3} K_{CH4} D_R^2 C_{R1} \qquad (3\text{-}11)$$

$$\text{Received signal} = G_{RH} K_{RH1} K_{RH2} K_{RH3} \left(\frac{D_T}{2}\right)^2 P_{RH} \qquad (3\text{-}12)$$

For equations (3-11) and (3-12), it is assumed that received signal eclipsing did not occur because of IF or LO switching. The duty cycle of the received signal in the fixed-gate channels is $\frac{1}{2}D_T^2$ since a particular receiver channel is active on alternate pulse intervals.

Figure 3-1 indicates that two calibrate signal levels are available to the horizontal receiver. These signals are alternately switched; one is used during the active time of the low-gain channel and the other is used during the active time of the high-gain channel.

The following relationship can now be established.

$$\frac{\text{Transmitter sample}}{\text{Calibrate signal}} = A = \frac{G_c K_{T2} K_{T1} D_T^2 P_o}{G_c K_{cc} C_c} \qquad (3\text{-}13)$$

The gain term cancels out and the relationship becomes

$$A = \frac{K_{T1} K_{T2} D_T^2 P_o}{K_{cc} C_c} \qquad (3\text{-}14)$$

For the horizontal receiver channel under consideration the relationship is:

$$\frac{\text{Received signal}}{\text{Calibrate signal}} = B = \frac{G_{RH} K_{RH1} K_{RH2} K_{RH3} \left(\frac{D_T}{2}\right)^2 P_{RH}}{G_{RH} C_{CH1} K_{CH3} K_{CH4} D_{RH}^2 C_{R1}} \qquad (3\text{-}15)$$

Removing the gain terms yield:

$$B = \frac{K_{RH1}K_{RH2}K_{RH3}D_T^2P_{RH}}{4K_{CH1}K_{CH3}K_{CH4}D_{RH}^2C_{R1}} \tag{3-16}$$

The values of A and B are measured quantities available from the recorded data.

The relationships given in equations (3-14), (3-16), and (3-9) can be combined to give:

$$\frac{P_{RH}}{P_{TH}} = \frac{\left(\frac{4K_{CH1}K_{CH3}K_{CH4}D_{RH}^2C_{R1}}{K_{RH1}K_{RH2}K_{RH3}}\right)B}{\left(\frac{K_{CC}K_{TH1}K_{TH2}}{K_{T1}K_{T2}}\right)C_cA} \tag{3-17}$$

Let

$$\left(\frac{4K_{CH1}K_{CH3}K_{CH4}}{K_{RH1}K_{RH2}K_{RH3}}\right) = K_{1HH}$$

$$\left(\frac{K_{CC}K_{TH1}K_{TH2}}{K_{T1}K_{T2}}\right) = K_{2HH} \tag{3-18}$$

$$\frac{C_{R1}}{C_c} = K_{3HH}$$

Then

$$\frac{P_{RH}}{P_{TH}} = \left(\frac{K_{1HH} \cdot K_{3HH}}{K_{2HH}}\right) D_R^2 \cdot \frac{B}{A} \tag{3-19}$$

Each receiver has a value for K_1, K_2, and K_3. D_R is established for each receiver and is a function of mode and range of operation.

The calibration constants are determined by measuring the individual components to establish values for K_1 and K_2. The value for K_3 requires a direct measurement of the power levels of C_{R1} and C_c, which are fixed power levels for all operating conditions. The quantity D_R, which is variable with the mode and range of operation, is established by measuring the calibrate signal level. In these measurements, the AGC is inoperative so that the receiver gain does not vary from measurement to measurement.

The system calibration constants are expressed by:

$$K_{HH} = \left(\frac{K_{1HH}K_{3HH}}{K_{2HH}}\right) D_R^2 \qquad (3\text{-}20)$$

When K_1, K_2, K_3, and D_R are obtained by direct measurement, the values of the calibration constants (K) can be computed from equation (3-20). The values are listed in table 3-1 for different polarizations, gain settings, and modes of operation.

The calibration constants listed in table 3-1 are the most recent data which reflect the changes introduced by the replace-

ment of parts and the addition of attenuators in the calibrate source. The values originally given by the Emerson Electric Company (ref. 8) were corrected by -22.7 dB for linear channels and -24.5 dB for cross channels. Corrections were made because of the installations of spare transmitter coupler and the output power divider of the calibrate channel with 20 dB pads added. Linear C_{R2}/C_C was +22.7 dB and then dropped to +3.8 dB. Cross C_{R1}/C_C was +11.62 dB and then dropped to -9.1 dB. The two-way antenna coaxial cable loss (L_s) of 8.4 dB was also measured in Building 15 of JSC.

The calibration channel coding is shown in table 3-2. From the frequency spectrum given in the calibrate channel, the values of the calibrate signal and the transmitter sample can be obtained along with the receiver gain position and the mode of operation. The calibration constants can be selected from table 3-1 when the receiver gain position and the mode of operation are known.

3.3 MEASURED SYSTEM PARAMETERS

After establishing the ratio of P_r to P_t by using the calibration constant for a specific polarization state, the gain setting of the receiver, and the measured antenna cable loss L_s, it is now possible to put all the parameters together and derive the final forms of the backscattering coefficient algorithms. The expression for equation (3-2) becomes

TABLE 3-1.– CALIBRATION CONSTANTS

[Values in negative dB]

Manual (1-5) mode, fixed gate

Channel	Gain position					
	1	2	3	4	5	6
VV	112.5	123.0	132.8	142.3	152.3	162.5
HH	112.8	122.8	132.8	142.7	152.1	161.8
VH	125.7	135.7	145.7	155.6	165.0	174.7
HV	125.4	135.9	145.7	155.2	165.2	175.4

TABLE 3-2.– CALIBRATION CHANNEL CODING

Mode	Code frequency, Hz
Manual (1-5)	403
Manual (4-20)	414
Horizontal receiver gain position	
1	514
2	531
3	547
4	564
5	581
6	597
Vertical receiver gain position	
1	666
2	689
3	711
4	733
5	754
6	776
Transmitter sample	500
Calibrate signal	1000

$$\sigma^{o}(\theta) = \frac{2(4\pi)^3 Vh^2 K(B/A)}{\lambda^3 \cos\theta\, G^2(\theta) B_\phi\, \Delta f_D L_s} \qquad (3\text{-}21)$$

where

B = the ratio of received signal to calibrate signal in the receiving channel

A = the ratio of transmitter sample to calibrate signal in the calibrate receiver

L_s = two-way antenna coaxial cable loss (-8.4 dB)

K = calibration constant for specific receiving polarizations and gain settings

The other parameters in the equation have been described previously. Similarly, the expression for equation (3-7) becomes

$$\frac{(B/A)}{\Delta f_D} = \frac{L_s\, \lambda^2}{K\, \Delta f_D (4\pi)^3} \sum_{i=1}^{N} \frac{G_t(\theta_i) G_r(\theta_i) \sigma^{o}(\theta_i)}{R^4(\theta_i)} \Delta A_i \qquad (3\text{-}22)$$

Note that in equation (3-22) the ratio of B over A is the relative receiver output power with respect to the transmitter sample power in the Doppler frequency band (Δf_D), which corresponds to the signal return from the ground cell defined by two isodopplers ($f_D + \frac{1}{2}\Delta f_D$ and $f_D - \frac{1}{2}\Delta f_D$) for a specific angle of incidence (θ) which generates f_D.

The values of K and L_s could change for different missions. The calibration constant K controls the power level of the calibrate signal, which is subject to the limitation of the dynamic range of the tape recorder. For a given surface of backscattering and aircraft altitude, K could be adjusted for an appropriate calibrate signal level using different values of attenuation pad to bring about the best signal-to-noise ratio for the data. The value of L_s depends on the length of the cables between the transmitter/receiver unit and the antenna, which can be changed from mission to mission. The values of K and L_s, measured for the functional check flight of Mission 347 will be used for the numerical calculations in section 5.

3.4 RESOLUTION CELL LENGTH REQUIREMENT

In the software processing algorithm, the resolution cell length L is assumed constant over all incidence angles and is expressed by:

$$L = \Delta\rho_f + \Delta\rho_t \tag{3-23}$$

where $\Delta\rho_f$ is the resolution length corresponding to the Doppler frequency bandwidth Δf_D as given in equation (3-3), and $\Delta\rho_t$ is the resolution length corresponding to the integration time.

$$\Delta\rho_t = \frac{V \times p_s}{f_s} \tag{3-24}$$

In equation (3-24), f_s is the sampling frequency of the digitizer, and P_s is the number of sample points for one cell as used in the program. For constant L and $\Delta\rho_t$, $\Delta\rho_f$ will be the same for all incidence angles; and from equation (3-3), it is easily seen that Doppler bandwidth Δf_D will decrease rapidly as the incidence angle increased from 0 to a larger value, say 60°.

Because scatterometers are, by definition, calibrated devices used in determining scattering information on an absolute scale, fading poses particular problems. Fading is caused by the constructive and destructive interference of the coherent signal components reflected by individual scatterers within a resolution cell. Making a single, instantaneous measurement of scattered power will introduce errors since there are no means by which we can determine how much fading is taking place. Thus, it is necessary to make a number of measurements which can be averaged to reduce fading effects. The signal must be observed long enough so that sufficient independent samples may be collected when averaging over a time period or spatial distance to reduce fading effects and thereby obtain meaningful values of $\sigma°$. Independent samples may arise from two causes: (1) independence within the Doppler bandwidth while illuminating a ground path from different angles and (2) a combination of return signals measured from completely separate ground patches. The number of independent samples occurring during the time the scatterometer passes a resolution cell length of L and a Doppler bandwidth of Δf_D is given (ref. 11) by:

$$N_i = \frac{L}{V} \Delta f_D = \frac{2L \Delta\rho_f \cos^3 \theta}{\lambda h} \qquad (3\text{-}25)$$

The relative standard deviation of the scattering coefficient is expressed by:

$$\frac{\sigma}{\mu} = \frac{1}{\sqrt{N_i}} = \left(\frac{\lambda h}{2L \Delta\rho_f \cos^3 \theta} \right)^{1/2} \qquad (2\text{-}26)$$

Because of the long wavelength of 75 centimeters (29.5 inches) of the 0.4-GHz scatterometer, a tradeoff must be made between a large Doppler bandwidth, which improves the data accuracy, and a small ground cell, which improves the length resolution of the data. Table 3-3 gives the number of independent samples and the standard deviation values for the 75-meter (246-foot) cell length, the 2500-Hz sample frequency, 1024 sample points, 77-meter (252.5 feet) per second aircraft ground speed, and 442 meters (1450 feet) altitude. Also included in the table are the center frequency and the Doppler bandwidth at incidence angles ranging from 0° to 60°.

There are less than 10 independent samples in the resolution cell when the incidence angle becomes larger than 40°. To attain more independent samples and thereby increase the accuracy, the cell length must be increased, especially at large incidence angles.

TABLE 3-3.— INDEPENDENT SAMPLE AND STANDARD DEVIATION FOR CONSTANT CELL LENGTH OF 75 METERS (246 FEET)

Incident angle, θ	Central Doppler frequency, f_D	Doppler frequency bandwidth, Δf_D	No. of individual sample, N_i	Standard deviation, σ/μ
5	17.9	20.0	19.4	0.227
10	35.7	19.3	18.7	.231
15	53.2	18.2	17.7	.238
20	70.3	16.8	16.3	.248
30	102.8	13.1	12.7	.280
40	132.2	9.1	8.8	.330
50	157.5	5.4	5.2	.438
60	178.1	2.5	2.5	.638

3.5 THE FUNCTIONAL DEPENDENCE OF P-BAND σ° ON θ

The ordinary approach of deriving the backscattering coefficient σ° by means of a Doppler shift frequency in the received signal frequency spectrum, such as the 0.4-GHz scatterometer, is to use the backscattering coefficient algorithm given by equation (3-21). The crosstrack dimension of a resolution cell is determined by the half-power beam width B_ϕ of the antenna, and the alongtrack dimension of a resolution cell is determined by the bandwidth Δf_D of a filter, centered at the Doppler frequency f_D, which corresponds to a selected angle of incidence. It was pointed out previously that as B_ϕ and Δf_D become larger, (especially when B_ϕ is too large to ignore for the 0.4-GHz scatterometer), a significant amount of error may be introduced in the derivation of σ°. To explore the amount of error introduced and to present an adequate standard for comparison, equation (3-22) is presented as the second form of the backscattering coefficient algorithm.

The derivation of σ° in equation (3-22) required an assumed functional dependence of σ° on θ. To see how the shape of the σ° versus θ curve affects the error in σ° estimation in equation (3-21), the measured values of σ° from both smooth and rough surfaces of backscattering are considered. For the smooth surface, the measurements by Guinard (ref. 12) at 0.428-GHz and for the HH polarization over a calm sea are adopted. For the rough surface, data presented by Dickey (ref. 13) at 0.4-GHz and for the HH polarization are used.

The results from both of these measurements are shown in figure 3-3. Roughness data are not available for the terrain measurement as presented by Dickey (ref. 13). However, it is not important in the present case where the primary interest is to have the functional forms of σ° dependence on θ for the numerical calculations of equation (3-22).

A quadratic regression was performed on the data from the measurements over the calm sea. The result is given by:

$$\sigma^\circ = 5.71 \times 10^{-3}\theta^2 - 0.971\theta - 2.85 \qquad (3\text{-}27)$$

The land measurements data (ref. 13) covered dry and irrigated conditions, with averaging over the entire test site. The result of the dry field data curve, with second-order polynomial approximation and smoothing, is expressed by

$$\sigma^\circ = 8.44 \times 10^{-3}\theta^2 - 1.01\theta + 9.85 \qquad (3\text{-}28)$$

In both equations (3-27) and (3-28), the unit of σ° is in dB and θ degree. Both of these expressions are used in the numerical calculations in section 5.2, where the two forms of the backscattering coefficient algorithms are compared.

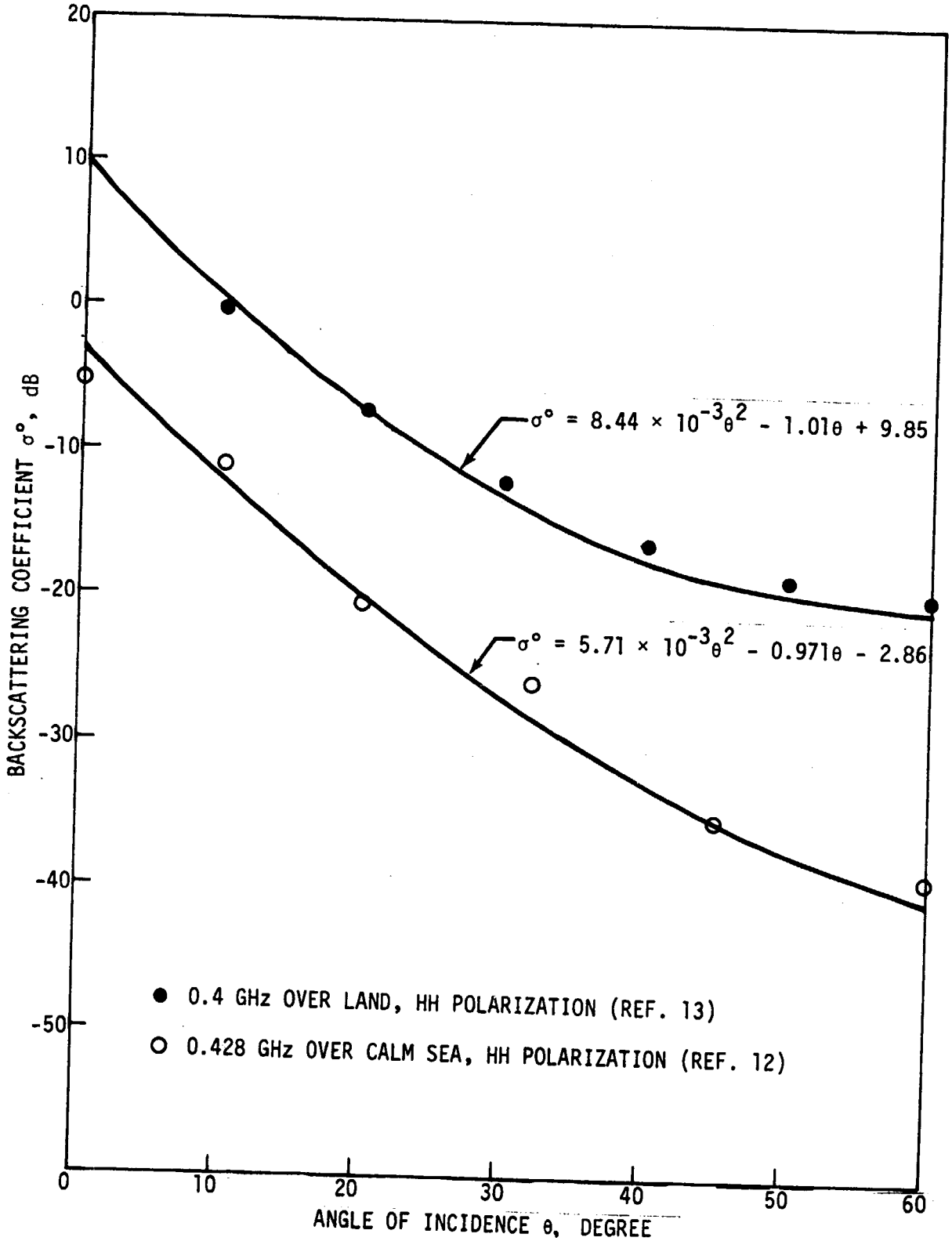

Figure 3-3.— The functional dependence of σ° on θ.

4. ANTENNA PATTERNS

4.1 MAIN LOBE

The antenna pattern data, both horizontal and vertical, were measured by the Physical Science Laboratory of New Mexico State University for every 2° interval in both the alongtrack and the crosstrack directions. The measurements were made with a set of two identical antennas without using a mockup to simulate the actual antenna system which is mounted on the C-130 aircraft. Consequently, the antenna pattern used in the present analysis might deviate from the real ones. The effects resulting from this deviation on the measurements of the backscattering coefficient σ° is not known. Calibration of the airborne system against the ground-based system may be necessary in order to determine the seriousness of this effect.

Since each of the horizontal and vertical antenna is used for the transmission and reception of the RF powers, the same antenna pattern is generated for the transmitting and receiving modes of operation. The horizontally transmitted and vertically received antenna pattern (two-way HV polarization) will be the same as the vertically transmitted and horizontally received antenna pattern (two-way VH polarization). Two-way gain of the HH and VV polarizations is the one-way gain of the corresponding horizontal and vertical antenna multiplied by two in dB. To see the spatial variations of the antenna patterns, the contour maps of

the two-way gain of HH, VV, and HV (or VH) polarizations are displaced in figures 4-1, 4-2, and 4-3, respectively. Each of the three maps covers the angular ranges of ϕ from -40° to 40° and of θ from 0° to 60°. The direction of nadir is located at $\theta = 0$ and $\phi = 0$. From these figures, it is clear that the RF powers of transmission and reception are mostly limited for ϕ in the region -40° to 40° (although the side-lobe level appears rather high at $\phi \simeq \pm 30°$) and for θ from 0° to 90°. The pattern for all polarizations (figs. 4-1, 4-2, and 4-3) displays an increase in gain with incidence angle and a rather high side lobe around nadir.

The variations of the alongtrack, two-way gains with the angles of incidence in the aft direction for all three polarizations are shown in figure 4-4. It is clear that the maximum of the two-way gains for HH and VV polarizations appears at $\theta = 66°$ and $\theta = 44°$, respectively. On the other hand, the maximum of the two-way gains for HV (or VH) polarization appears at $\theta \simeq 52°$ which is about half way between the maximum of HH and VV polarizations.

From equations (3-2), it is observed that the backscattered power, P_r, is proportional to $G^2(\theta)$, $\sigma°$, and R^{-4}. Since both $\sigma°$ and R^{-4} generally decrease with increasing θ, P_r would be small at large angles of incidence. For VV polarization, the decrease in the two-way antenna gain $G^2(\theta)$ for $\theta > 44°$ further depressed

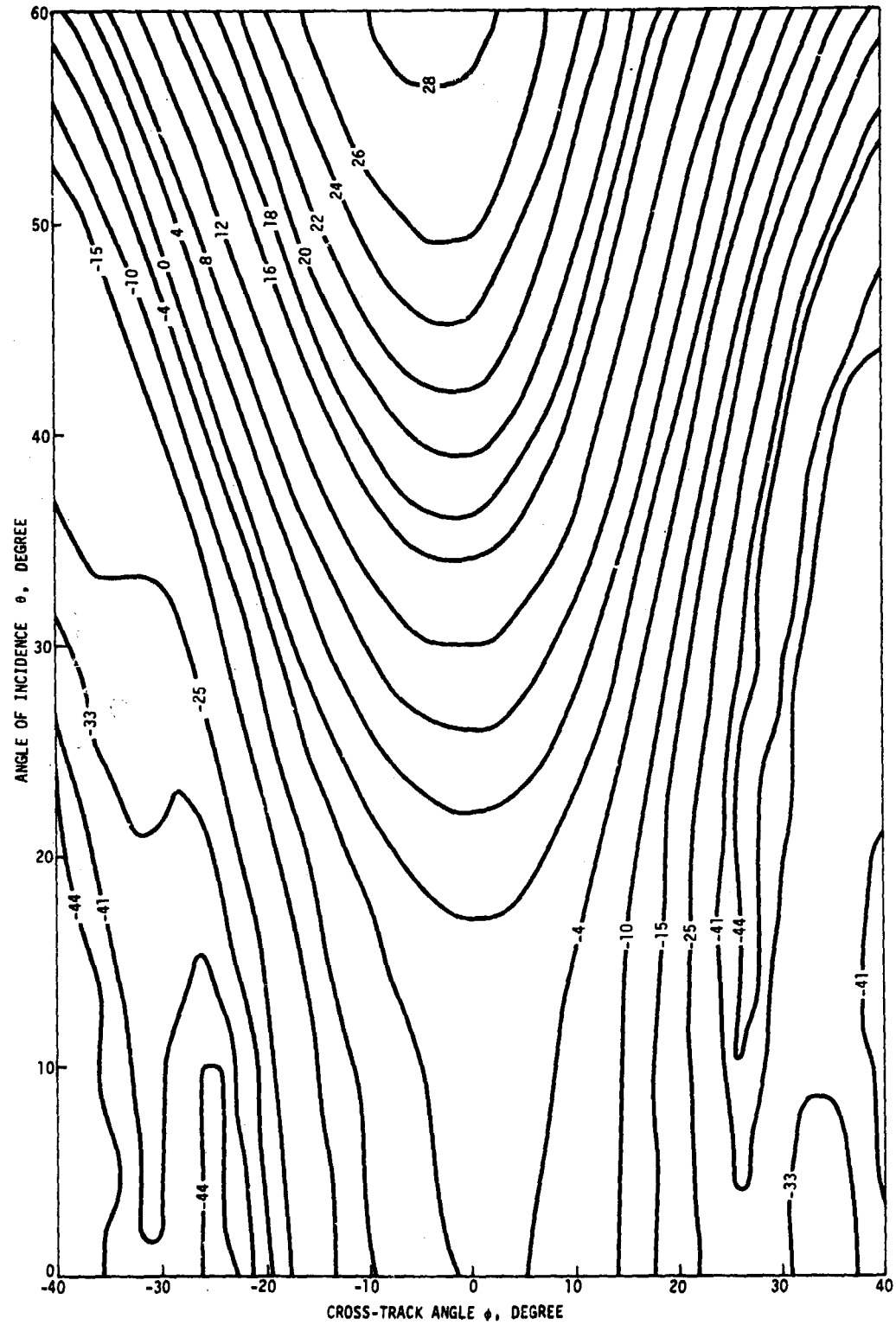

Figure 4-1.– The two-way gain contour of HH polarization.

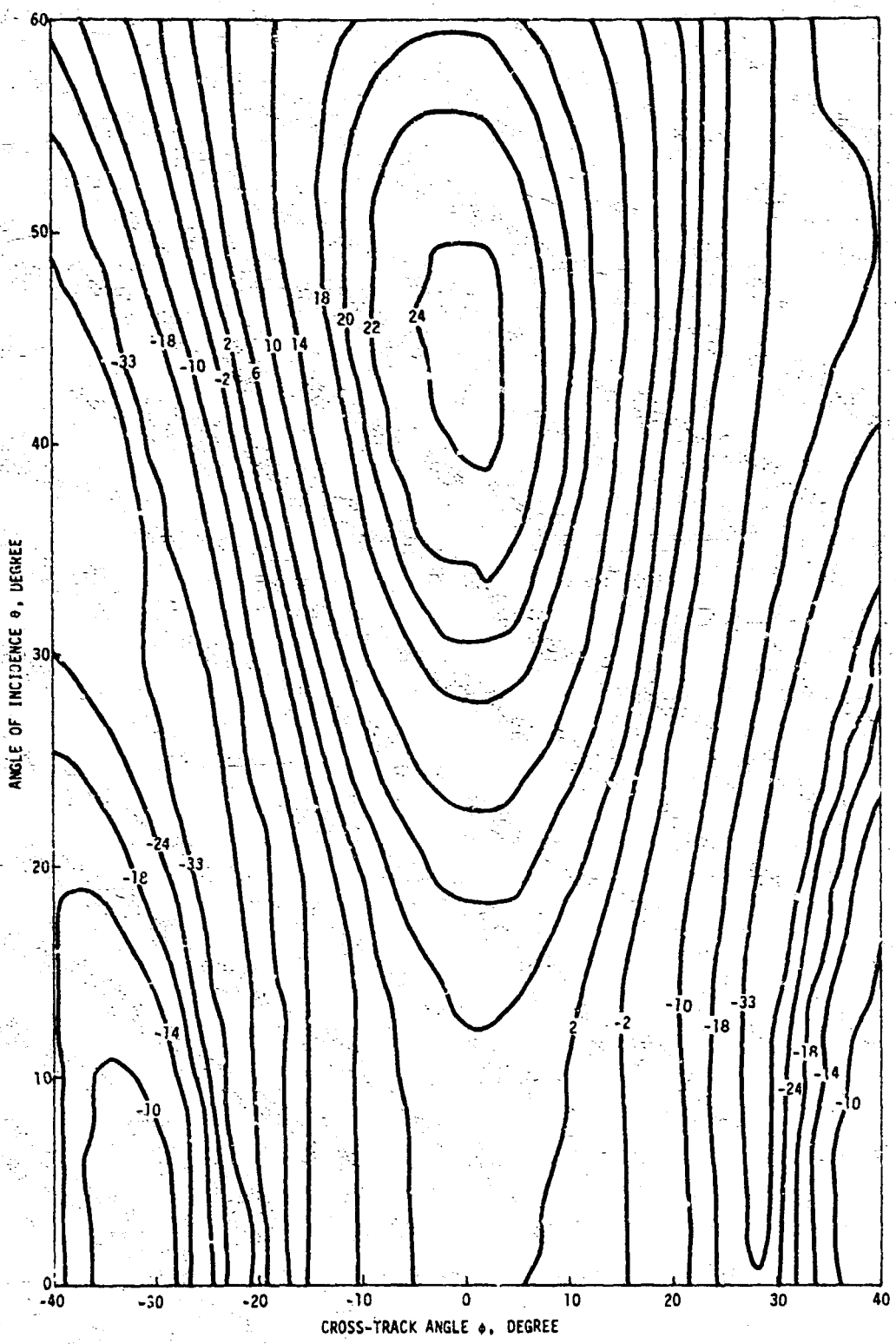

Figure 4-2.— The two-way gain contour of VV polarization.

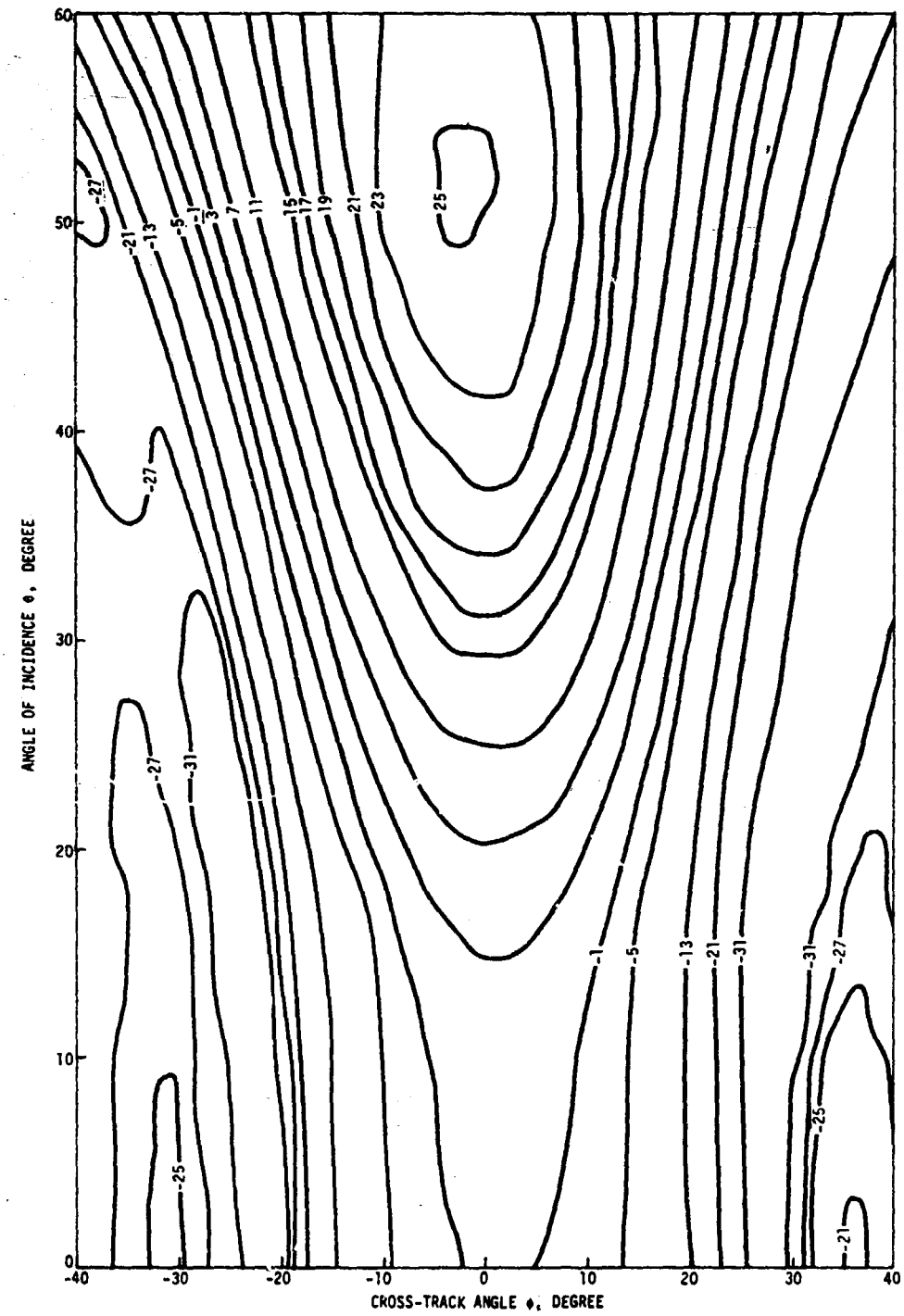

Figure 4-3.— The two-way gain contour of HV (or VH) polarization.

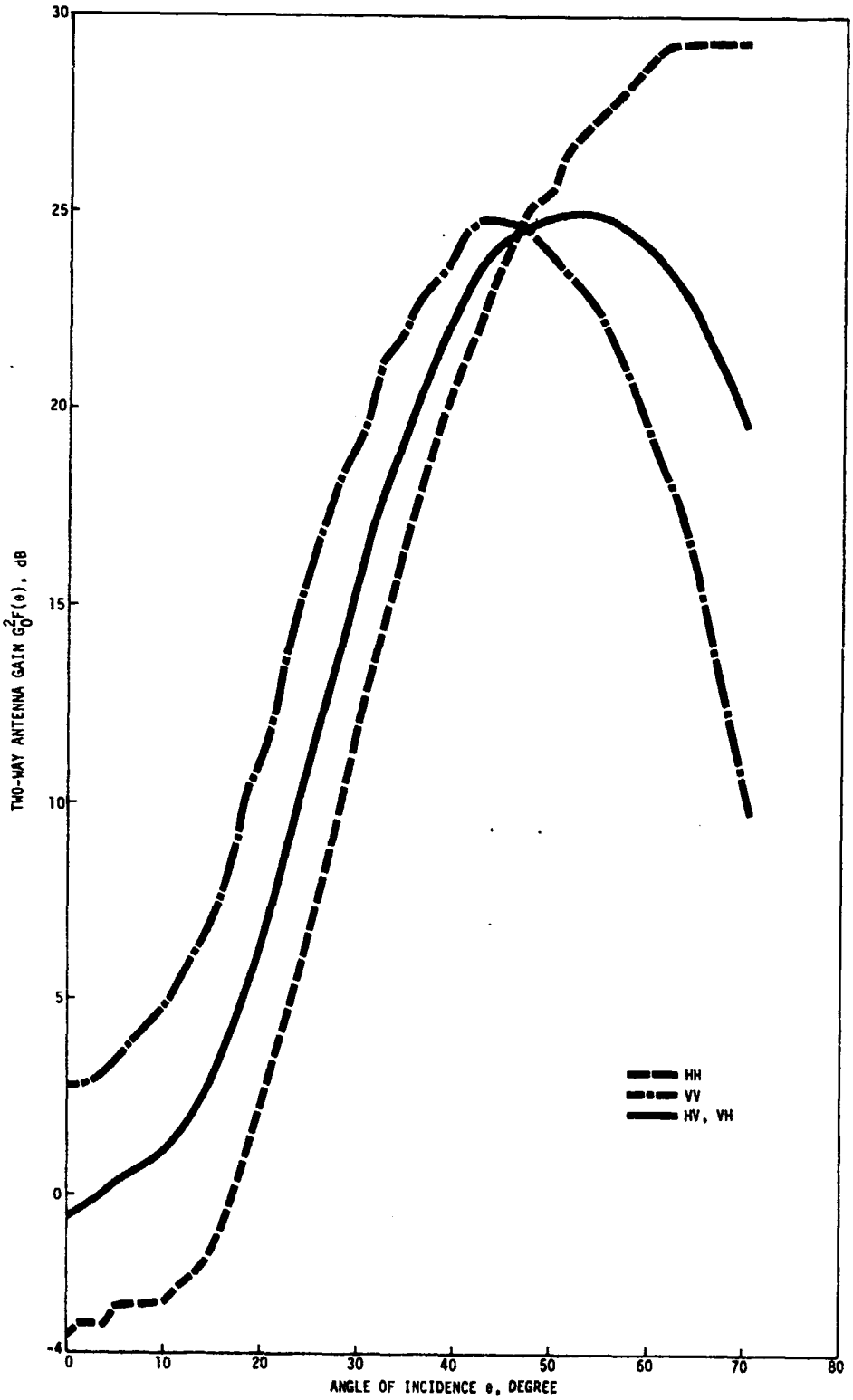

Figure 4-4.— The variation of two-way antenna gains with angle of incidence.

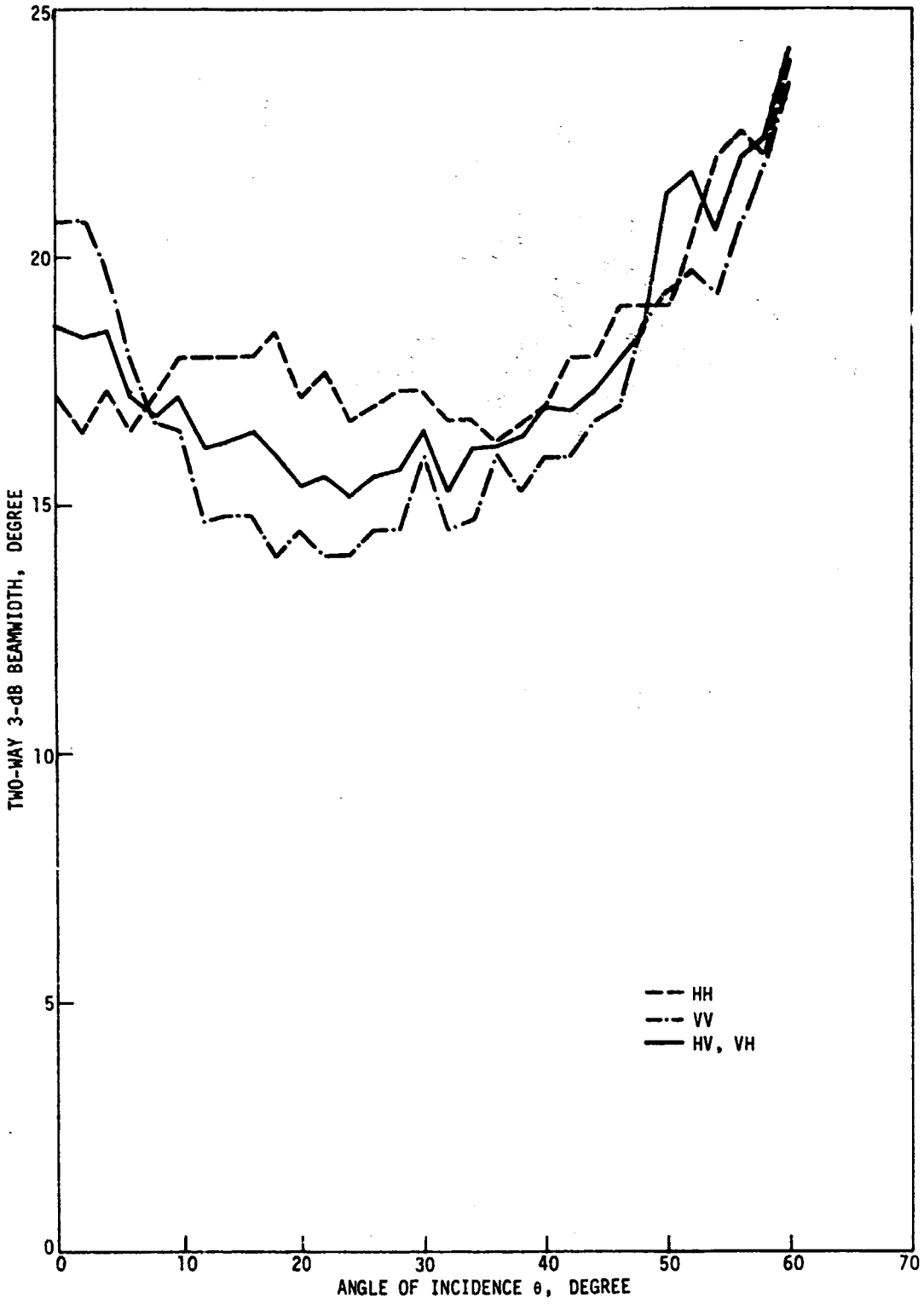

Figure 4-5.— The variation of the 3-dB beam width with angle of incidence.

is the results of the existence of the rather high side-lobe level in this region which generates the pattern broadening effect (figs. 4-6 and 4-7). As expected for HV (or VH) polarization, the variation of the antenna beam width, with respect to the incidence angle, stays half way between HH and VV polarizations. In general, the beam width variation for VV polarization is from 14° to 24°; for HH polarization, it is from 17° to 24°. From this, it can be stated that VV polarization has better cross-track resolutions in the region of θ from 12° to 35°.

The second method of defining a beam width is given by:

$$B_\phi = \frac{\int_{\phi_1}^{\phi_2} G_0^2 F(\theta)\, f\ (\theta,\phi) d\phi}{G_0^2 F(\theta)} \qquad (4\text{-}1)$$

where ϕ_1 and ϕ_2 are the crosstrack angles where the null points of the main-lobe antenna gain occur. The function $f(\theta,\phi)$ defines the crosstrack gain variation and $G_o^2 F(\theta)$, which is expressed in numerical value and not in dB and has the same meaning as before. The results of the calculations based on equation (4-1) are tabulated in table 4-1 for incidence angles ranging from 0° to 60° at 2° intervals. The corresponding 3-dB beam widths are also included in the table for comparison. It is clear from the table that for all angles of incidence and all polarizations the values of the beam width as derived from equation (4-1) are larger than the corresponding ones obtained from the 3-dB method. On

TABLE 4.1– COMPUTED TWO-WAY ANTENNA BEAM WIDTH IN DEGREE

Incidence angle Θ, degree	Method 1			Method 2		
	HH	VV	HV,VH	HH	VV	HV,VH
0	17.2	20.7	18.6	17.8	22.4	19.3
2	16.5	20.7	18.4	17.7	22.0	19.6
4	17.3	19.8	18.5	18.4	21.6	19.3
6	16.5	18.0	17.2	17.7	20.1	17.9
8	17.2	16.7	16.8	18.0	19.0	17.8
10	18.0	16.5	17.2	18.7	18.3	18.2
12	18.0	14.7	16.2	19.1	17.3	17.5
14	18.0	14.8	16.3	19.0	16.3	17.4
16	18.0	14.8	16.5	18.9	16.1	17.2
18	18.5	14.0	16.0	18.8	15.9	16.9
20	17.2	14.5	15.4	18.1	15.6	16.3
22	17.7	14.0	15.6	18.6	15.3	16.6
24	16.7	14.0	15.2	18.4	15.0	16.5
26	17.0	14.5	15.6	17.9	15.4	16.3
28	17.3	14.5	15.7	18.3	16.2	16.7
30	17.3	16.0	16.5	18.3	17.1	18.4
32	16.7	14.5	15.3	17.9	15.8	16.4
34	16.7	14.7	16.2	18.0	16.4	17.1
36	16.3	16.0	16.2	17.7	17.6	17.5
38	16.7	15.3	16.4	17.4	17.0	17.5
40	17.0	16.0	17.0	17.8	16.6	17.1
42	18.0	16.0	16.9	19.7	17.0	18.0
44	18.0	16.7	17.3	19.0	17.6	18.2
46	19.0	17.0	17.9	19.7	18.4	18.8
48	19.0	18.7	18.5	20.0	19.6	19.5
50	19.0	19.3	21.3	20.2	20.8	20.4
52	20.3	19.7	21.7	22.1	21.0	21.5
54	22.0	19.3	20.5	23.1	21.2	22.0
56	22.5	20.7	22.0	24.3	22.6	23.4
58	22.0	22.0	22.4	23.2	23.8	23.2
60	24.0	23.3	24.2	25.5	25.0	25.2

the average, the difference in beam width, calculated by the two methods, is approximately 1.5°.

The antenna beam width, as defined by equation (4-1), has been used for sensitivity calculation and will be used in the numerical calculations discussed in section 5.

4.2 SIDE LOBES

From figures 4-1, 4-2, and 4-3, it appears that the contribution of the power returned from the side lobes is not significant compared to that returned from the main lobe for $\theta > 20°$, but might be significant for $\theta < 20°$. To carefully examine the relative levels of the main and side lobes, the two-way gains at incidence angles 0° and 10° are plotted as a function of the crosstrack angle ϕ in figures 4-6 and 4-7 for HH and VV polarizations. For VV polarization, the first side lobe levels are approximately 11 dB and 14 dB down from the main lobe at $\theta = 0°$ and $\theta = 10°$, respectively. On the other hand, the HH polarization first side lobe levels are approximately 27 dB and 32 dB down from the main lobe at $\theta = 0°$ and $\theta = 10°$, respectively. It is also clear that the size of the first side lobe for HH polarization is much smaller than for VV polarization. Therefore, it is expected that there are more side lobe contributions from VV polarization than from HH polarization. The gain of each of the remaining side lobes is comparable to that of the first side lobe in each of the two polarizations. In general, the side lobe gains become

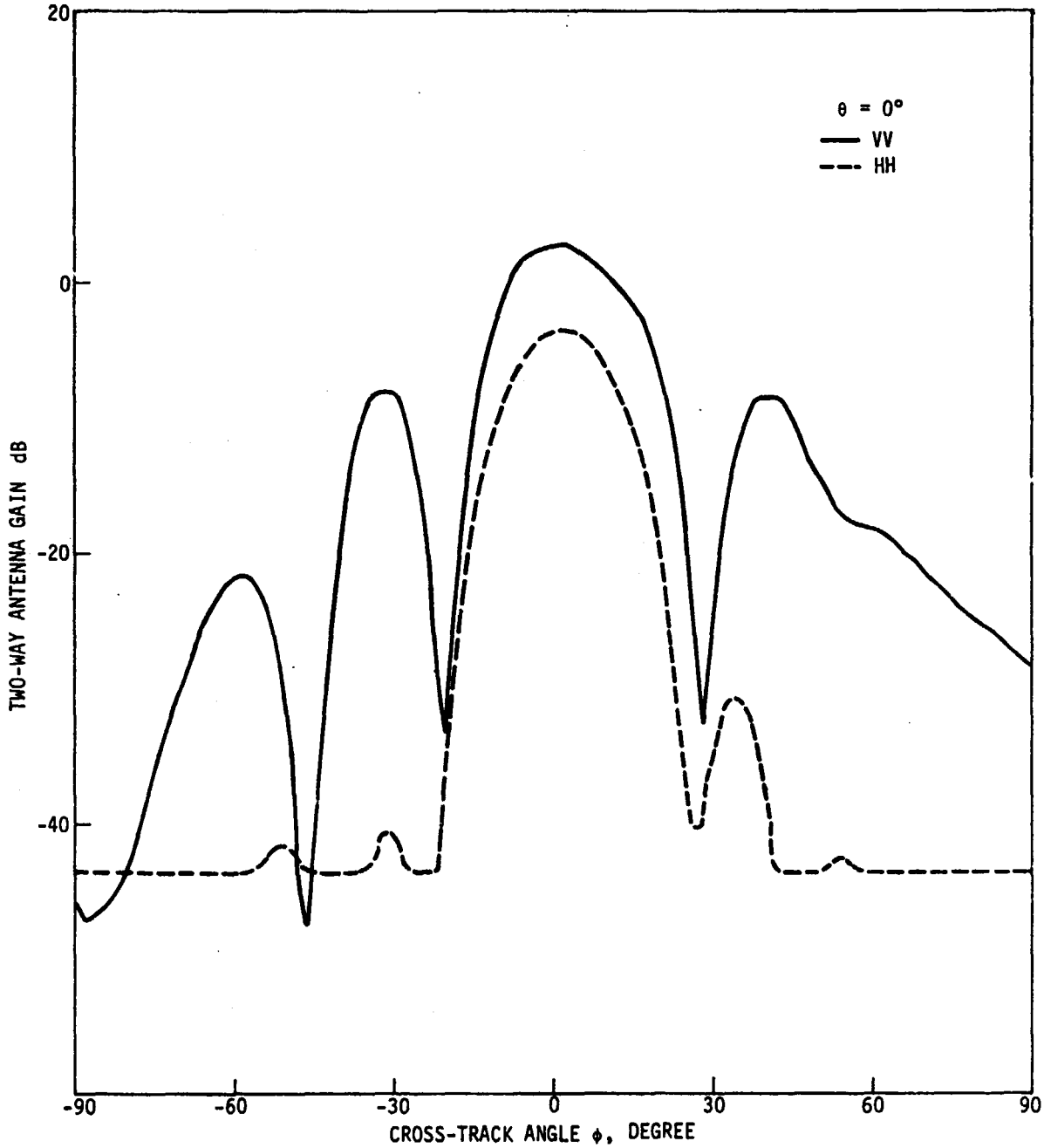

Figure 4-6.— The variation of the two-way antenna gains with crosstrack angles.

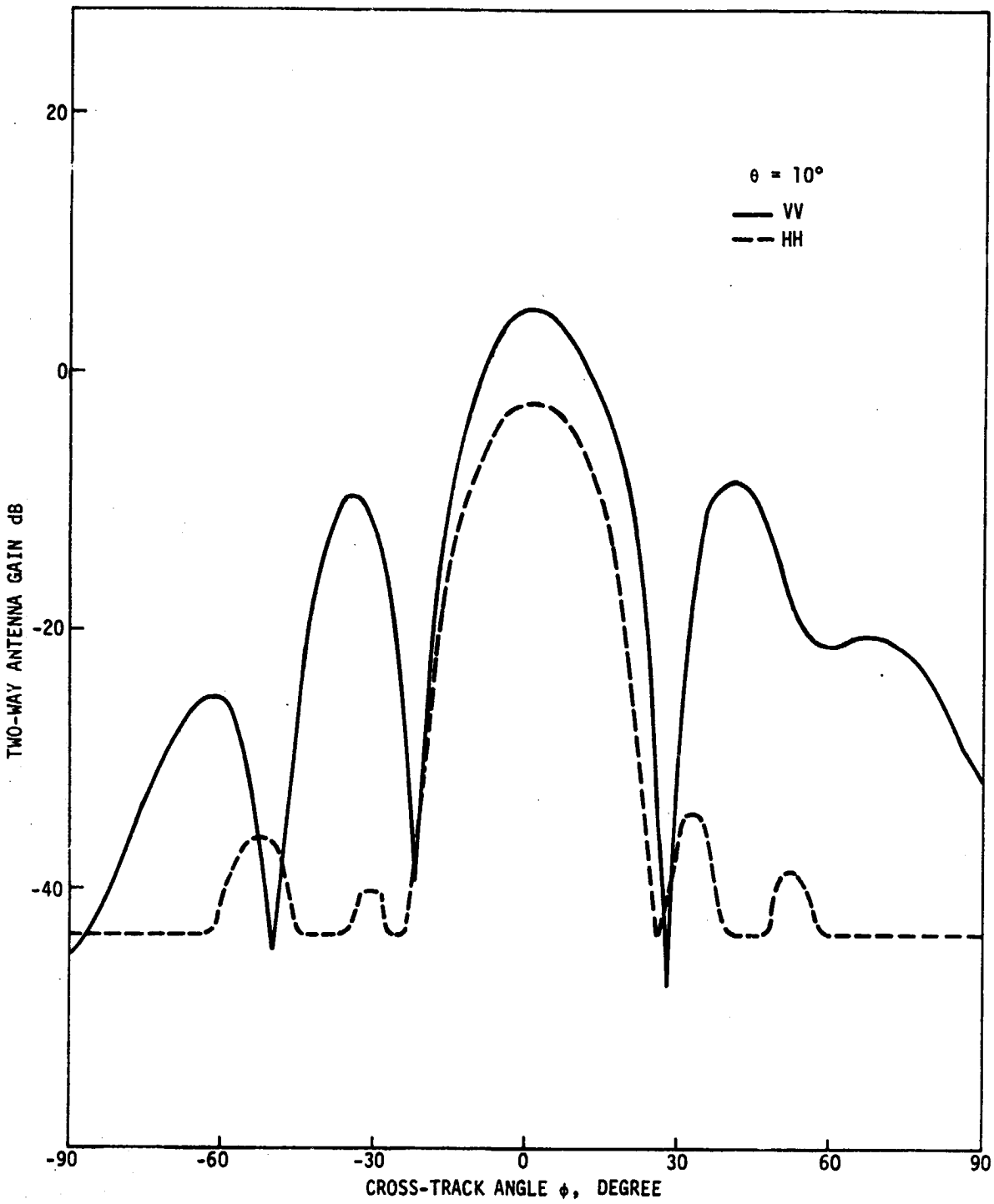

Figure 4-7.— The variation of the two-way antenna gains with crosstrack angles.

progressively smaller as $|\phi|$ increases. For the estimation of the side lobe effect, it is desirable to obtain the total contribution from all of the side lobes.

The derivation of the backscattering coefficient σ° normally includes the ground cell associated only with the main lobe antenna pattern. However, the power return at the scatterometer receiver includes contributions from other areas, where the side lobe gains are finite, and from the antenna coupling effect, which is discussed in section 4.3. At a given Doppler frequency band, associated with the alongtrack incidence angle θ and angular width $\Delta\theta$, the side lobe contribution to the power return is

$$P_s(\theta) = \frac{P_t \lambda^2}{(4\pi)^3} \int_{A_s} \frac{G_t G_r \sigma^\circ}{R^4} \, dA \qquad (4\text{-}2)$$

where the integration is carried out over the area defined by the Doppler frequency band and all side lobes. To make a rough but reasonable numerical estimate of $P_s(\theta)$, the area element of integration is to be approximated by the one shown in figure 4-8. The two isodopplers determine the total ground area, which back scatters the RF power in the corresponding Doppler frequency band. Curves L_1 and L_2 represent the surface loci of the 3-dB points of a given side lobe. Point C_i is the intersection between the isodoppler, corresponding to the central Doppler frequency and the curve tracing the two-way gain maximum of the side lobe. The area

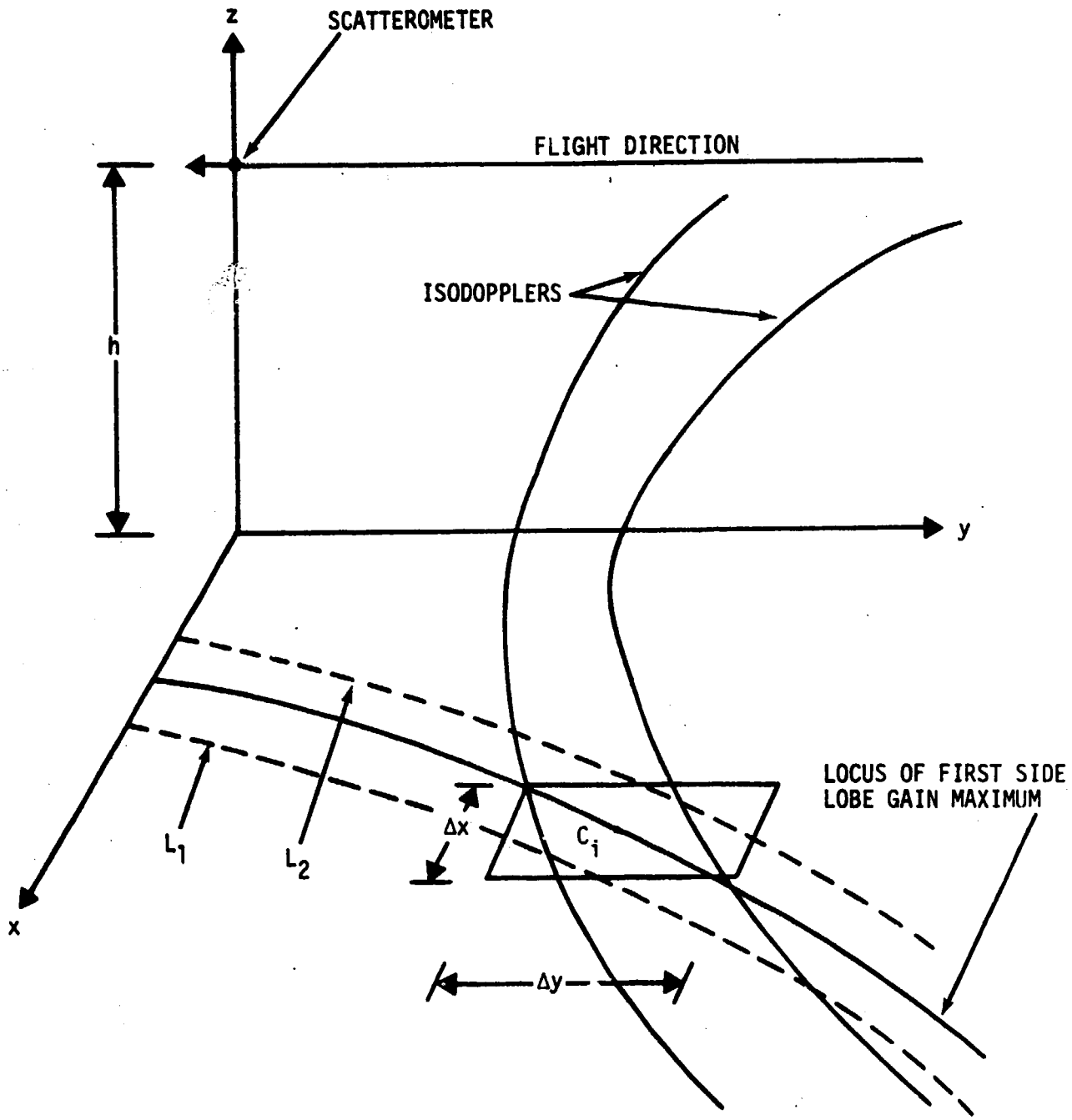

Figure 4-8.– An area element used in the calculation of side lobe contribution to total signal.

element from this side lobe is approximately given by:

$$\Delta A_i = \Delta X_i \Delta Y_i \tag{4-3}$$

and equation (4-2) can be written:

$$P_s(\theta) = \frac{P_t \lambda^2}{(4\pi)^3} \sum_{i=1}^{N} \frac{G_i^2 \sigma_i^\circ}{R_i^4} \Delta X_i \Delta Y_i \tag{4-4}$$

where G_i^2 is the side lobe maximum two-way gain at point C_i for the area element ΔA_i. The values of σ_i° and R_i refer to point C_i. The summation is over all the side lobe area elements within the two isodopplers.

The estimated values for $P_s(\theta)$ are presented in section 5, where the results from all numerical calculations are summarized and discussed.

4.3 ANTENNA CROSS-POLARIZATION AND ITS COUPLING EFFECT

Since the nature of the horizontal and vertical antennas and the isolation between them are not perfect, undesired signals are generated because of antenna coupling effects which appear in the receiver data channel as portions of the backscattered signals. The relative contribution of the undesired signals to the total signal power level has important bearing in the data analysis and in the interpretation of the backscattering process of the RF waves. Thus, it is necessary to estimate the relative signal contribution resulting from the effect of antenna coupling in order to correctly interpret the measured results.

Since the backscattered signal in the 0.4-GHz scatterometer is delay gated with a predetermined time period for corresponding aircraft altitude which ensures that the return signals are only from the target, the direct power leakage into the receiver data channels results from the coupling between the transmit/receive antennas would be gated out and would not appear as power return in the data channel. The main source of the undesired signals are from the coupling effect of the antenna cross-polarization of the horizontal and vertical antennas. Antenna cross-polarizations are mainly due to the nature of the practical antenna, where a horizontal antenna will generate, simultaneously, a vertically polarized pattern in a much smaller magnitude when compared to the main horizontally polarized pattern; the same is true for a vertical antenna.

To see how this source of undesired signals are generated, a specific example is described below. Note that the expression $P_{rHH}(\theta)$, which is the power level of the signal return at an incidence angle θ in the horizontal-transmit and horizontal-receive data channel including the antenna coupling effect, can be written by:

$$P_{rHH}(\theta) = \frac{\lambda^2 \Delta A P_t}{(4\pi)^3 R^4(\theta)} \left[G_H^2(\theta)\sigma^\circ_{HH}(\theta) + G_{HC}(\theta)G_H(\theta)\sigma^\circ_{VH}(\theta) + G_H(\theta)G_{HC}(\theta)\sigma^\circ_{HV}(\theta) + G_{HC}^2(\theta)\sigma^\circ_{VV}(\theta) \right] \quad (4\text{-}5)$$

where

G_H = one-way horizontal antenna gain, either in the transmitting or the receiving mode of operation

G_{HC} = one-way cross-polarized horizontal antenna gain, either in the transmitting or the receiving mode of operation

The first term inside the bracket in equation (4-5) is the dominant term which represents the backscattered signals of interest. The three remaining terms are contributions of the undesired signals resulting from antenna cross-polarization and, thus, its coupling effect. These three terms in sequential order, represent:

a. The return signal in the horizontal receiver caused by the signal transmitted by the cross-polarized component of the horizontal antenna, backscattered in the horizontal polarization, and received by the prime component of the horizontal antenna

b. The return signal in the horizontal receiver caused by the signal transmitted by the prime component of the horizontal antenna, backscattered in the vertical polarization, and received by the cross-polarized component of the horizontal antenna

c. The return signal in the horizontal receiver caused by the signal transmitted by the cross-polarized component of the horizontal antenna, backscattered in the vertical polarization, and received by the cross-polarized component of the horizontal antenna

Expressions similar to equation (4-5) were derived for the other three power returns of different polarizations, namely, P_{rHV}, P_{rVH}, and P_{rVV}. The results were summarized in table 4-2, including the one for P_{rHH} discussed above. For each of the four power returns in the table, the first term always gives the dominant term of interest from which the associated backscattering coefficient σ° is derived. The other three terms, representing the undesired signal returns, would have to be estimated and their relative contribution to the total power level would have to be assessed in the derivation of σ°. In table 4-2, if the cross-polarized backscattering coefficients σ°_{HV} and σ°_{VH} are assumed to be the same (namely, $\sigma^\circ_{HV} = \sigma^\circ_{VH}$ for all incidence angle), then further simplification of the results are given in table 4-3. The assumption is reasonable because backscattering coefficients obey the reciprocity theorem in general, and the experimentally measured data of the two coefficients usually show that they are about the same in magnitude. Table 4-3 will be used in the calculations presented in section 5.

To show the level of antenna coupling, the peak one-way gains of both prime and cross (coupling) polarizations for the horizontal and vertical antennas were plotted as a function of θ in the aft direction from 0° to 70° (figs. 4-9 and 4-10). For the horizontal antenna (fig. 4-9), the cross-polarization level is generally about 16 dB or more below that of the prime polarization; it reaches a maximum difference of 25 dB at θ = 22°. To reduce the

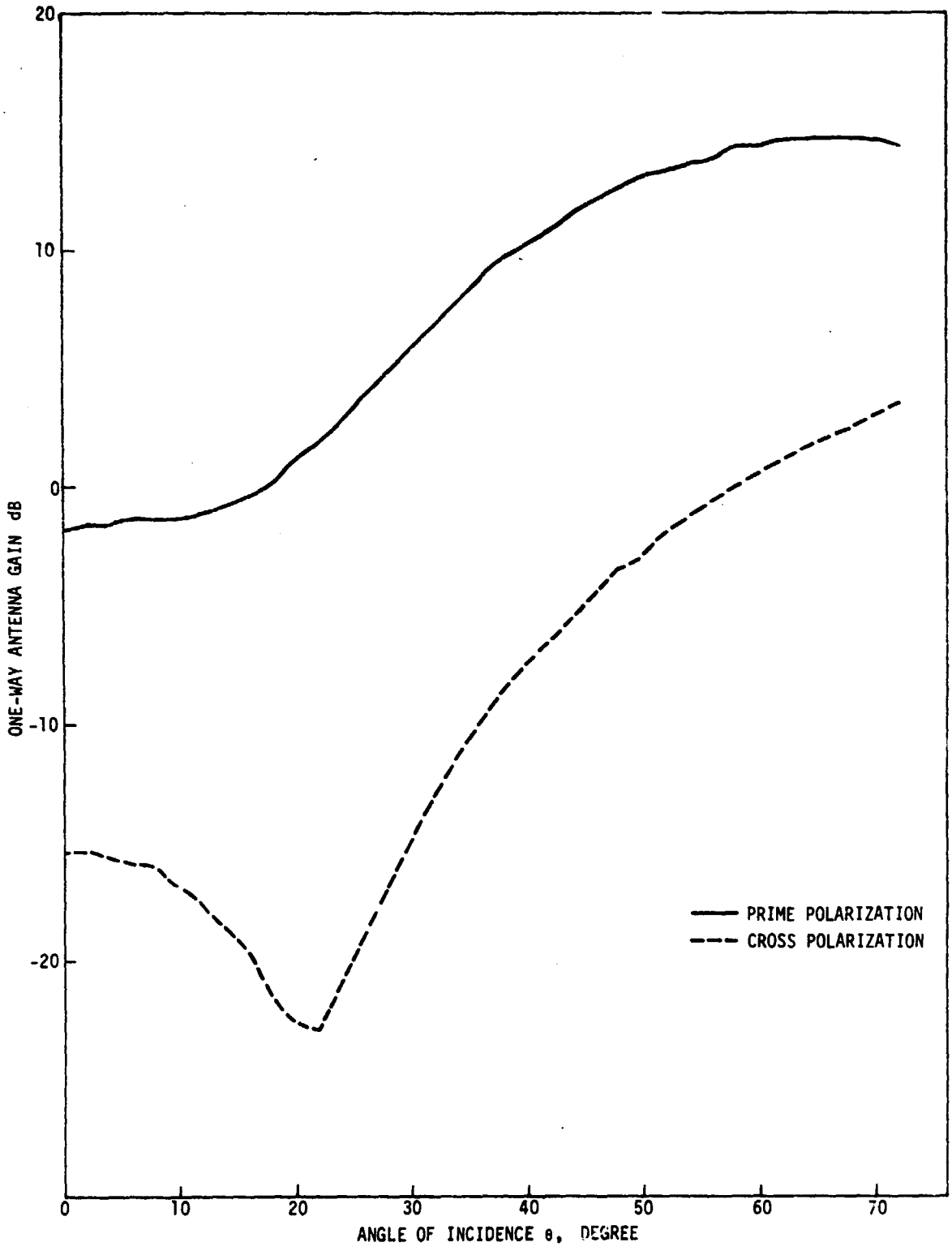

Figure 4-9.— The variation of peak one-way gain of the horizontal antenna with incidence angle for both prime and cross polarizations.

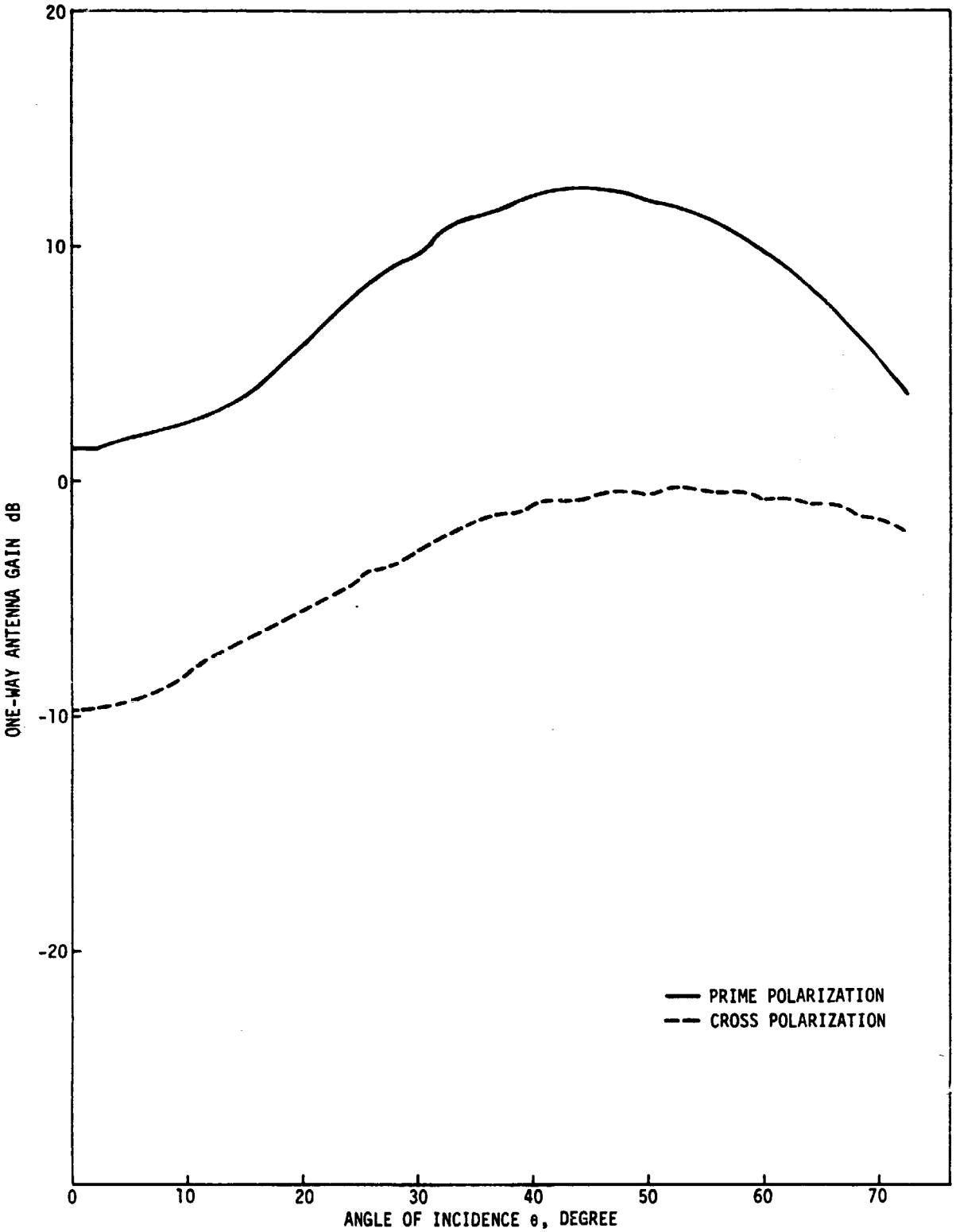

Figure 4-10.— The variation of peak one-way gain of the vertical antenna with incidence angle for both prime and cross polarizations.

TABLE 4-2.— THE COMPONENTS OF THE BACKSCATTERED SIGNAL IN RECEIVER DATA CHANNELS

Power return	Components of backscattered signal
P_{rHH}	1. $G_H \sigma^\circ_{HH} G_H$ 2. $G_{HC} \sigma^\circ_{VH} G_H$ 3. $G_H \sigma^\circ_{HV} G_{HC}$ 4. $G_{HC} \sigma^\circ_{VV} G_{HC}$
P_{rHV}	1. $G_H \sigma^\circ_{HV} G_V$ 2. $G_{HC} \sigma^\circ_{VV} G_V$ 3. $G_H \sigma^\circ_{HH} G_{VC}$ 4. $G_{HC} \sigma^\circ_{VH} G_{VC}$
P_{rVH}	1. $G_V \sigma^\circ_{VH} G_H$ 2. $G_{VC} \sigma^\circ_{HH} G_H$ 3. $G_V \sigma^\circ_{VV} G_{HC}$ 4. $G_{VC} \sigma^\circ_{HV} G_{HC}$
P_{rVV}	1. $G_V \sigma^\circ_{VV} G_V$ 2. $G_{VC} \sigma^\circ_{HV} G_V$ 3. $G_V \sigma^\circ_{VH} G_{VC}$ 4. $G_{VC} \sigma^\circ_{HH} G_{VC}$

TABLE 4-3.– THE COMPONENTS OF THE BACKSCATTERED SIGNAL IN RECEIVER DATA CHANNELS

[Assuming $\sigma^{\circ}_{HV} = \sigma^{\circ}_{VH}$]

Power return	Components of backscattered signal
P_{rHH}	1. $G_H^2\sigma^{\circ}_{HH}$ 2. $G_H G_{HC}\sigma^{\circ}_{HV}$ 3. $G_H G_{HC}\sigma^{\circ}_{HV}$ 4. $G_{HC}^2\sigma^{\circ}_{VV}$
P_{rHV} (or P_{rVH})	1. $G_H G_V\sigma^{\circ}_{HV}$ 2. $G_{HC} G_V\sigma^{\circ}_{VV}$ 3. $G_H G_{VC}\sigma^{\circ}_{HH}$ 4. $G_{HC} G_{VC}\sigma^{\circ}_{HV}$
P_{rVV}	1. $G_V^2\sigma^{\circ}_{VV}$ 2. $G_V G_{VC}\sigma^{\circ}_{HV}$ 3. $G_V G_{VC}\sigma^{\circ}_{HV}$ 4. $G_{VC}^2\sigma^{\circ}_{HH}$

coupling effect, the backscattering coefficient should be measured in the region from 15° to 35° where the cross polarization level is about 20 dB below the prime polarization level.

For the vertical antenna (fig. 4-10), the cross-polarization level is generally about 11 dB or more below that of the prime polarization level and attains a maximum difference of 13 dB at θ = 40° to 44°. Comparing figures 4-9 and 4-10, it is clear that the horizontal antenna has less antenna coupling effect than the vertical antenna, especially for θ in the range of 15° to 35°.

Generally, the peak gain cross-polarization level (figs. 4-9 and 4-10) is not located at ϕ = 0°, where the peak prime polarization gain usually would be located. This is illustrated in figures 4-11, 4-12, 4-13, and 4-14, where the one-way gains of both prime and cross polarizations were plotted as a function of ϕ at θ = 30° and θ = 60° in the aft direction for the horizontal and vertical antennas. The peak cross-polarization gain occurs at ϕ = -10° for both the horizontal and vertical antennas when the incidence angle is 30°, and it occurs at ϕ = -25° when the incidence angle becomes 60°. Also, from figures 4-11 through 4-14, it is seen that at θ = 60° the cross-polarization level is higher than at θ = 30° for both the horizontal and vertical antennas. This is in agreement with what is shown in figures 4-9 and 4-10. There are two cross-polarization lobes in the antenna main beam (figs. 4-12, 4-13, and 4-14); only one with comparatively smaller

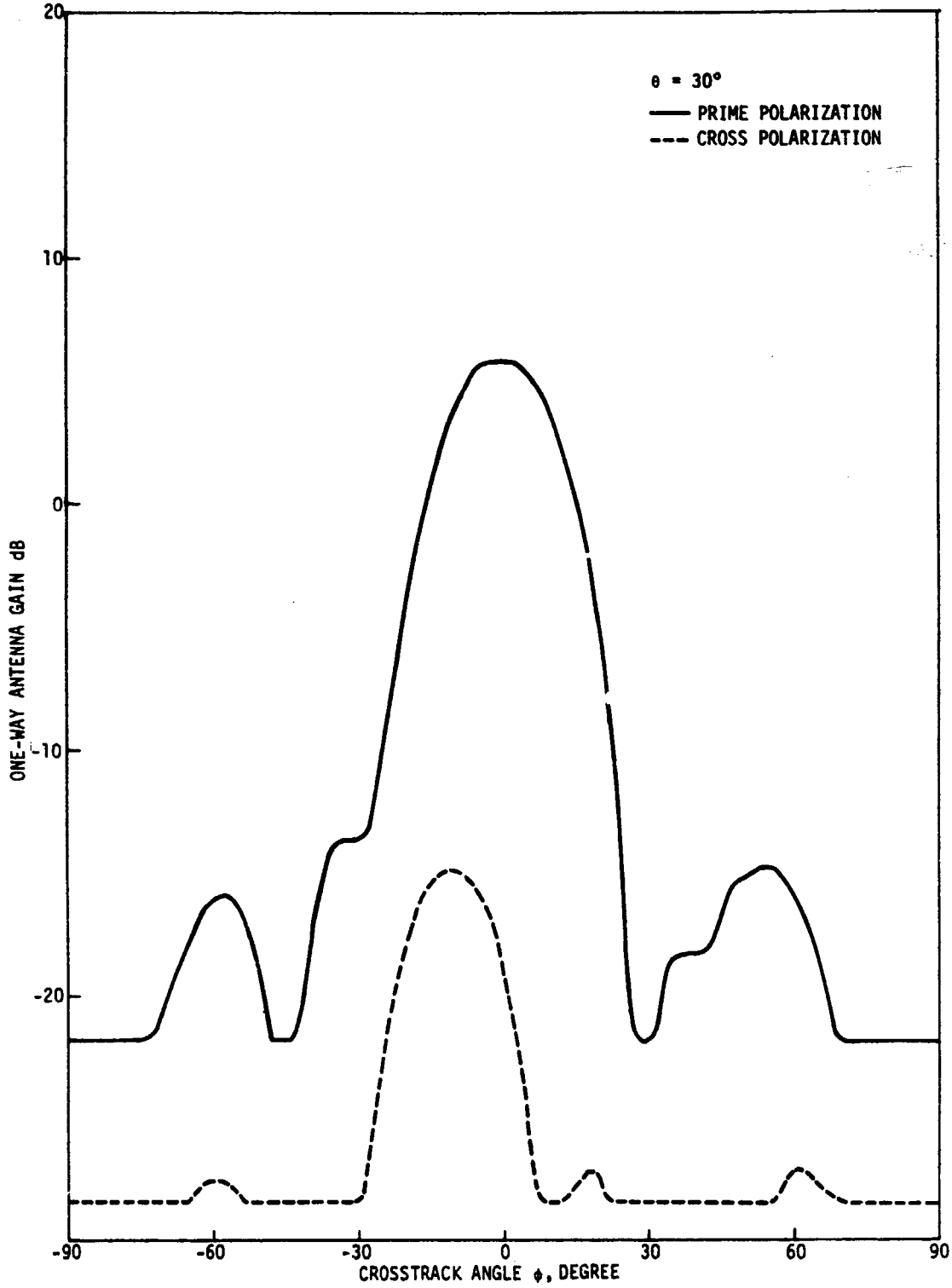

Figure 4-11.— The variation of one-way horizontal antenna gain with crosstrack angle for both prime and cross polarizations.

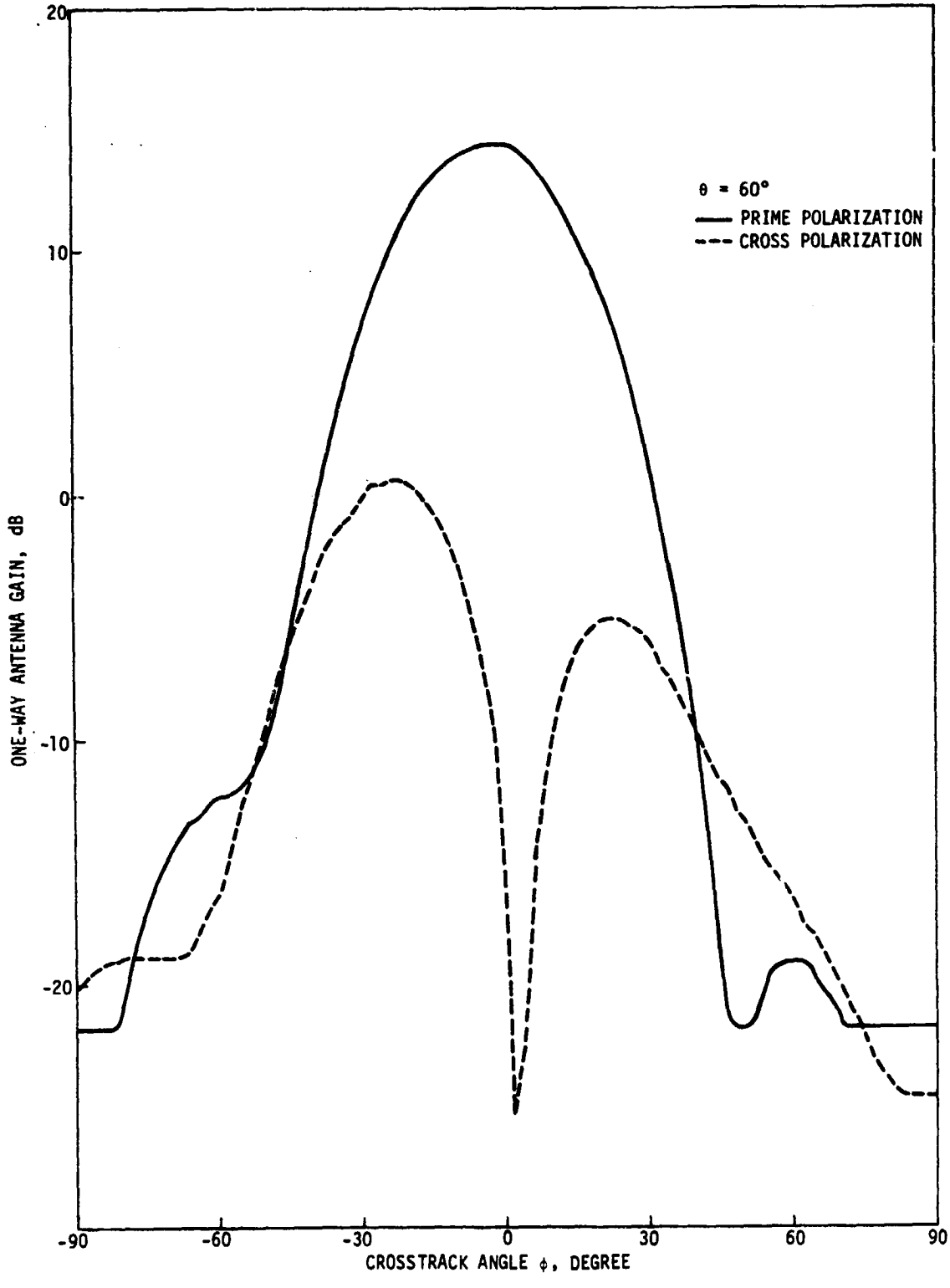

Figure 4-12.– The variation of one-way horizontal antenna gain with crosstrack angle for both prime and cross polarizations.

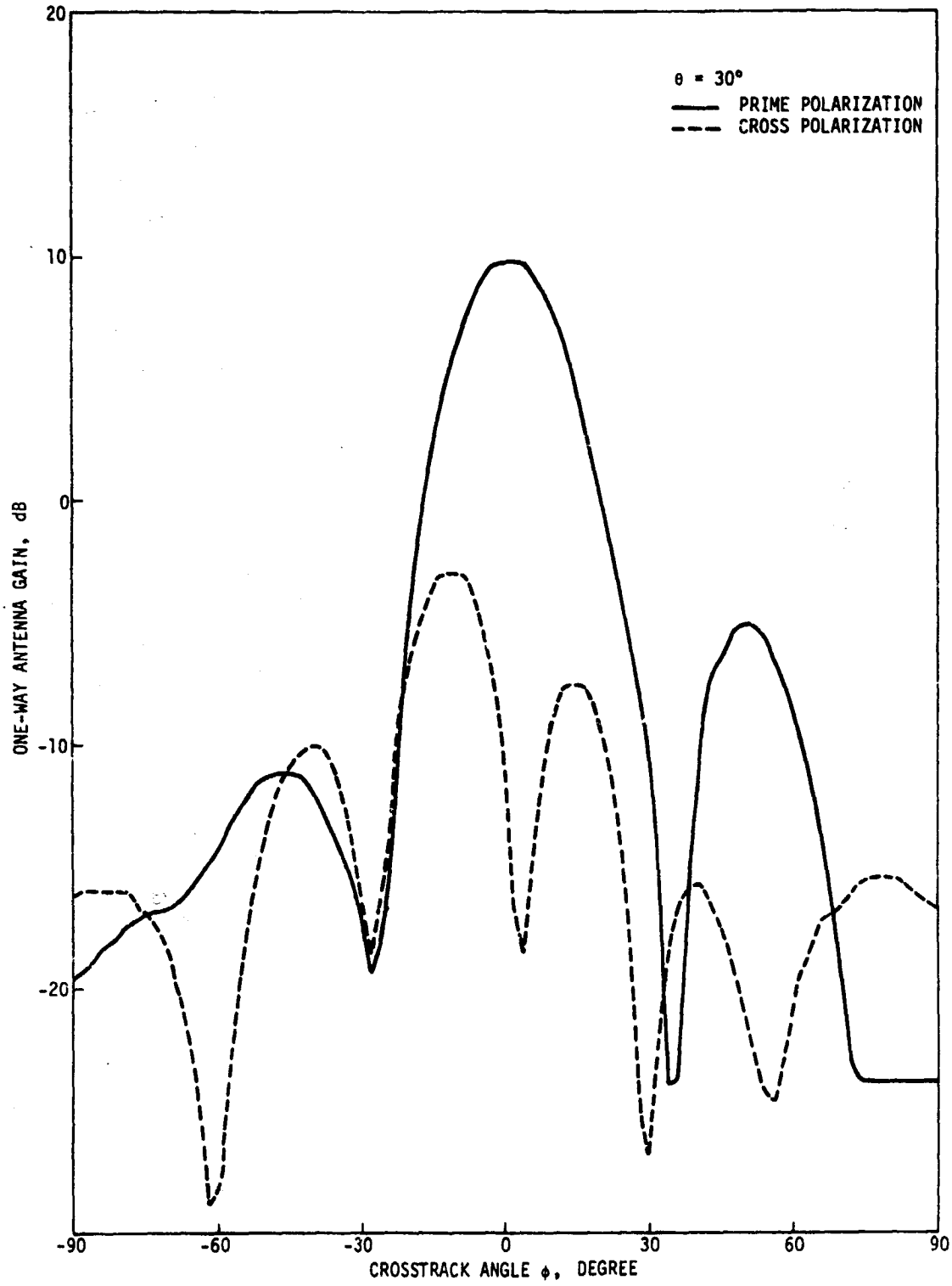

Figure 4-13.— The variation of one-way vertical antenna gain with crosstrack angle for both prime and cross polarizations.

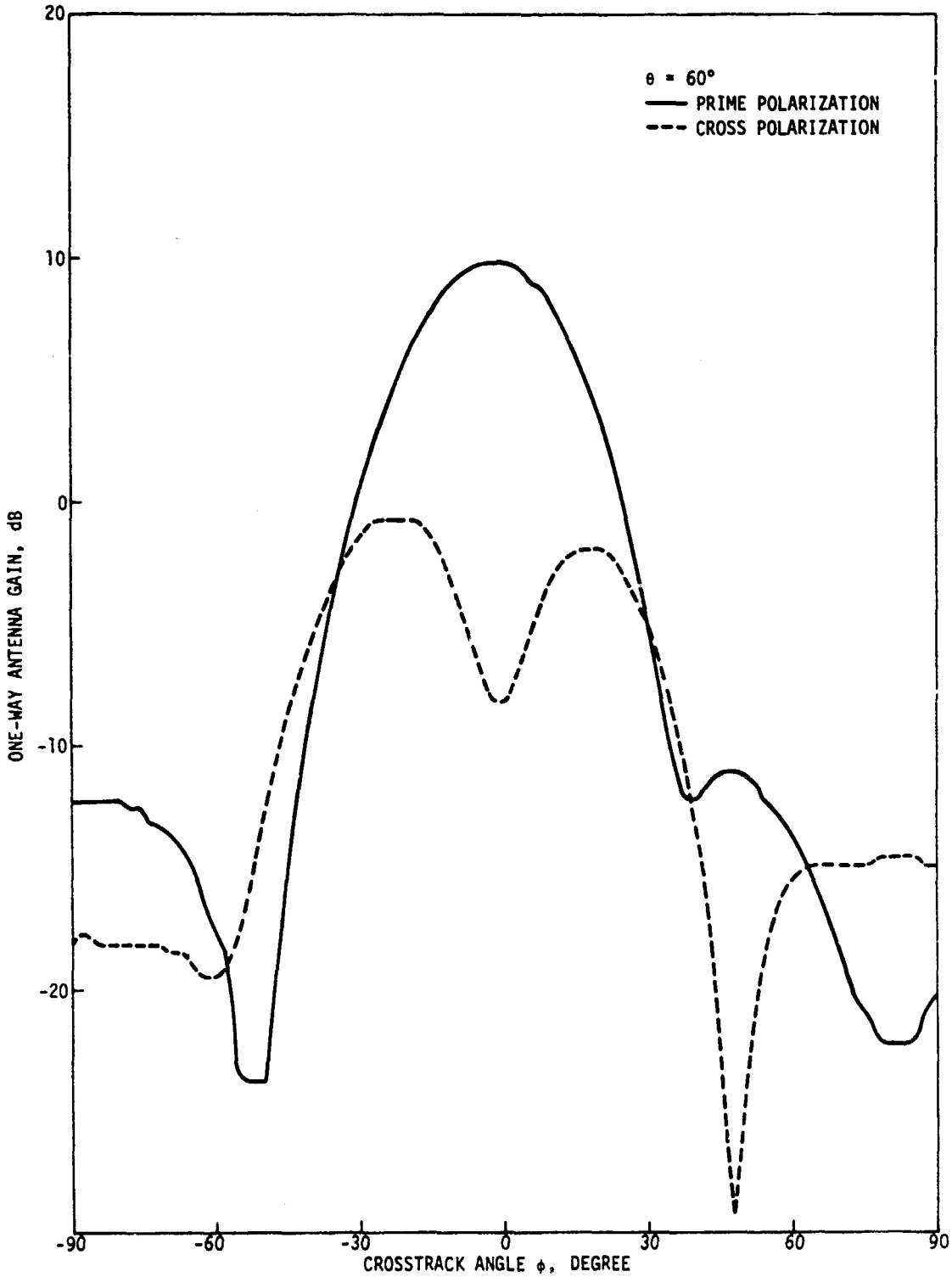

Figure 4-14.— The variation of one-way vertical antenna gain with crosstrack angle for both prime and cross polarizations.

magnitude appears in figure 4-11. This indicates that the horizontal antenna at $\Theta = 30°$ contains less antenna coupling effects when compared to the other three cases shown in figures 4-12 through 4-14.

Based on figures 4-11, 4-12, 4-13, and 4-14 and table 4-3, the relative contributions caused by antenna coupling could be estimated, at some selected locations, for each of the four power returns P_{rHH}, P_{rHV}, P_{rVH}, and P_{rVV}.

The results are summarized in table 4-4 for $\Theta = 30°$ and $\Theta = 60°$, each with two values of ψ where the prime and cross-polarization gains attain the peak values. For $\Theta = 30°$, the values for ϕ are 0° and -10°; for $\Theta = 60°$, 0° and -25°, respectively. All of the relative power returns and $\sigma°$'s in the table are expressed in dB.

The components of the backscattered signals are listed in the same sequence as those in table 4-3. Since the values of $\sigma°_{HH}$ and $\sigma°_{VV}$ are generally observed to be about 10 to 15 dB greater than those for $\sigma°_{HV}$ or $\sigma°_{VH}$ (ref. 14), it is immediately clear that for ΔP_{rHH} and ΔP_{rVV} the contributions from the undesired signals are approximately 20 dB or more below that of the signal of interest at $\Theta = 30°$. At $\Theta = 60°$ and $\phi = -25°$, the difference between the signal of interest and the undesired signals becomes less than 10 dB for ΔP_{rVV} but is about 20 dB for ΔP_{rHH}. For the

TABLE 4-4.— THE RELATIVE CONTRIBUTIONS TO THE TOTAL BACKSCATTERED SIGNALS

Power return	Components of backscattered signal, dB			
	$\theta = 30°$		$\theta = 60°$	
	$\phi = 0°$	$\phi = -10°$	$\phi = 0°$	$\phi = -25°$
ΔP_{rHH}	$\sigma°_{HH}$ + 11.8	+ 8.4	$\sigma°_{HH}$ + 28.8	+19.2
	$\sigma°_{HV}$ - 13.1	-10.6	$\sigma°_{HV}$ - 1.6	+10.2
	$\sigma°_{HV}$ - 13.1	-10.6	$\sigma°_{HV}$ - 1.6	+10.2
	$\sigma°_{VV}$ - 38.0	-29.6	$\sigma°_{VV}$ - 32.0	+ 1.2
ΔP_{rHV} (or $\Delta P_{r}VH$)	$\sigma°_{HV}$ + 15.7	+10.6	$\sigma°_{HV}$ + 24.2	+13.4
	$\sigma°_{VV}$ - 9.2	- 8.4	$\sigma°_{VV}$ - 6.2	+ 4.4
	$\sigma°_{HH}$ - 5.6	+ 1.2	$\sigma°_{HH}$ + 6.2	+ 8.8
	$\sigma°_{HV}$ - 30.5	-17.8	$\sigma°_{HV}$ - 24.2	- 0.2
ΔP_{rVV}	$\sigma°_{VV}$ + 19.6	+12.8	$\sigma°_{VV}$ + 19.6	+ 7.6
	$\sigma°_{HV}$ - 1.7	+ 3.4	$\sigma°_{HV}$ + 1.6	+ 3.0
	$\sigma°_{HV}$ - 1.7	+ 3.4	$\sigma°_{HV}$ + 1.6	+ 3.0
	$\sigma°_{HH}$ - 23.0	- 6.0	$\sigma°_{HH}$ - 16.4	- 1.6
Antenna gains	G_H = 5.9	4.2	G_H = 14.4	9.6
	G_{HC} = -19.0	-14.8	G_{HC} = -16.0	0.6
	G_V = 9.8	6.4	G_V = 9.8	3.8
	G_{VC} = -11.5	-3.0	G_{VC} = -8.2	-0.8

remaining two power returns ΔP_{rHV} and ΔP_{rVH}, the undesired signal contributions may be significant or even larger than the signal of interest. For example, at $\phi = -10°$ and $\Theta = 30°$, the third term undesired signal level may be as high as the signal of interest; whereas at $\phi = -25°$ and $\Theta = 60°$, it may reach approximately 5 dB larger than the signal of interest. These results suggest that, depending upon locations, the contributions of the undesired signal could be three times higher than the signal of interest for either ΔP_{rHV} or ΔP_{rVH}.

The power at a given Doppler frequency band, as observed by the 0.4-GHz scatterometer, represents the total backscattered signal from the entire ground cell corresponding to that frequency band. Therefore, the comparisons made in table 4-4 at selected locations are clearly not sufficient to give a valuable assessment of the antenna coupling effect. A reasonable approach for estimating the effect is to integrate the power of each of the backscattered signal components, desired and undesired, over the entire ground cell and compare the results. This is done by numerical integration described in section 5.

It is noted (fig. 4-11) that the measurements of the antenna gains are limited to the levels above approximately -28 dB. This suggests that the actual cross-polarized gain levels could be lower than the measured values in some regions. However, the

estimate on the total undesired signal contribution is heavily weighted towards the components having the higher power returns associated with higher antenna cross-polarization levels. Consequently, the saturation in the cross-polarized gain measurements does not introduce significant errors in the numerical estimates of the antenna coupling effect performed in section 5.

The coupling in the side lobes also makes undesired contributions to the total signal power return. However, the contribution to the total signal caused by the prime side lobe gains is small (sections 4.2 and 5.3). The undesired signal level caused by the antenna coupling in the side lobes is expected to be even smaller; therefore, these should not be explored.

5. NUMERICAL RESULTS AND DISCUSSION

5.1 INTRODUCTION

The numerical computations of the receiver signal output for various polarizations were performed according to equation (3-22). The area elements with the relative coordinates are shown in figure 5-1. The center of the area element lies on the isodoppler corresponding to the incidence angle θ_i and the crosstrack angle ϕ_i. The integration of ϕ_i is made from alongtrack ($\phi_i = 0$) to offtrack ($\phi_i \neq 0$) depending on the antenna beam width which must be included. The offtrack incidence angle θ_i is related to the alongtrack (y-axis) incidence angle θ_o by:

$$\theta_i = \cos^{-1} (\cos \theta_o \cos \phi_i) \tag{5-1}$$

and the offtrack distance $R(\theta_i)$ to alongtrack distance $R(\theta_o)$ by:

$$\begin{aligned} R(\theta_i) &= R(\theta_o)/\cos \phi_i \\ &= h/\cos \theta_i \end{aligned} \tag{5-2}$$

The area element ΔA_i is given by:

$$\Delta A_i = \Delta x_i \cdot \Delta y_i \tag{5-3}$$

where Δy_i for offtrack ΔA_i is related to alongtrack Δy_o by:

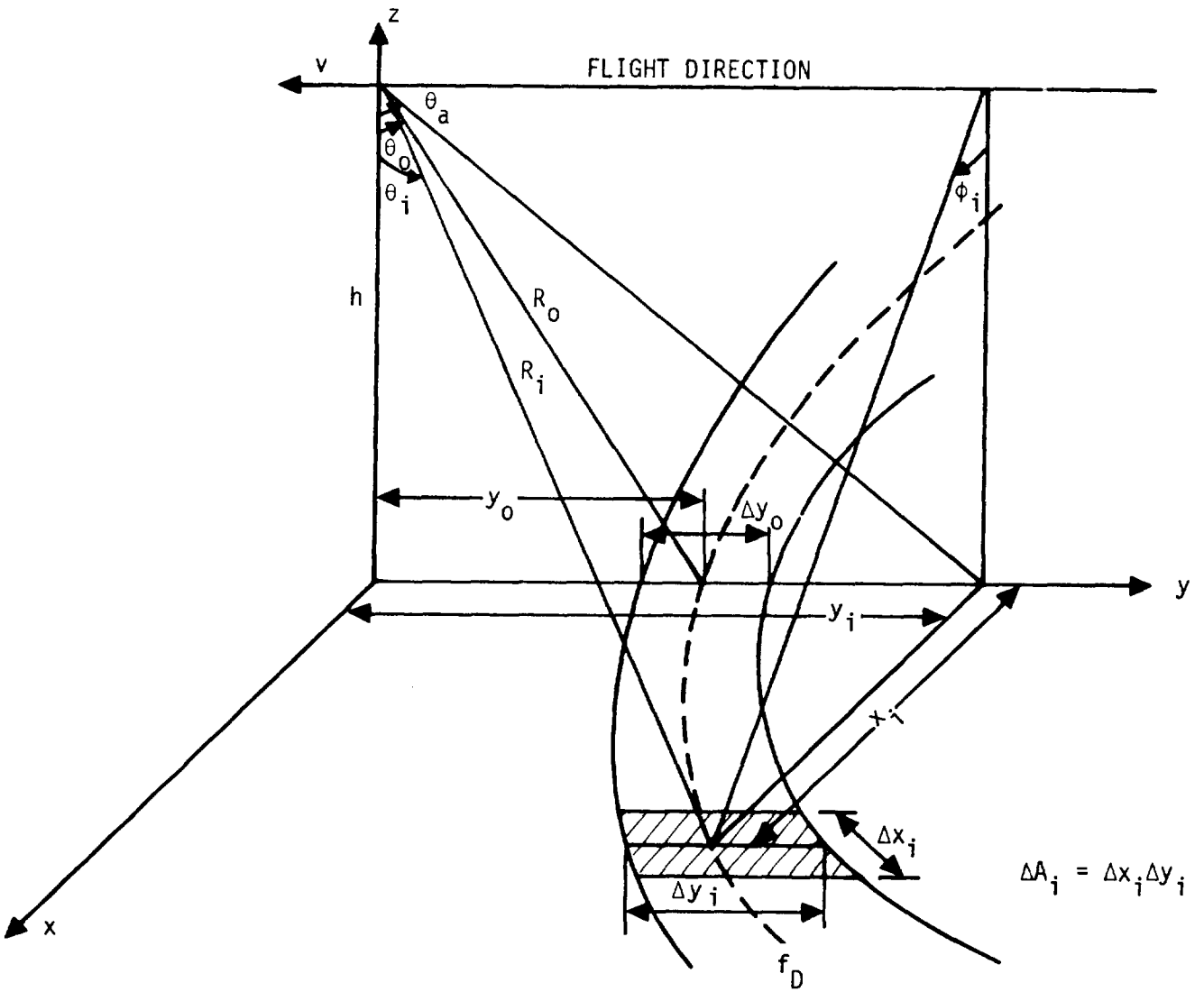

Figure 5-1.— The coordinates of the area element ΔA_i.

$$\Delta y_i = \Delta y_o / \cos \phi_i \qquad (5\text{-}4)$$

where Δy_o is 50 meters (164 feet) in the computation. The width Δx_i is defined to be the distance substended by 2° of the cross-track angular increment and can be written as:

$$\Delta x_i = h \left[\tan(\phi_i + 1) - \tan(\phi_i - 1) \right] \qquad (5\text{-}5)$$

where h is the aircraft altitude and is taken to be 460 meters (1510 feet).

The antenna gains $G_t(\theta_i)$ and $G_r(\theta_i)$, the backscattering coefficient $\sigma°(\theta_i)$, and the distance $R(\theta_i)$ inside the summation sign of equation (3-22) were evaluated at the centers of the ΔA_i's. When these centers did not fall on the positions where the actual measurements of $G_t(\theta_i)$ and $G_r(\theta_i)$ were made, linearly interpolated values from the immediate neighbors were used. The summation was carried out to $\phi_i = \pm 60°$, where the antenna crosstrack patterns indicate that almost all the powers are inside this angular range. To make the estimate of the antenna coupling effect simple and reasonable, a single ±60° crosstrack boundary was applied to the calculations of all four components of desired and undesired signal returns for the three polarizations as shown in table 4-3.

The computer program, designed and implemented by J. R. Wang (ref. 10) for the 1.6-GHz scatterometer, was modified to calculate

the receiver power return for the 0.4-GHz scatterometer. The modified version given in the appendix can evaluate the power outputs in accordance with equation (3-22). Eight angles of incidence at 5°, 10°, 15°, 20°, 30°, 40°, 50°, and 60° were chosen for the computations. Since the alongtrack cell length is a fixed value of 50 meters (164 feet), the bandwidth Δf_D changes when the angle of incidence decreases from 22 Hz at Θ = 5° to 3.8 Hz at Θ = 60°. The values of the antenna feed-line loss L_s and the calibration constant K were treated as constants in the program.

The program, coded in Fortran, consisted of one main program and two subroutines. The first subroutine was used to obtain the values of the two-way antenna gain for the calculation of signal returns, given the incidence angle Θ_o and the crosstrack angle ϕ_i. The second subroutine was used to evaluate the backscattering coefficient $\sigma°$, given the incidence angle Θ_i at the area element ΔA_i. The functional dependence of $\sigma°_{VV}$ and $\sigma°_{HH}$ on Θ_i is given in equations (3-27) and (3-28) for water and land, respectively. The values of $\sigma°_{HV}$ (or $\sigma°_{VH}$) were assumed to be 15 dB lower than $\sigma°_{HH}$ or $\sigma°_{VV}$ at all incidence angles. The program was executed on the UNIVAC 1110 computer at JSC.

The two-way antenna gains for each of 10 combinations in table 4-3 were previously saved on a magnetic tape, one file for each combination. For a $\sigma°$ versus Θ curve, all the signal outputs

corresponding to 10 components listed in table 4-3 can be obtained with a single computer run.

5.2 THE σ° DEVIATION

As discussed in section 3, it is necessary to assume a functional dependence of σ° on the incidence angle θ in equation (3-22) of σ° derivation. This assumption was made according to equations (3-27) and (3-28) for backscattering from water and land, respectively. The receiver signal outputs in terms of $(B/A)/\Delta f_D$ from the computer runs are shown in figures 5-2 and 5-3 for backscattering over water and land, respectively. These signal outputs could be compared with those actually obtained from observations to determine the validity of the assumed σ° dependence on θ. The procedure is straightforward and will not be performed here. Instead, a comparison will be made between the first [as represented by equation (3-21)] and the second [as represented by equation (3-22)] methods of derivation. To make this comparison, the data displayed in figures 5-2 and 5-3 were taken to be the receiver output signals for both methods. Then the σ° dependence on θ, as derived from the second method, will be given by equation (3-27) for water and equation (3-28) for land. The numerical values from these equations at the incidence angles of 5°, 10°, 15°, 20°, 30°, 40°, 50°, and 60° are listed under the σ° columns in tables 5-1 and 5-2. The σ°'s for both linear and cross polarizations over water and land were given in tables 5-1 and 5-2, respectively. Note that no distinction is made between σ°_{HH}

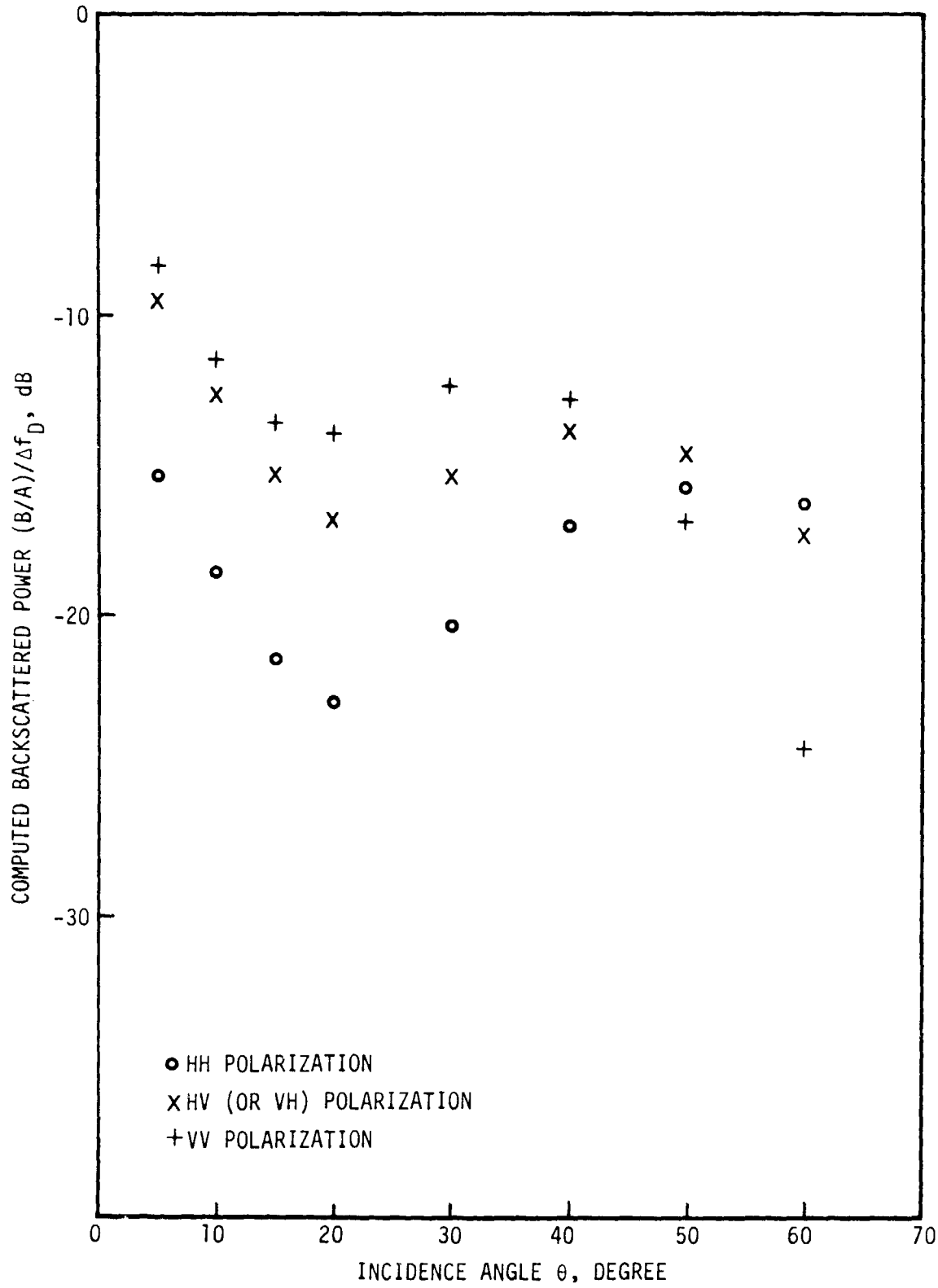

Figure 5-2.— The computed backscattered signals over water for all four polarizations.

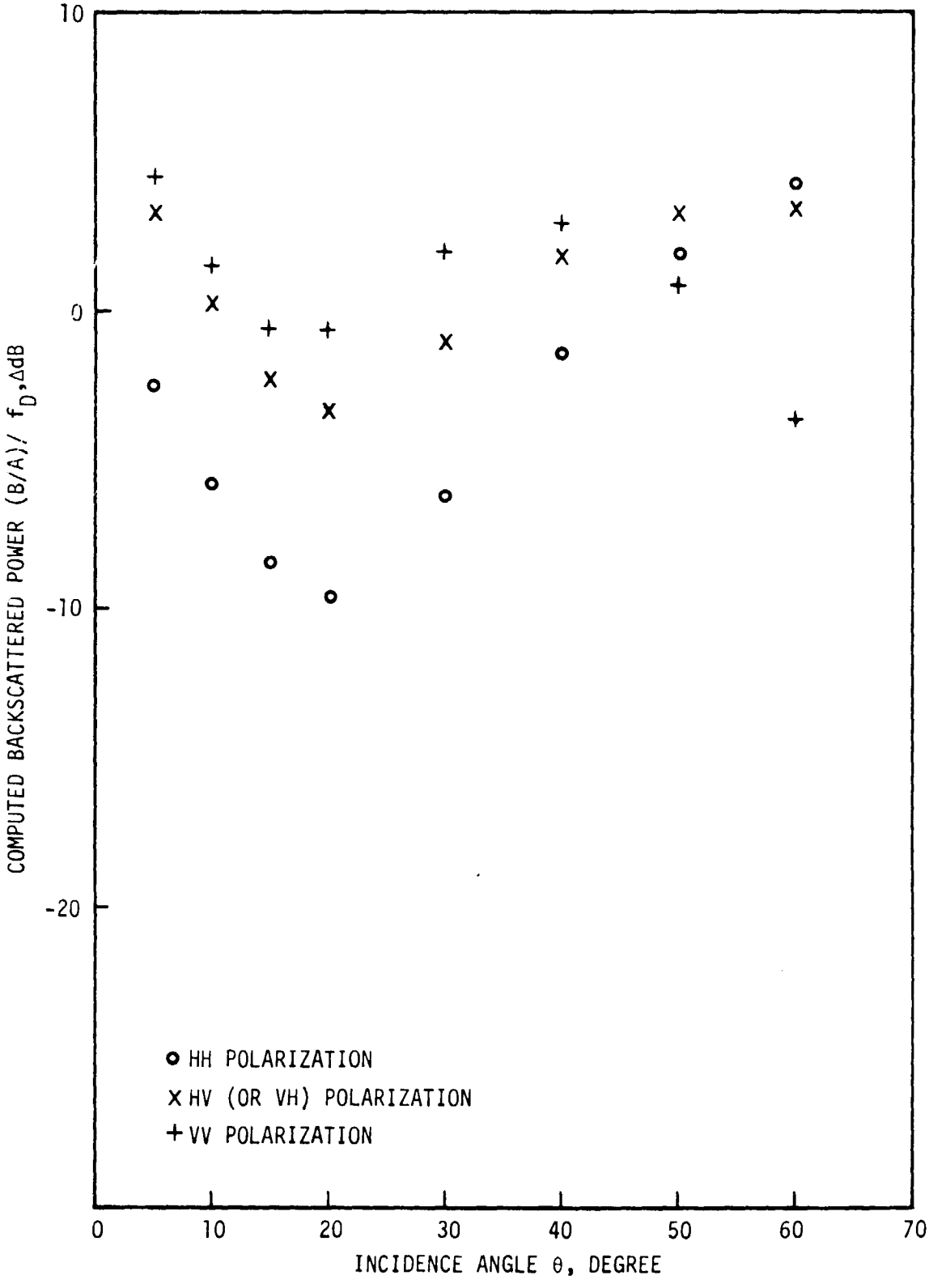

Figure 5-3.— The computed backscattered signals over land for all four polarizations.

and σ°_{VV} and between σ°_{VH} and σ°_{HV} in this second method of σ° derivation (section 5.1).

The corresponding values of the σ°'s derived from the first method of equation (3-21) were given in tables 5-1 and 5-2 under the σ°_{HH}, σ°_{VV}, and σ°_{HV} columns. The same numerical values for the parameters such as altitude, aircraft speed, cell length, antenna feed loss, and calibration constant K were used in equations (3-21) and (3-22). From tables 5-1 and 5-2, it is seen that the results of the linear polarizations are more similar for the two method than are the results of cross polarization power return. This is because the cross polarization power return contains significant amounts of the antenna coupling term, which will be discussed in later subsections. The inclusion of the antenna coupling effect increases the results derived from the first method by 2 to 5 dB higher than from the second method. For linear polarization, with negligible antenna coupling effects the results derived from the first method is approximately 0 to 2 dB lower than from the second method.

5.3 EFFECT OF ANTENNA SIDE LOBES

The side lobe contribution to the total power return can be estimated by using equation (4-4). However, to compare the power levels between the main beam and the side lobe signal returns, it is more convenient to write equation (4-4) in a form similar

TABLE 5-1. — A COMPARISON OF σ° VALUES
DERIVED FROM TWO DIFFERENT APPROACHES OVER WATER

[dB]

Incidence angle Θ, degree	Linear polarization			Cross polarization	
	σ°	σ°_{HH}	σ°_{VV}	σ°	σ°_{HV} or σ°_{VH}
5	- 7.57	- 9.80	- 9.68	-22.57	-20.36
10	-12.00	-13.30	-13.49	-27.00	-24.01
15	-16.14	-17.37	-17.83	-31.14	-28.38
20	-20.00	-22.20	-21.74	-35.00	-33.14
30	-26.85	-28.80	-28.17	-41.85	-40.48
40	-32.56	-33.95	-33.10	-47.56	-45.45
50	-37.14	-37.85	-36.69	-52.14	-48.64
60	-40.56	-40.74	-39.30	-55.56	-50.07

TABLE 5-2. — A COMPARISON OF σ° VALUES DERIVED FROM TWO DIFFERENT APPROACHES OVER LAND

[dB]

Incidence angle θ, degree	Linear polarization			Cross polarization	
	σ°	σ°_{HH}	σ°_{VV}	σ°	σ°_{HV} or σ°_{VH}
5	5.01	3.02	3.14	- 9.99	- 7.53
10	0.59	- 0.45	- 0.63	-14.41	-11.12
15	- 3.40	- 4.35	- 4.82	-18.40	-15.33
20	- 6.97	- 8.90	- 8.45	-21.97	-19.81
30	-12.85	-14.56	-13.94	-27.85	-26.20
40	-17.05	-18.21	-17.38	-32.05	-29.66
50	-19.55	-20.08	-18.93	-34.55	-30.76
60	-20.37	-20.33	-18.94	-35.37	-29.49

to equation (3-22). This is readily done and the final expression for the side lobe signal return is:

$$(B/A)/\ f_D = \frac{\lambda^2\ L_s}{(4\pi)^3\ K\ \Delta f_D} \sum_{i=1}^{N} \frac{G_i^{\ 2}\sigma_i^{\ \circ}}{R_i^{\ 4}}\ \Delta x_i\ \Delta y_i \qquad (5\text{-}6)$$

where N is the number of the side lobe area elements contributing to the power return at the Doppler frequency f_D and bandwidth Δf_D; L_s and K have the same meaning and values as in equation (3-22); and G_i^2, σ_i°, Δx_i, and Δy_i were defined in section 4.2. The variation of σ° with incidence angle θ were again determined by equations (3-27) and (3-28) for backscattering over water and land, respectively. From equation (5-6), the side lobe power level can be estimated in terms of $(B/A)/\Delta f_D$ and compared directly with the main beam power return shown in figures 5-2 and 5-3.

Only the VV polarization contains a significant amount of side lobe power; therefore, only the contributions of power return from the first side lobe on both sides of the main beam of the VV polarization were computed and plotted in figures 5-4 and 5-5 for water and land, respectively. Also included in figures 5-4 and 5-5 is the depressed 30 dB main lobe power return. From figures 5-4 and 5-5, it is clear that the side lobe power level for VV polarization is about 30 dB or more lower than that of the main lobe power. As observed in section 4, the other polarizations contain much smaller amounts of side lobe level as compared to VV polarization; thus, it can be concluded that the side

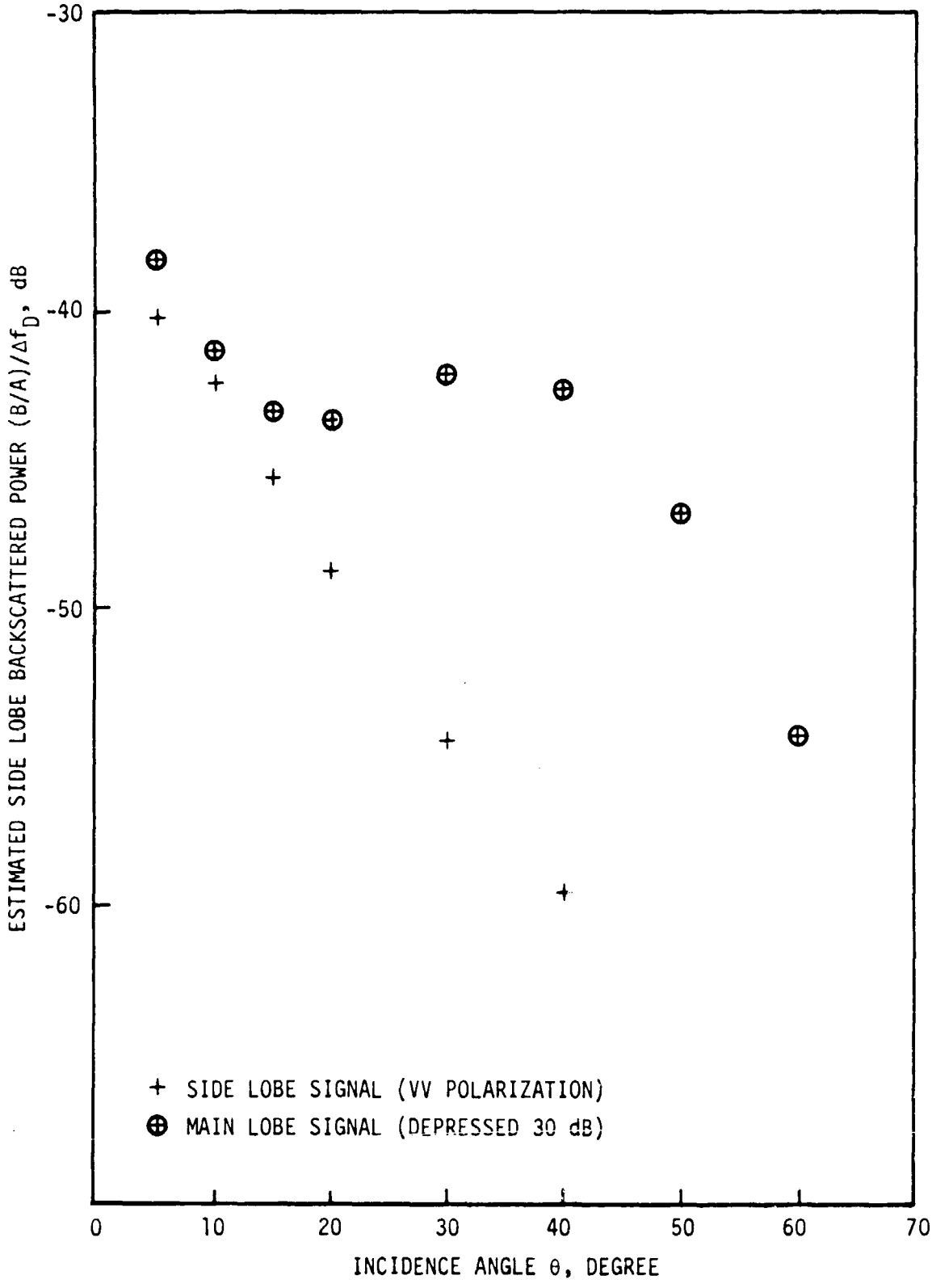

Figure 5-4.– Estimated side lobe signal return over water corresponding to the indicated main beam incidence angle.

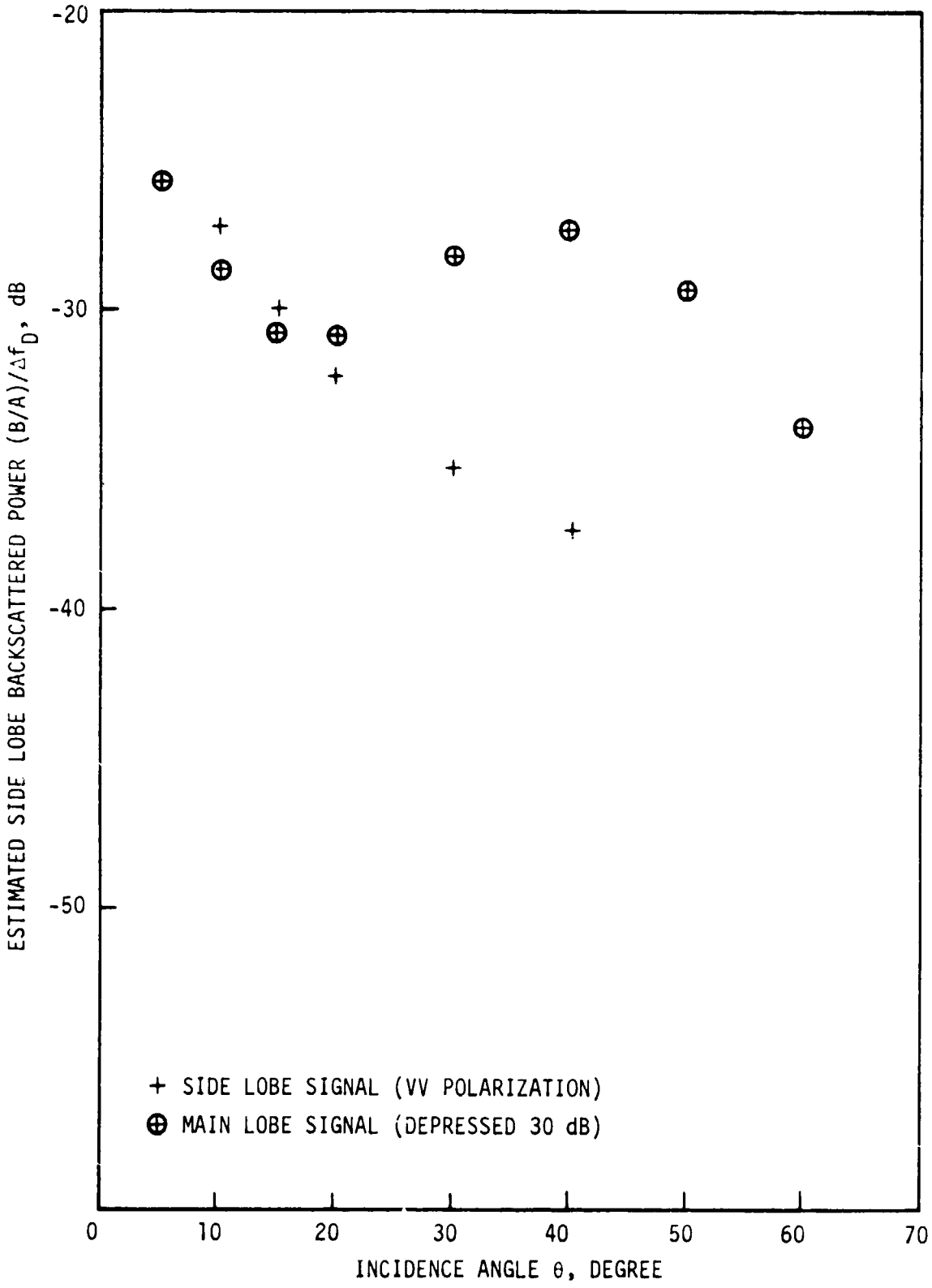

Figure 5-5.– Estimated side lobe signal return over land corresponding to the indicated main beam incidence angle.

lobe contributions to the backscattered signal powers are insignificant for all polarizations.

5.4 ANTENNA COUPLING EFFECT

The computer outputs of the backscattered signals are displayed in sequential order in tables 5-3, 5-4, and 5-5 for HH, HV, and VV polarizations, respectively. The computed signal outputs were derived for backscattering over water and land and for incidence angles of 5°, 10°, 20°, 30°, 40°, 50°, and 60°. The assignment of the backscattered signal components under columns 1, 2, 3, and 4 was the same as that given in table 4-3. Consequently, the values in column 1 were the backscattered power of interest, and those under the other three columns were the backscattered powers caused by antenna coupling. The values in the Total column give the sum of the first four columns. The values for σ°_{HV} or σ°_{VH} were taken to be 15 dB less than those for σ°_{HH} and σ°_{VV} in the computations. It is clear from tables 5-3 and 5-5 that by comparing columns 1 and Total, the contribution to the backscattered signal caused by antenna coupling is totally negligible in these cases. Therefore, it is not necessary to consider the effect of antenna coupling when deriving σ°_{HH} or σ°_{VV}.

The results shown in table 5-4 indicate a significant contribution from columns 2 and 3 to the total power. The contributions from column 2 are larger than those of column 1, which indicate that the antenna coupling effect overshadows the power return of interest.

TABLE 5-3.– NUMERICAL VALUES OF THE BACKSCATTERED SIGNALS FOR HORIZONTAL TRANSMIT AND HORIZONTAL RECEIVE

[IN TERMS OF $B/A/\Delta f_D$]

Incidence angle θ, degree	HH (water)					HH (land)				
	1	2	3	4	Total	1	2	3	4	Total
5	-15.33	-49.20	-49.20	-48.08	-15.32	-2.510	-36.36	-36.36	-35.19	-2.504
10	-18.58	-52.55	-52.55	-51.95	-18.57	-5.723	-39.64	-39.64	-38.97	-5.717
15	-21.40	-56.78	-56.78	-58.37	-21.40	-8.384	-43.68	-43.68	-45.18	-8.381
20	-22.85	-60.99	-60.99	-66.96	-22.85	-9.549	-47.63	-47.63	-53.48	-9.547
30	-20.33	-58.66	-58.66	-64.25	-20.33	-6.088	-44.36	-44.36	-49.82	-6.087
40	-17.09	-52.72	-52.72	-53.85	-17.09	-1.357	-36.84	-36.84	-37.74	-1.354
50	-15.76	-49.55	-49.55	-48.18	-15.75	2.018	-31.52	-31.52	-29.78	2.020
60	-16.24	-48.21	-48.21	-44.49	-16.23	4.162	-27.41	-27.41	-23.23	4.176

TABLE 5-4.– NUMERICAL VALUES OF THE BACKSCATTERED SIGNALS FOR HORIZONTAL TRANSMIT AND VERTICAL RECEIVE

[IN TERMS OF $B/A/\Delta f_D$]

Incidence angle θ, degree	HV or VH (water)					HV or VH (land)				
	1	2	3	4	Total	1	2	3	4	Total
5	-14.05	-12.63	-17.59	-43.22	- 9.53	-1.237	0.2031	-4.742	-30.36	3.297
10	-17.21	-15.51	-21.13	-46.22	-12.61	-4.358	-2.617	-8.210	-33.27	0.275
15	-19.71	-17.90	-25.42	-50.39	-15.26	-6.698	-4.837	-12.33	-37.23	-2.213
20	-20.61	-19.34	-29.08	-55.60	-16.66	-7.324	-5.985	-15.72	-42.13	-3.334
30	-18.51	-18.70	-27.55	-54.26	-15.32	-4.277	-4.361	-13.28	-39.83	-1.041
40	-17.18	-17.58	-23.87	-49.50	-13.90	-1.462	-1.723	-8.042	-33.45	1.887
50	-18.55	-17.99	-23.23	-47.87	-14.61	-0.786	-0.0275	-5.266	-29.58	3.27
60	-22.45	-19.75	-25.32	-47.70	-17.16	-2.079	0.8982	-4.618	-26.55	3.418

TABLE 5-5.– NUMERICAL VALUES OF THE BACKSCATTERED SIGNALS FOR VERTICAL TRANSMIT AND VERTICAL RECEIVE

[IN TERMS OF $B/A/\Delta f_D$]

Incidence angle C, degree	VV (water)					VV (land)				
	1	2	3	4	Total	1	2	3	4	Total
5	- 8.414	-36.76	-36.76	-33.03	-8.386	4.406	-23.92	-23.92	-20.16	4.434
10	-11.47	-39.71	-39.71	-35.54	-11.44	1.392	-26.81	-26.81	-22.58	1.422
15	-13.63	-42.20	-42.20	-36.99	-13.60	-0.619	-29.13	-29.13	-23.85	-0.586
20	-13.92	-43.50	-43.50	-38.05	-13.89	-0.631	-30.15	-30.15	-24.61	-0.604
30	-12.25	-43.27	-43.27	-39.23	-12.23	1.986	-28.95	-28.95	-24.79	2.002
40	-12.81	-43.95	-43.95	-40.36	-12.80	2.907	-28.12	-28.12	-24.36	2.922
50	-16.88	-46.92	-46.92	-42.64	-16.86	0.870	-29.01	-29.01	-24.45	0.892
60	-24.23	-52.06	-52.06	-45.60	-24.18	-3.870	-31.48	-31.48	-24.62	-3.819

While there were comparable contributions at all eight incidence angles under investigation, the least severe ones appeared to be at $\Theta = 30°$ where the value of column 2 is about the same as that of column 1. At all other incidence angles, the values of column 2 are larger than those of column 1. To account for the antenna coupling effect in the derivation of $\sigma°_{HV}$ or $\sigma°_{VH}$, a correction factor shall be included in the data processing algorithm. The values of the correction factor will be the difference between the columns labelled Total and 1 in table 5-4, assuming $\sigma°_{HV}$ or $\sigma°_{VH}$ to be 15 dB less than those of $\sigma°_{HH}$ and $\sigma°_{VV}$.

The effect of the antenna coupling on the backscattered signal power level is expected to depend strongly on the relative values of $\sigma°_{HV}$ or $\sigma°_{VH}$ with respect to $\sigma°_{HH}$ and $\sigma°_{VV}$. To make a rough estimate of this dependence, a similar computation was performed with $\sigma°_{HH}$ and $\sigma°_{VV}$ again given by equations (3-27) and (3-28) for backscattering over water and land, respectively. But the values of $\sigma°_{HV}$ or $\sigma°_{VH}$ were assumed to be 10 dB less than those of $\sigma°_{HH}$ and $\sigma°_{VV}$. The results of this computation are shown in tables 5-6, 5-7, and 5-8 for HH, HV, and VV polarizations, respectively. Again, it is clear from tables 5-6 and 5-8 that the contribution to the backscattered signal caused by antenna coupling is still negligible in the linear polarization cases. Therefore, it is not necessary to consider the effect of antenna coupling when $\sigma°_{HV}$ was assumed to be either 15 dB or 10 dB less than those for $\sigma°_{HH}$ for the linear polarization cases.

TABLE 5-6.– NUMERICAL VALUES OF THE BACKSCATTERED SIGNALS FOR HORIZONTAL TRANSMIT AND HORIZONTAL RECEIVE

[IN TERMS OF $B/A/\Delta f_D$]

Incidence angle θ, degree	HH (water)					HH (land)				
	1	2	3	4	Total	1	2	3	4	Total
5	-15.33	-44.20	-44.20	-48.08	-15.32	-2.510	-31.36	-31.36	-35.19	-2.496
10	-18.58	-47.55	-47.55	-51.95	-18.57	-5.723	-34.64	-34.64	-38.97	-5.710
15	-21.40	-51.78	-51.78	-58.37	-21.39	-8.384	-36.88	-38.68	-45.18	-8.375
20	-22.85	-55.99	-55.99	-66.96	-22.85	-9.549	-42.63	-42.63	-53.48	-9.545
30	-20.33	-53.66	-53.66	-64.25	-20.33	-6.088	-39.36	-39.36	-49.82	-6.084
40	-17.09	-47.72	-47.72	-53.85	-17.08	-1.357	-31.84	-31.84	-37.74	-1.348
50	-15.76	-44.55	-44.55	-48.18	-15.75	-2.018	-26.52	-26.52	-29.78	-1.980
60	-16.24	-43.21	-43.21	-44.49	-16.22	4.162	-22.41	-22.41	-23.23	4.189

TABLE 5-7.– NUMERICAL VALUES OF THE BACKSCATTERED SIGNALS FOR HORIZONTAL TRANSMIT AND VERTICAL RECEIVE

[IN TERMS OF $B/A/\Delta f_D$]

Incidence angle Θ, degree	HV or VH (water)					HV or VH (land)				
	1	2	3	4	Total	1	2	3	4	Total
5	- 9.05	-12.63	-17.59	-38.22	- 7.06	3.763	0.2031	-4.742	-25.36	5.757
10	-12.21	-15.51	-21.13	-41.22	-10.18	0.642	-2.617	-8.210	-28.27	2.693
15	-14.71	-17.90	-25.42	-45.39	-12.76	-1.698	-4.837	-12.33	-32.23	0.269
20	-15.61	-19.34	-29.08	-50.60	-13.94	-2.324	-5.985	-15.72	-37.13	-0.632
30	-13.51	-18.70	-27.55	-49.26	-12.23	0.723	-4.361	-13.28	-34.83	2.027
40	-12.18	-17.58	-23.87	-44.50	-10.86	3.538	-1.723	-8.042	-28.45	4.899
50	-13.55	-17.99	-23.23	-42.87	-11.88	4.214	-0.0275	-5.266	-24.58	5.948
60	-17.45	-19.75	-25.32	-42.70	-15.01	2.921	0.8982	-4.618	-21.55	5.492

TABLE 5-8.– NUMERICAL VALUES OF THE BACKSCATTERED SIGNALS FOR VERTICAL TRANSMIT AND VERTICAL RECEIVE

[IN TERMS OF $B/A/\Delta f_D$]

Incidence angle Θ, degree	VV (water)					VV (land)				
	1	2	3	4	Total	1	2	3	4	Total
5	-8.414	-31.76	-31.76	-33.03	-8.359	4.406	-18.92	-18.92	-20.16	4.461
10	-11.47	-34.71	-34.71	-35.54	-11.41	1.392	-21.81	-21.81	-22.58	1.451
15	-13.63	-37.20	-37.20	-36.99	-13.57	-0.619	-24.13	-24.13	-23.85	-0.560
20	-13.92	-38.50	-38.50	-38.05	-13.87	-0.631	-25.15	-25.15	-24.61	-0.583
30	-12.25	-38.27	-38.27	-39.23	-12.22	1.986	-23.95	-23.95	-24.79	2.017
40	-12.81	-38.95	-38.95	-40.36	-12.78	2.907	-23.12	-23.12	-24.36	2.937
50	-16.88	-41.92	-41.92	-42.64	-16.84	0.870	-24.01	-24.01	-24.45	0.911
60	-24.23	-47.06	-47.06	-45.60	-24.15	-3.870	-26.48	-26.48	-24.62	-3.787

It can be shown that even if the values of σ°_{HV} or σ°_{VH} are comparable to those of σ°_{HH} and σ°_{VV}, the effect of antenna coupling remains negligible in σ°_{HH} and σ°_{VV} estimations. For both water and land backscatterings, the results in table 5-7 indicate a 1- to 2.5-dB contribution caused by antenna coupling, which is smaller than that shown in table 5-4. The contributions from column 2 become smaller than those of column 1 because of increasing values of σ°_{HV}.

The smallest coupling effect occurs at $\theta = 30°$, where the values in column 2 are about 5 dB less than those in column 1. By comparing tables 5-4 and 5-7, it can be seen that the larger the difference is between the assumed values of σ°_{HV} and σ°_{HH}, the larger the contributions are from the antenna coupling effect. This is because a decrease in σ°_{HV} results in a decrease in column 1; simultaneously, the unchanged values in column 2 will result in a larger share of contribution from column 2. This is what happens in column 1 of tables 5-4 and 5-7, where exactly 5 dB difference is shown between the two tables. As a result of the undesirable contribution from antenna coupling, σ°_{HV} or σ°_{VH} would be overestimated in the data processing algorithm. A correction would be required which would depend on the relative level of σ°_{HV} with respect to σ°_{HH}. For σ°_{HV} to be 10 dB less than those of σ°_{HH} and σ°_{VV}, the value difference between the Total column and column 1 in table 5-7 should be employed.

5.5 OUTPUT SIGNAL PRECISION

5.5.1 ANTENNA PATTERN MEASUREMENTS

The uncertainty in the antenna pattern measurements was not recorded and supplied with the gain values. Since the New Mexico State University measured both the 1.6-GHz and 0.4-GHz antenna patterns, it is assumed that the same degree of uncertainty is placed to the 0.4-GHz system. An uncertainty of approximately ±0.5 to ± 1 dB in one-way gain results in the uncertainty of ± 0.7 to ± 1.3 dB for the two-way gain used in the σ° estimates. Another source of uncertainty, which is significant for the 0.4-GHz scatterometer because of its large antenna array, comes from the fact that the gain measurements were made without a mockup to simulate the effect of the C-130 aircraft. It is expected that, after the antennas were installed in the aircraft, the gain pattern would differ from that measured in the laboratory. The magnitude of this antenna pattern change cannot be estimated.

5.5.2 MEASUREMENT OF CALIBRATION CONSTANTS

An uncertainty exists in the measurements of the calibration constants K for various polarizations and gain settings. A reasonable estimate placed this uncertainty to be no more than ±0.5 dB for each of these measurements.

5.5.3 AIRCRAFT PARAMETERS

Factors associated with aircraft motion, such as roll, pitch, drift, vertical velocity, speed, and altitude changes, could

introduce errors in the received signals. The effects of roll, pitch, and vertical velocity alter the incidence angle θ and were studied by Krishen (ref. 4) with respect to the 13.3-GHz scatterometer system. Following the same approach, the errors introduced by these factors in the σ° estimates are presented in tables 5-9, 5-10, and 5-11 for all four polarizations. In making these error calculations, the aircraft speed is assumed to be 77 m/sec (253 ft/sec), the vertical velocity is 4 m/sec (13.1 ft/sec), and both roll and pitch angles are 5°. Clearly, the change in θ, caused by pitch and vertical speed, could be either plus or minus. Tables 5-10 and 5-11 list larger modified incidence angles only.

Changes in both aircraft speed and drift would introduce changes in the Doppler frequency which is associated with a given θ. For example, at $\theta = 30°$, a change of speed from 77 m/sec (253 ft/sec) to 70 m/sec (230 ft/sec) would give a corresponding change in Doppler frequency from 103 Hz to 93 Hz. Similarly, a drift of approximately 10° would shift the Doppler frequency from 103 Hz to 101 Hz. These Doppler frequency changes, if not corrected for in data processing, could result in erroneous σ° estimates.

The variation in aircraft altitude would also introduce error in the σ° estimate. From equation (3-22), σ° is observed to be proportional to R^4 and inversely proportional to the area A of the ground cell. Since R is proportional to altitude h and A to h^2, σ° varies with h^2. Thus, if h changes from 460 to 440 meters

TABLE 5-9. — ERRORS INTRODUCED IN THE σ° ESTIMATE DUE TO AN AIRCRAFT ROLL OF 5°

Incidence angle, degree	Modified incidence angle, degree	Error in σ° (dB)		
		HH	HV or VH	VV
5	7.07	-0.25	-0.35	-0.50
10	11.17	-0.29	-0.41	-0.59
15	15.79	-0.40	-0.40	-0.40
20	20.59	-0.44	-0.53	-0.59
30	30.38	-0.38	-0.38	-0.38
40	40.26	-0.13	-0.09	-0.07
50	50.18	-0.05	0	0.05
60	60.13	-0.02	0.05	0.07

TABLE 5-10. – ERRORS INTRODUCED IN THE σ° ESTIMATE DUE TO AN AIRCRAFT PITCH OF 5°

Incidence angle, degree	Modified incidence angle, degree	Error in σ° (dB)		
		HH	HV or VH	VV
5	10	-0.25	-0.75	-1.25
10	15	-1.50	-2.00	-2.50
15	20	-3.50	-3.70	-4.00
20	25	-4.50	-4.65	-4.75
30	35	-5.00	-3.95	-3.25
40	45	-3.00	-1.75	-0.50
50	55	-1.25	0.15	1.50
60	65	-0.50	1.65	3.75

TABLE 5-11. – ERRORS INTRODUCED IN THE σ° ESTIMATE DUE TO AN AIRCRAFT VERTICAL SPEED OF 4 M/SEC (13 ft/sec)

Incidence angle, degree	Modified incidence angle, degree	Error in σ°(dB)		
		HH	HV or VH	VV
5	7.97	-0.25	-0.45	-0.75
10	12.97	-0.75	-1.10	-1.50
15	17.97	-1.50	-2.00	-2.50
20	22.97	-2.50	-2.80	-3.00
30	32.97	-3.00	-2.60	-2.50
40	42.97	-1.75	-1.10	-0.50
50	52.97	-0.75	0	0.75
60	62.97	-0.50	0.80	2.00

(1510 to 1443 feet), the error in the σ° estimate would be approximately 0.39 dB.

5.5.4 COMMENT

The uncertainty introduced in the antenna pattern measurements and by the presence of the aircraft body is difficult to correct. But this uncertainty can be treated as a bias and should not affect the repeatability of the data taken from one mission at another level. The calibrate signal level could be adjusted to accommodate a particular mission. For each adjustment, a new calibration constant K would have to be measured; therefore, the measurement should be made as precisely as possible. The changes in aircraft parameters could introduce large error in σ° estimation (tables 5-9, 5-10, 5-11). This type of error could be minimized by making corrections to the aircraft parameters during data processing. The error sources from the antenna coupling could be corrected by proper data reduction and manipulation using tables 5-4 and 5-7 for cross polarization power returns. However, if the measured data indicate an irregular variation, the data should be used with reservation.

6. CONCLUSIONS AND RECOMMENDATIONS

A system analysis was performed on the 0.4-GHz airborne scatterometer. The principle of the scatterometer operation, calibration procedures, resolution cell length requirement, and data handling were described. The antenna gain patterns were studied, and the effect of the antenna cross coupling effects were analyzed. Several error sources in the estimation of σ° were briefly discussed. In the course of the entire analysis, only the immediate relationship between the power input to the power output from the scatterometer system was examined. The interacting process of the RF waves with terrain surfaces was completely omitted. The terrain surface characteristics were reflected through the assumed functional forms of the backscattering coefficient $\sigma^\circ(\theta)$. The major conclusions that resulted from this study are listed below:

a. To obtain a sufficient independent sample within a resolution cell, the cell length should be made larger than 75 m as described in section 3.3, especially at large incidence angles.

b. The gain patterns for the vertical and horizontal antenna are quite different. The gain maximum occurs at $\theta = 66^\circ$ for the horizontal antenna, and it occurs at $\theta = 42^\circ$ for the vertical antenna. The beam width variations (with θ) of the two antennas closely follow one another, with the vertical antenna having the smaller beam width.

c. The cross-polarization effects, measured for the two antennas, have important bearing on the receiver signal outputs of both HV and VH polarizations. If σ°_{HV} or σ°_{VH} is less than σ°_{HH} and σ°_{VV} by approximately 15 dB, the power contributions caused by the antenna cross-polarization effects were larger than the return power of interest for the HV or VH receiver. If σ°_{HV} or σ°_{HV} is less than σ°_{HH} and σ°_{VV} by approximately 10 dB, the cross polarization effects were found to be comparable to the return power of interest. Thus, in general conditions, a correction factor should be added to make the estimation meaningful for the HV or VH receiver. The magnitude of the correction may be obtained from tables 5-4 and 5-7.

d. The side lobe contributions to the receiver signal outputs are negligible. For the cases examined, the backscattered power levels from the side lobes are approximately 30 dB or more below that from the main beam.

e. The variations of the aircraft parameters affect the estimation of σ°. For example, a pitch of 5° could result in an error of approximately 5.0 dB in some cases.

The following recommendations should be considered in order to improve the performance of the system and the quality of the final report.

a. The effect of the aircraft body on the antenna pattern cannot be estimated. To improve the accuracy of σ° measurements,

it is desirable to calibrate the aircraft scatterometer with a well-calibrated ground system on a homogeneous terrain surface.

b. The antenna cross-polarization effects should be considered in the estimations of σ°_{HV} or σ°_{VH}. If information provided by σ°_{HV} or σ°_{VH} is indispensable in the aircraft remote sensing of soil moisture, carefully interpolated correction factors should be used to obtain a reasonable estimate of σ°_{HV} or σ°_{VH}. In other cases, the measured data of σ°_{HV} or σ°_{VH} should be used with reservation.

c. Since aircraft parameter variations significantly affect the estimation of σ°, corrections to the variation of the aircraft parameters should be made in the data processing.

7. REFERENCES

1. Krishen, K.: Joint Soil Moisture Experiment Project Plan.

2. Krishen, K.; Vlahos, N.; Brandt, O.; and Graybeal, G.: Results of Scatterometer System Analysis for NASA/MSC Earth Observations Sensor Evaluation Program. Proc. of the 7th Inter. Symp. on Remote Sensing of Environment, Univ. of Mich. (Ann Arbor, Mich.), May 1971.

3. Bradley, G. A.: Remote Sensing of Ocean Winds Using a Radar Scatterometer. Univ. of Kansas/Center for Research, Inc., Technical Report 177-22, Sept. 1971.

4. Nordhaus, W. D.: The Development of a Signal Processing Network for a Real-Time Arctic Sea Ice Classification System. Texas A&M Univ., Technical Report, RSC-46, Aug. 1973.

5. Rosenkranz, W. A.: A Model of the 13.3-GHz Scatterometer. LEC-8795, June 1976.

6. Wang, J. R.: A Model of the 1.6-GHz Scatterometer. LEC-10521, July 1977.

7. Reid, S. C.: Joint Soil Moisture Experiment (JSME) Scatterometer Systems. LEC-7195, Oct. 1975.

8. 400-MHz Scatterometer Maintenance Manual, Volume I. Emerson Electric Co., Electronics and Space Division, Document No. 2200, rev. A., Aug. 1968.

9. 400-MHz Scatterometer Final Report. Emerson Electric Co., Electronics and Space Division, Document No. 2236, rev. A., Oct. 1969.

10. Burdic, W. S.: Radar Signal Analysis. Ch. 2. Prentice Hall Inc. (New Jersey), 1968.

11. Manual of Remote Sensing – Microwave Remote Sensors, Chapter 9. American Society of Photogrammetry (publisher), 1975.

12. Guinard, N. W.: The NRL Four-Frequency Radar System. Report on NRL Progress. May 1969, pp. 1-10.

13. Dickey, F. M.; King, C.: Holtzman, J. C.; and Moore, R. K.: Moisture Dependency of Radar Backscatter from Irrigated and Nonirrigated Fields at 400 MHz and 13.3 GHz. IEEE Transaction of Geoscience Electronics, vol. GE-12, no. 1, Jan. 1974, pp. 19-21.

14. Skalnik, M. I.: Radar Handbook, Chapter 25. McGraw-Hill Book Company, 1970.

APPENDIX

THE COMPUTER PROGRAM LISTING

```
      DIMENSION THETA(8),POW(8,2),BUF(92)
      DATA THETA/5.,10.,15.,20.,30.,40.,50.,60./
      COMMON/B/IDADD,IX,IY,IXMAX,IYMAX
C ENTER CONSTANT PARAMETERS.
      ALOSS=8.4
      PIE=3.1416
      HA=460.
      VA=77.
      SLAMD=0.75
      CELEN=50.
      PI=PIE/180.
      IFIL=1
      IX=92
      IY=36
      IXMAX=92
      IYMAX=36
      CALL RINIT(IDADD,NWRDS)
      IEOF=IFIL+10
 50   CONTINUE
C GET DISC AREA
      NS=IFIL
      K=IDADD
C PUT ANTENNA FOOTPRINT ON DISC
 100  READ(1,4000,END=200)(BUF(NR),NR=1,92)
C     WRITE(6,5000)(BUF(NR),NR=1,92)
      CALL RWRITE(K,BUF,IX,NSTAT)
5     IF(NSTAT.EQ.1) GO TO 5
      K=K+IX
      GO TO 100
 200  CONTINUE
C ENTER MAIN LOOP OF COMPUTATION.
C ALONG-TRACK COMPUTATION.
      DO 500 I=1,8
      THTA=THETA(I)*PI
      FDOP=2.*VA*SIN(THTA)/SLAMD
      DF=2.*VA*(COS(THTA)**3)*CELEN/HA/SLAMD
      CLAMD=SLAMD**2
      CPI=(4.*PIE)**3
      SUM=0.
C CROSS-TRACK COMPUTATION.
      IF(I.LT.7) JJ=21
      IF(I.GE.7) JJ=21
      DO 600 M=1,2
      DO 400 J=1,JJ
      PHI=(J-1)*PI*2.
      PHIL=((J-1)*2.-1.)*PI
      PHIR=((J-1)*2.+1.)*PI
      DX=HA*(TAN(PHIR)-TAN(PHIL))
      DY=CELEN/COS(PHI)
      DA=DX*DY
      R=HA/COS(THTA)/COS(PHI)
      RR=R**4.
      THINC=ACOS(HA/R)
      THINC=THINC/PI
      CALL BCOFF(THINC,SIGMA,NS,M)
      AI=ATAN(TAN(THTA)/COS(PHI))
      AI=AI/PI
      CALL GAI(PGL,PGR,I,J,AI)
      SIG=10.**(SIGMA/10.)
      IF(J.EQ.1)PGR=0.
      SUM=SUM+((PGL+PGR)*SIG*DA/RR)
```

```
62*       C       WRITE(6,6000)PSL,PGR,SIGMA,SIG,DA,RR,SUM
63*        400    CONTINUE
64*       C CALCULATE POWER OUTPUT FOR AN INCIDENT ANGLE.
65*               PAC=SUM*CLAMD/CPI/DF
66*               PAC=10.*ALOG10(PAC)
67*               IF(NS.EQ.1.OR.NS.EQ.7.OR.NS.EQ.8) SCAL=122.8
68*               IF(NS.EQ.2.OR.NS.EQ.3.OR.NS.EQ.4.OR.NS.EQ.5) SCAL=135.7
69*               IF(NS.FQ.6.OR.NS.EQ.9.OR.NS.EQ.10) SCAL=123.
70*               POW(I,M)=PAC-ALOSS+SCAL
71*        600    CONTINUE
72*       C       WRITE(6,6000)PAC,FDOP,DF,CLAMD,CPI,ALOSS,SCAL
73*        500    CONTINUE
74*       C       WRITE(6,3000)IFIL,NS,M
75*               WRITE(6,1000)
76*               WRITE(6,2000)((POW(I,M),I=1,8),M=1,2)
77*               IFIL=IFIL+1
78*               IF(IFIL.LT.IEOF)GO TO 50
79*               STOP
80*        1000   FORMAT(2H ,'INCIDENT ANGLE AT',3X,'5',11X,'10',10X,'15',10X,'20'
81*          C    10X,'30',10X,'40',10X,'50',10X,'60',/)
82*        2000   FORMAT(16X,8D12.4)
83*        3000   FORMAT(3I10)
84*        4000   FORMAT(22F6.1)
85*        5000   FORMAT(20F6.1)
86*        6000   FORMAT(7D12.4)
87*               END
```

```
 1*               SUBROUTINE GAT(GL,GR,I,J,AI)
 2*               COMMON/B/IDADD,IX,IY,IXMAX,IYMAX
 3*               DIMENSION BUF1(92),BUF2(92)
 4*       C DETERMINE THE POSITION OF THE ANTENNA FOOTPRINT.
 5*               AI=AI/2.
 6*               IA=36-AINT(AI)
 7*               AAI=36.-AI
 8*               IAP1=IA-1
 9*               IP1=IA*IX+IDADD
10*               IP2=(IA-1)*IX+IDADD
11*       C READ ANTENNA RECORDS.
12*               CALL RREAD(IP1,BUF1,IX,IST)
13*        5      IF(IST.EQ.1)GO TO 5
14*               IF(IST.NE.0)WRITE(6,1000)IA
15*               CALL RREAD(IP2,BUF2,IX,IST)
16*        6      IF(IST.EQ.1)GO TO 6
17*               IF(IST.NE.0)WRITE(6,1000)IAP1
18*       C PERFORM LINEAR INTERPOLATION.
19*               IF(J.EQ.1)GO TO 7
20*               PL1=BUF1(47-J)
21*               PL2=BUF2(47-J)
```

```
22*              PR1=BUF1(45+J)
23*              PR2=BUF2(45+J)
24*              PL1L=10.**(PL1/10.)
25*              IF(J.GT.5.AND.PL1.EQ.0.)PL1L=0.
26*              PL2L=10.**(PL2/10.)
27*              IF(J.GT.5.AND.PL2.EQ.0.)PL2L=0.
28*              PR1L=10.**(PR1/10.)
29*              IF(J.GT.5.AND.PR1.EQ.0.)PR1L=0.
30*              PR2L=10.**(PR2/10.)
31*              IF(J.GT.5.AND.PR2.EQ.0.)PR2L=0.
32*              GL=(((AAI-IA)/(IAP1-IA))*(PL2L-PL1L))+PL1L
33*              GR=(((AAI-IA)/(IAP1-IA))*(PR2L-PR1L))+PR1L
34*              GO TO 8
35*       7      P1=BUF1(46)
36*              P2=BUF2(46)
37*              P1=10.**(P1/10.)
38*              P2=10.**(P2/10.)
39*              GL=(((AAI-IA)/(IAP1-IA))*(P2-P1))+P1
40*              GR=GL
41*       8      CONTINUE
42*      C       WRITE(6,4000)P1,P2,PL1,PL2,PR1,PR2,GL,GR,AAI,IA,IAP1
43*              RETURN
44*       1000   FORMAT(1H ,'DISC READ PROBLEM FOR ANGLE',I5)
45*       2000   FORMAT(1H ,F6.2,5X,3I10)
46*       3000   FORMAT(1H ,7F12.4)
47*       4000   FORMAT(1H ,9F8.2,2I10)
48*              END
```

```
 1*              SUBROUTINE BCOFF(A     ,SIGMA,N,M)
 2*              IF(M.EQ.1) SIGMA=0.00571*A**2-0.971*A-2.86
 3*              IF(M.EQ.2) SIGMA=0.00844*A**2-1.01*A+9.85
 4*              IF(N.EQ.1.OR.N.EQ.2.OR.N.EQ.5.OR.N.EQ.6) SIGMA=SIGMA-10.
 5*              RETURN
 6*              END
```